**School of Civil and Mechanical Engineering**
**Department of Civil Engineering**

# Nutrient Adsorption onto Sawdust for the Treatment of Stormwater

**Kadek Diana Harmayani**

**This thesis is presented for the Degree of**
**Doctor of Philosophy**
**of**
**Curtin University**

**June 2013**

# DECLARATION

To the best of my knowledge and belief this thesis contains no material previously published by any other person except due acknowledgement has been made.

This thesis contains no material which has been accepted for the award of any degree or diploma in any university.

Signature:

Date: June 2013

# ABSTRACT

Stormwater runoff contains significant amount of nutrients including nitrogenous compounds such as ammonia-nitrogen ($NH_3$-N), nitrate-nitrogen ($NO_3$-N), and nitrite-nitrogen ($NO_2$-N). These compounds are known as potential stormwater contaminants and they are a threat to the environment. It is crucial to determine an optimum adsorption medium for removing these contaminants from stormwater.

In this study, the sawdust of Radiata pine wood was chosen as an adsorption medium to remove these pollutants from synthetic stormwater. A series of batch experiments was carried out to investigate the effect of different parameters for removing these pollutants. Five particle sizes of sawdust (<300 µm, 300µm-600µm, 600µm-1.18mm, 1.18-2.36 mm, and >2.36mm) with initial concentration range of 0.5-5 mg/L and dosages of 2-20 mg of sawdust were used in the experiments. The effects of pH were checked, for pH range of 4-9.

The adsorption of nutrients ($NH_3$-N, $NO_3$-N, and $NO_2$-N) from aqueous solutions onto sawdust were also investigated using fixed-bed packed columns for different flow rates, concentrations, and different heights of beds under saturated conditions. The solution contaminated by nutrients was placed into the feed tank and injected through a column at up-flow mode, and the effluent was collected in an effluent tank. The effluent sample was collected using a two-way valve at a predetermined time and analysed using Aquakem 200.

Results revealed that pH and particle size do not significantly affect the removal process. However, dosage, initial concentration and contact time had a significant effect on the removal of these compounds. An increase of adsorbent dosage increased the removal of all nutrients. The maximum removal of 100% was found for $NO_3$-N, and $NO_2$-N while $NH_3$-N removal was found 55%. A lower initial concentration revealed a higher removal rate. The maximum removal of $NO_3$-N and $NH_3$-N was obtained within 10 minutes, while it took 45 hrs to reach maximum removal of $NO_2$-N. Different adsorption isotherms were also checked and found the Freundlich model fitting better, with varying degree of regression coefficient.

Furthermore, the second-order model was found to be suitable to describe the kinetics of the removal of all nutrients in the batch. The rate constants of pseudo-

second order were found 0.038-0.539 g/mg min, 0.0003-0.133 g/mg min, and 0.001-0.039 g/mg min for $NH_3$-N, $NO_3$-N, and $NO_2$-N adsorption respectively. Moreover, it was found that chemisorptions acted as the rate controlling step for $NH_3$-N and $NO_3$-N transfer to a solid surface. The mechanism of $NO_2$-N transfer to the solid surface includes diffusion through the fluid film around the sawdust particles and diffusion through the pores to the internal sites. This is due to the fact that the transfer of solute onto the solid surface is faster at the beginning, and the solute then takes more time to transfer from the solid surface to the internal adsorption sites through the pores. During this time, intraparticle diffusion becomes the dominant process.

The dynamic behavior of $NH_3$-N, $NO_3$-N, and $NO_2$-N adsorption was tested in columns. The breakpoint time was found to decrease with an increase in flow rate, inlet concentration, and bed-depth. The models of Clark (1987) and Yoon-Nelson (1984) were used to predict breakthrough curves to determine the column's kinetic parameters. Both models were found to be effective for predicting $NO_2$-N adsorption, while $NH_3$-N was well predicted by the Clark model (1987) and $NO_3$-N was effectively predicted by the Yoon and Nelson model (1984). The length of the unused bed (*LUB*) was calculated which may be used in designing the fix-bed reactor. The *LUB* indicates how much sawdust was active in the adsorption process prior to breakthrough. The value of the *LUB* can be added to the stoichiometric length of the bed needed. This makes the actual column longer in terms of accounting for any unused adsorption capacity under real conditions.

Fixed-bed adsorption processes were then investigated and the axial dispersion ($D_a$), the external fluid-phase mass transfer resistance ($k_f$) and the surface diffusion of mass transfer resistance ($D_s$) were calculated. The surface diffusion was found to be concentration-dependent and it varied in the range of 3.87-4.4×$10^{-6}$$cm^2$/s for $NH_3$-N adsorption, 3.7-4.58×$10^{-6}$$cm^2$/s for $NO_3$-N adsorption and 4.35-7.92×$10^{-9}$$cm^2$/s for $NO_2$-N adsorption respectively for a concentration range of 0.5-5 mg/L. The axial dispersion coefficient were found in the range of 1.05-1.8×$10^{-3}$ $cm^2$/s for $NH_3$-N and $NO_3$-N adsorption respectively for the flow rate of 9-22ml/min but it was found zero for $NO_2$-N adsorption. This was due to the surface diffusion being predominant over axial dispersion for $NO_2$-N adsorption. The external mass transfer coefficients ($k_f$) were also found to be dependent on the flow rate. The value of $k_f$ obtained was in the

range of 2.41–8.94×$10^{-4}$ cm/s, 2.48–5.6×$10^{-4}$ cm/s, and 0.677–6.17×$10^{-4}$ cm/s for $NH_3$-N, $NO_3$-N, and $NO_2$-N adsorption respectively.

Finally, the liquid-solid phase mass transfer was studied for nutrient adsorption onto sawdust. A stepwise regression analysis was carried out and an optimum mass transfer correlation for $NH_3$-N adsorption onto sawdust was found to be $Sh=0.4059Re^{1.02}Sc^{1/3}$ (standard error of estimate =±0.12; $0.74<Re<1.77$). $NH_3$-N was chosen for developing this correlation due to the dimensionless Biot number of different nutrients and their isotherms. The correlation shows that the mass transfer coefficient of the dissolved $NH_3$-N is proportional to the flow rate to the power of 1.02. This value is higher compared to other reported research. This might be due to the experiment in this research being conducted under a laminar flow while some of the previous research was carried out under turbulent conditions. In addition, mass transfer is affected by the porous characteristics of the medium. Other studies used porous mediums that did not show intraparticle diffusion, while sawdust is an intraparticle adsorbate medium.

Based on the results found in this research, it was revealed that a favourable denitrification process may be driven by sawdust from Radiata pine wood under saturated condition. Sawdust is a waste material and can be used as a renewable resource for the treatment of stormwater. The findings of this research may be useful for designing biofiltration/bioretention systems for treating stormwater using Radiata pine sawdust.

# DEDICATION

This thesis is dedicated to:
my lovely husband, I Nyoman Yoga Wedana
my lovely daughters, Putu Hardayani Utami,
Kadek Laksmi Satyawati, and Komang Sasti Anantari
I thank them for their support, patience and best wishes throughout the time of my research and thesis preparation.

# ACKNOWLEDGEMENTS

It is an honour for me to acknowledge the people who made this thesis possible. I would like to give my sincere thanks to my academic supervisor, Dr. Faisal Anwar, for his clarity and comments, and for his patience in understanding my abilities and supporting me step by step in my research work. In addition, I am also deeply grateful to Prof. Hamid Nikraz, the Head of Department of Civil Engineering, for his supervisory attention, guidance and technical support during my study.

I would also like to express my special gratitude to the greatly supportive staff in the Department of Civil Engineering, School of Civil and Mechanical Engineering, Curtin University, who assisted in bringing my research to bear on time.

My thanks also go to my sponsors, the DIKTI of the Ministry of Education, Indonesia for being financially supportive of my study. I am also grateful to all the postgraduate students at Curtin University and to the DIKTI Scholarship members of Udayana University for listening to some of the problems I encountered during my research and for sharing their thoughts and experiences over the course of my studies.

Finally, I owe my deepest gratitude to my beloved family in Bali for their spirit, patience and empathy whilst we have been separated during my time in Perth, Western Australia.

Perth, June 2013

**Kadek Diana Harmayani**

# TABLE OF CONTENTS

# LIST OF ABBREVIATIONS

*ANZECC* = Australian Water Quality Guidelines for Fresh and Marine Waters, Australian and New Zealand Environment and Conservation Council

*APE* = Average Percentage Error

*BMPs* = Best Management Practices

*BOD* = Biochemical Oxygen Demand

*BTC* = Breakthrough Curve

*COD* = Chemical Oxygen Demand

*DIN* = Dissolved Inorganic Nitrogen

*DON* = Dissolved Organic Nitrogen

*FAWB* = Facility for Advancing Water Biofiltration

*FRP* = Filterable Reactive Phosphorus

*LUB* = Length of Unused Bed (cm)

*Org-N* = Organic Nitrogen

*SAZ* = the Saturated Zone

*TOC* = Total Organic Carbon

*TKN* = Total Kjeldahl Nitrogen

*TN* = Total Nitrogen

*TP* = Total Phosphorus

*TSS* = Total Suspended Solid

# LIST OF FIGURES

# LIST OF SYMBOLS

$a$ = external particle surface area ($m^2/m^3$ solid)

$A$ = the area under the breakthrough curve ($m^2$)

$A_C$ = the Clark constant

$b$ = a constant related to the affinity of the binding sites

$C_e$ = the equilibrium nutrients concentrations (mg/L)

$C_{ad}$ = the nutrients adsorbed concentration which is taken as influent concentration $C_o$ – effluent concentration $C$, (mg/L).

$C_{eq}$ = the unadsorbed nutrients concentration at equilibrium in the column (mg/L)

$C_i$ = the concentration of the solute in the liquid at the particle/liquid interface

$C_0$ = the initial nutrients concentration (mg/L)

$c`_o$, $c_o$ = initial ($t < 0$) and final ($t \geq 0$) steady state values of $c$

$C_t$ = the liquid phase concentration at any time (mg/L)

$D_a$ = the axial dispersion coefficient ($cm^2/s$)

$D_m$ = the solute molecular diffusivity in the fluid phase ($cm^2/min$)

$D_s$ = the solute diffusivity in the solid phase ($cm^2/min$)

$d_p$ = the particle diameter (cm)

$F$ = $q_t/q_e$ is the fractional attainment of equilibrium

$G_s$ = flow rate of solvent per unit of cross-sectional area in Clark model ($m^3 min^{-1} m^{-2}$)

$H$ = the column height (cm)

$h$ = the initial adsorption rate (mg/g min)

$K$ = constant involving adsorption capacity (Freundlich equation) (mg/g)

$K_{ads}$ = the measure of affinity of adsorbate for adsorbent (unitless)

$K_{db}$ = the distribution ratio; equal to $q_o/c_o$

$K_T$ = mass-transfer coefficient in Clark model (1/min)

$k_a$ = rate constant of adsorption

$k_f$ = the convective fluid phase external film mass transfer coefficient (cm/min)

$k_{fd}$ = the adsorption rate constant of liquid film diffusion model (1/min)

$k_{di}$ = the intraparticle diffusion rate constant (mg/g $h^{1/2}$) at stage $i$.

$k_{ds}$ = rate constant of desorption

$k_{YN}$ = the rate constant of Yoon and Nelson model (1/min)

$k_1$ = the rate constant adsorption (1/min) of pseudo-first-order kinetic model

$k_2$ = the rate constant of second-order adsorption (g/mg h)

$L_a$ = mass velocity of adsorbent to keep the mass-transfer zone stationary (Clark model) (mg/ h $m^2$)

$m_{total}$ = total amount of adsorbate ions driven to column

$M_i$ = the intercept of stage $i$

$n$ = constants involving adsorption intensity (Freundlich equation)

$Q$ = the volumetric flow rate (mL/min)

$Q_\circ$ = the maximum amount of nutrient per unit weight of sawdust to form a complete monolayer on the surface bound at high $C_{eq}$

$q_e$ = the amounts of nutrients adsorbed (mg/g) at equilibrium

$q_e$ (cal) = the calculated $q_e$

$q_e$ (exp) = the experimental $q_e$

$q_m$ = the maximum capacity constant of adsorbent for adsorbate (mg/g)

$q`_o$, $q_o$ = initial and final values of $q$ ($q_o$ is in equilibrium with $c_o$, $q`_o$ is in equilibrium with $c`_o$)

$q(r)$ = the local values of $q$ in the solid

$q_s$ = the surface concentration (just inside solid) (mg/g)

$q_t$ = the amount of nutrient adsorbed by sawdust at time $t$ (mg/g)

$q_{total}$ = total quantity nutrient adsorbed in the column for a fix feed concentration and flow rate of $Q$ (mg)

$\bar{q}$ = the average concentration of solute in the solid phase (mass of solute per unit volume of solid)

$q^*$ = the $q$ value in equilibrium with the bulk concentration in the liquid

$R$ = the particle radius (mm)

$R_L$ = the dimensionless parameter of equilibrium or adsorption intensity (additional analysis of Langmuir equation)

$r$ = the Clark constant (1/min)

$r_d$ = the radial position coordinate originating in the centre of the solid spherical particle

$S$ = the cross sectional area of column ($mm^2$)

$t$ = the contact time (min)

$t^{0.5}$ = the square root of contact time

$t_{breakthrough}$ = the breakthrough time (min)

$t_{total}$ = the total flow time (min)

$t`$ = the time required for the first parcel of the solute-rich feed stream to transverse the length of the bed $H/v$

$V$ = the initial volume of nutrient solution (mL)

$V_{eff}$ = the effluent volume ($mL^3$)

$v$ = the interstitial fluid phase velocity (cm/min)

$W$ = the weight of oven-dried sawdust (g)

$W_e$ = the dynamic adsorption capacity of sawdust (mg/g)

$x$ = the weight of sawdust (g)

$Z$ = the axial distance coordinate (mm)

***Greek symbols***

$\varepsilon$ = void fraction in the bed

$\tau$ = the time required for 50% adsorbate breakthrough in Yoon and Nelson odel (min)

$\alpha$ = the velocity of constant pattern front; equal to $\varepsilon v/[\varepsilon+(1-\varepsilon)K]$

$\gamma_f$ = $[\alpha^2(1-\varepsilon)/3\varepsilon]$ $(RK_{db}^2/k_fD_a)$

$\gamma_p$ = $[\alpha^2(1-\varepsilon)/15\varepsilon](R^2K_{db}/D_sD_a)$

$\theta$ = the dimensionless residence time; $\theta = t/t`=1$

$\rho$ = the fluid phase density ($g/cm^3$)

$\mu$ = the fluid phase viscosity (g/cm min).

$\Delta q$ = validity of kinetics model (%)

$\Delta Z$ = a short length of sawdust of cross-sectional area (mm)

Common Dimensionless Group

$Bi = k_f d_p/2K_{db}D_s$ = Biot Number

$j_D = (k_f/\varepsilon v)Sc^{2/3}$ = Colburn Factor

$Re = d_p \varepsilon v \rho / \mu$ = Reynolds Number

$Sc = \mu / \rho D_m$ = Schmidt Number

$Sh = k_f d_p / D_m$ = Sherwood Number

# LIST OF TABLES

# List of Publications Out of This Thesis

**Conference Papers:**

Harmayani, K.D. and Anwar, A. H. M. F., 2012. Nutrients adsorption on sawdust in dynamic conditions, In Proc. of *13th International Conference Wetland Systems for Water Pollution Control,* IWA specialist conference, Perth, WA. 25-29 November.

**Journal Papers:**

Harmayani, K. D. and Anwar, A. H. M. F., 2012. Adsorption of Nutrients from Stormwater Using Sawdust. *International Journal of Environmental Science and Development*, 3(2): 114-117.

Harmayani, K. D. and Anwar, A. H. M. F., 2013. Nutrient removal from stormwater using Radiata pine sawdust: Adsorption Kinetics and Equilibrium Studies. *Clean Soil Air Water* (to be submitted).

Harmayani, K. D. and Anwar, A. H. M. F., 2013. Dynamic Adsorption of Nutrients onto Sawdust in Column Study. *Chemospere* (to be submitted).

Harmayani, K. D. and Anwar, A. H. M. F., 2013. Mass Transfer Characteristics for Nutrient Adsorption onto Sawdust. *Chemosphere* (to be submitted).

# CHAPTER 1
# INTRODUCTION

## 1.1.Background Overview

Stormwater runoff contains varieties of contaminants such as, hydrocarbons, trace metals and nutrients. This contaminated water is harmful to human health and surrounding ecosystems if it is received by water bodies in an untreated condition. Nutrients include phosphorous and nitrogenous compounds such as ammonia-nitrogen ($NH_3$-N), nitrate-nitrogen ($NO_3$-N), and nitrite-nitrogen ($NO_2$-N). These nutrients, transported by stormwater, normally result from auto-emissions, fluid leaks from vehicles, home use fertiliser and pesticides, refuse, and pet faeces. This type of pollutant in stormwater has adverse effects on groundwater quality, particularly in urban areas (Fetter, 1999) and the pollutants are also responsible for eutrophication in receiving water (Taylor et al., 2005).

The treatment of stormwater is receiving attention all over the world in that efforts are being made to remove unwanted pollutants and to ensure good-quality water. Nutrients can be removed through either physiochemical or microbiological processes or both. Physiochemical processes include reverse osmosis, electrodialysis, activated carbon adsorption and ion exchange with synthetic resins (Wanielista and Chang, 2008). Microbiological processes such as bio-infiltration are designed to remove nutrients using different sorption media and these are used in urban watersheds (Wanielista and Chang, 2008).

Nitrification and Denitrification are two of the main processes that help remove nitrogenous compounds from stormwater runoff. Nitrification oxidizes ammonia and denitrification reduces nitrate into nitrogen gas before it is released into the air. Only the denitrification process under anaerobic conditions can permanently remove nitrate from stormwater runoff (Wanielista and Chang, 2008; Xuan et al., 2010). It has also been found that nitrogen removal can be enhanced through denitrification under sustained anoxic conditions, in the presence of carbon sources from organic materials and the presence of mature, dense vegetation (Collins et al., 2010).

Many researchers have used different types of sorption media to remove nitrogenous compounds from contaminated water (Lee, 2002; Kim, et al., 2003; Öztürk and Bekta, 2004; Karadag et al., 2006; Wang et al., 2006; Ray et al., 2006; Hossain et al., 2009). Using renewable resources for contaminant removal through adsorption is becoming more cost-effective. Some materials tested for this purpose include sepiolite (Öztürk and Bekta, 2006), bittern (Lee, 2002), clinoptilolite (Karadag et al., 2006; Wang et al., 2006), hardwood mulch (Ray et al., 2006), and sawdust (Kim et al., 2003; Hossain et al., 2009). Sawdust has been used together with other media for contaminant adsorption. For example, Xuan et al. (2010) considered a mixture of 68% fine sand, 25% tire crumbs, and 7% sawdust as adsorption medium, which resulted in a 96% nitrate removal rate. It was also found that sawdust acts as an electron donor if part of the medium becomes anaerobic. Hossain et al. (2009) used a mixture of 50% sand, 20% limestone, 15% sawdust, and 15% tire crumbs in their experiments and concluded that the mixture was efficient and effective for the removal of nitrate and nitrite at lower concentrations. Kim et al. (2003) selected different materials as potential electron donors to treat stormwater. They performed three sets of experiments containing various materials: (i) Set 1 contained alfalfa, newspaper, and leaf mulch compost, (ii) Set 2 contained sawdust, wood chips, and wheat straw, and (iii) Set 3 contained small sulfur-limestone, large sulfur-limestone, and large sulfur only particles. They found that Set 1 removed 100 % of the nitrate; Set 2 achieved 95% nitrate removal and Set 3 removed 91% of the nitrate. Based on these results, they reported that the mixture of newspaper, wood chips, and small sulfur-limestone acts as the best electron donor for nutrient removal.

Despite the various researches mentioned above, there have, as yet, been no studies documented in the literature where sawdust from Radiata pine wood has been used for nutrient removal in stormwater. As this wood is found large volumes in Australia as a waste material, this study investigates the possibility of using it for the removal of nutrients from stormwater. Radiata Pines (*Pinus radiate)* are grown on a large scale in Australia and New Zealand, and in Chile where they are the basis of the pulp and paper industries (Uprichard, 2002). Radiata Pine is also widely used in engineering applications, construction industries and for decorative purposes (Radiata Pine, 2013) and as a result, large volumes of waste wood and sawdust are left over. Moreover, the sawdust from Radiata pine contains cellulose, lignin, and tannins or

other phenolic compounds which are active ion exchange compounds (Shukla et al., 2002). Lignin is a hydrophobic polymer which is generally recognised as the principal wood sorbent (Boving and Neary, 2007).

Therefore, the main purpose of this research is to examine the physicochemical behaviour of sawdust in its removal of $NH_3$-N, $NO_3$-N, and $NO_2$-N through the sorption process.

## 1.2.Objectives and Scope of the Research

To assess the suitability of sawdust as an adsorbent for removing dissolved nitrogenous compounds such as $NH_3$-N, $NO_3$-N, and $NO_2$-N in stormwater, the adsorption characteristic of sawdust must be comprehensively understood. It is well-known that two important physicochemical aspects for the evaluation of a sorption process as a unit operation are the equilibrium of the sorption and sorption kinetics. Sorption equilibrium is described by isotherms which express the surface properties and affinity of the sorbent. Thus to achieve an effective design of sorption systems, an accurate mathematical description of the equilibrium isotherm which is based on a correct sorption mechanism, is essential. The main aim of this research is to investigate the adsorption characteristics of nutrients using sawdust for stormwater treatment. To achieve this aim, several specific objectives were set:

- To investigate the capability of Radiata pine sawdust to remove nutrients from stormwater in batches of varying nutrient concentrations, pH, particle sizes, dosages and contact time.
- To understand the isotherms and kinetics of nutrient adsorption onto sawdust for the removal of dissolved nutrients.
- To investigate the dynamic characteristics of nutrient adsorption in column studies.
- To develop a mass transfer correlation for the nutrient adsorption onto sawdust for stormwater treatment.

## 1.3.Research Significance

Due to the increase in impervious surfaces (such as roads, carparks, and rooftops) in urban and sub-urban areas, a greater fraction of impinging precipitation cannot infiltrate into the soil and therefore becomes runoff, mobilising deposited

pollutants (Hsieh and Davis, 2005). These include several nitrogenous compounds such as ammonia, nitrate, and nitrite which are frequently present in stormwater (Taylor et al. 2005). Increased nutrient inflows can stimulate excessive and unbalanced growth of plants and algae, leading to oxygen depletion and eventual eutrophication of the water body (Bratieres et al 2008). Therefore, it is very important to remove the pollutants before they enter the water stream.

In response to this, such techniques are often referred to as low impact development (LID) systems in the USA, water sensitive urban designs (WSUD) in Australia, and sustainable urban drainage systems (SUDS) in the UK (Bratieres et al 2008). Of the range of WSUD treatment technologies available and as one of urban stormwater's best management practices (BMPs); a component of the LID, biofiltration/bioretention is becoming popular and it is widely used to reduce runoff quantity and improve quality in a natural, aesthetically pleasing manner (Davis et al., 2001; Kim et al., 2003; Hsieh and Davis, 2005; Bratieres et al., 2008; Read et al., 2008; Cho et al., 2009; Trowsdale and Simcock, 2010; Zinger et al., 2013).

Bioretention materials generally consist of a porous medium supporting a vegetative layer, with a surface layer of hardwood mulch. A ponding area serves as a reverse space for runoff storage and provides additional time for water to infiltrate into the media during and after rainfall events. Bioretention media remove pollutants from stormwater through a variety of mechanisms, including sedimentation, filtration, sorption, and precipitation (Hsieh and Davis, 2005).

This combination of a naturally-engineered system is a simple but cost-effective strategy to manage stormwater runoff from small (0.1 ha to 0.8 ha) development areas (Davis et al, 2001). Besides being flexible in terms of size, this system is also flexible in terms of location, configuration, and appearance. For example, a biofilter might be employed in the form of vegetative strips along roadsides, or public open spaces, or it might be incorporated into street-trees within the landscape (Bratieres et al., 2008).

Water quality treatment in stormwater biofilters has generally been found to be effective and reliable. For example, total suspended solid (TSS), heavy metal and commonly, phosphorus removal is very efficient and the removal rates both in laboratory experiments and field tests often exceed 80% - 90% (Davis et al, 2001; Zinger et al 2013). But it has been reported that the removal of nitrogenous compound

was found less than 50%-60% in stormwater biofilters (Kim et al., 2003; Collins et al., 2010; Bratieres et al., 2008; Zinger et al., 2013). While aerobic nitrification occurs in the usually well-drained filter media, anaerobic denitrification is often lacking. This has been identified as the main reason for insufficient N removal or leaching (Kim et al., 2003; Zinger et al., 2013).

If nitrogen removal is of concern, one potential approach is to enhance anaerobic denitrification in the filter media which incorporates a continuously submerged anoxic/saturated zone (SAZ). An additional carbon source is included in the SAZ as an electron donor to facilitate denitrification (Kim et al., 2003; Zinger et al., 2013). However, the cost of activated carbon to remove these nutrients is relatively high; therefore many researchers have tried to find "a green adsorbent", that is not only cheap but also environmental friendly. On the other hand, to control process efficiency, finding the best performing but lowest cost adsorbent is still an objective.

For this reason, Radiata pine wood has been chosen for this study as the sorption medium for removing nutrients. Radiata pine is a tall evergreen conifer which grows up to 50m tall in high quality plantation areas. Radiata pine is abundantly grown in Australia, New Zealand and Chile where it is the basis of pulp and paper industries (Uprichard, 2002). By 2003 there were over 716,500 ha of Radiata pine in Australia (Radiata pine, 2013b). Radiata pine is also widely used in engineering applications, construction industries and for decorative purposes (Radiata pine, 2013a) and large volumes of waste wood and sawdust are left over. This research therefore, is significant in that it will investigate this promising waste material for its properties of nutrient removal and this should prove beneficial for both the environment and wood agriculture. Polluted streams across the world could be cleaned and a new market for this sawdust could be created.

### 1.4. Conceptual Framework of Research

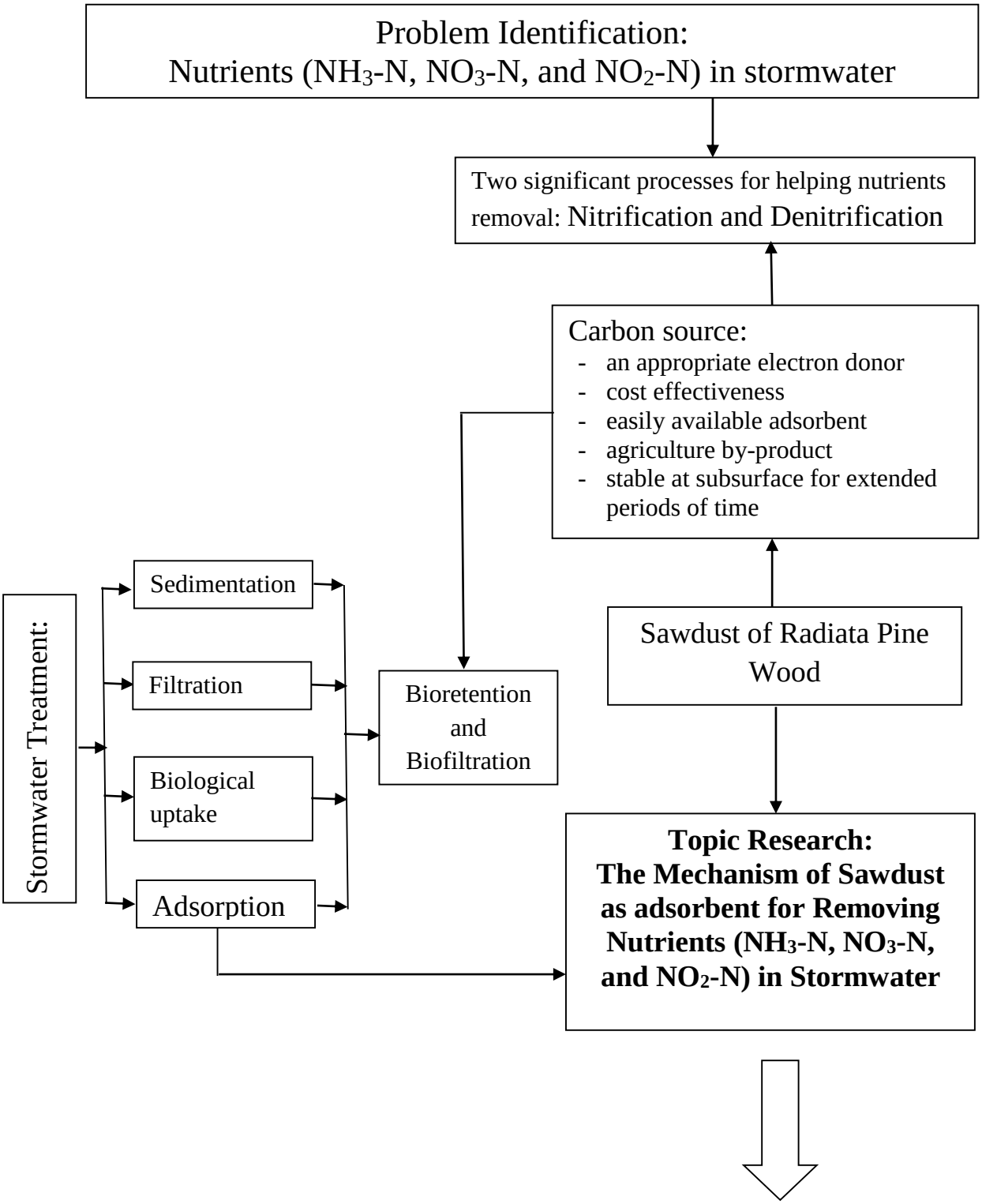

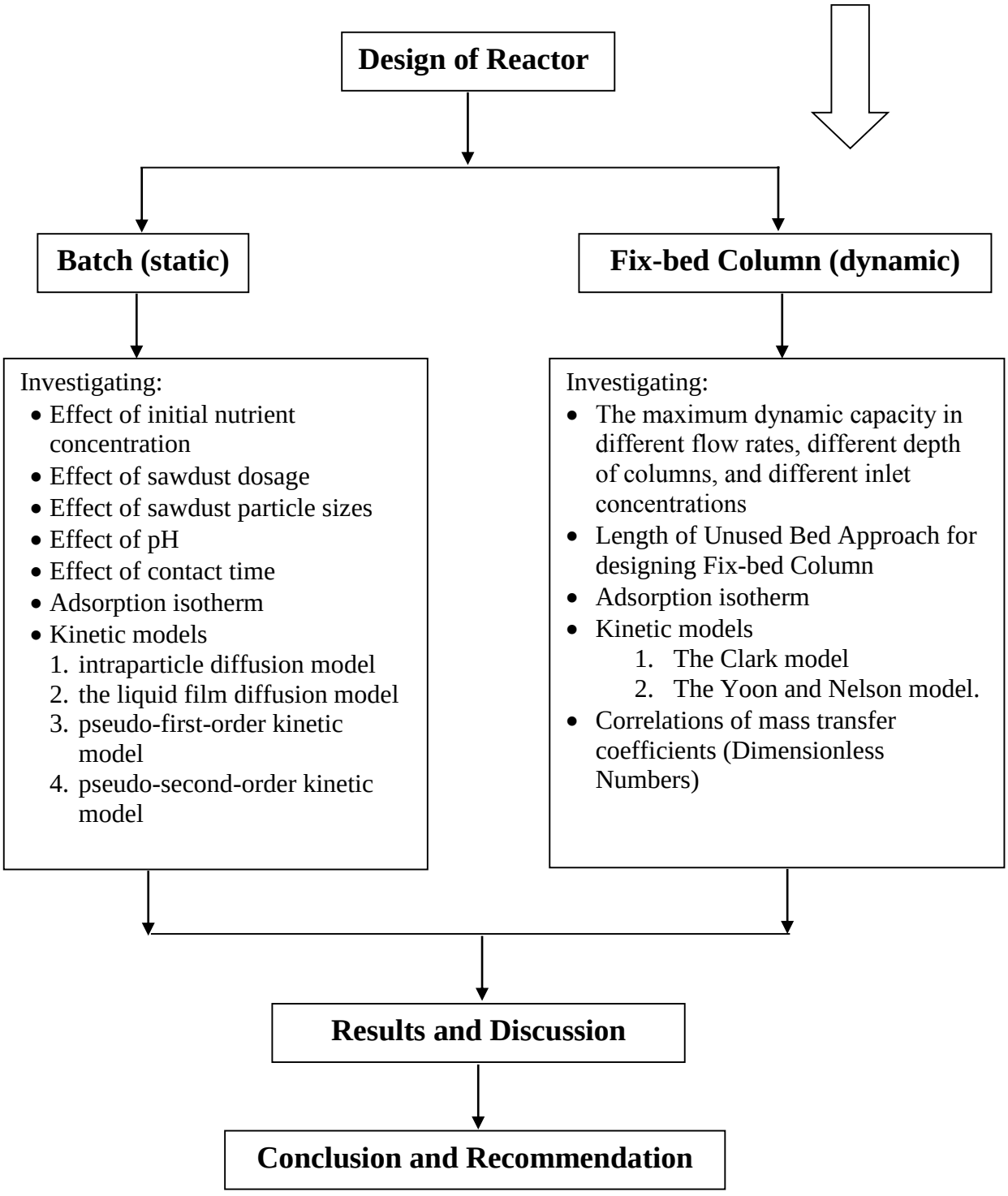
Design of Reactor
Batch (static)
Fix-bed Column (dynamic)
Investigating:
Effect of initial nutrient concentration
Effect of sawdust dosage
Effect of sawdust particle sizes
Effect of pH
Effect of contact time
Adsorption isotherm
Kinetic models
1. intraparticle diffusion model
2. the liquid film diffusion model
3. pseudo-first-order kinetic model
4. pseudo-second-order kinetic model
Investigating:
The maximum dynamic capacity in different flow rates, different depth of columns, and different inlet concentrations
Length of Unused Bed Approach for designing Fix-bed Column
Adsorption isotherm
Kinetic models
1. The Clark model
2. The Yoon and Nelson model.
Correlations of mass transfer coefficients (Dimensionless Numbers)
Results and Discussion
Conclusion and Recommendation

## 1.5. Composition of Thesis

Based on the conceptual framework above, this thesis has been divided into several chapters to provide an overview of the research:

**Chapter 1** begins with the problem identification of nitrogenous compounds ($NH_3$-N, $NO_3$-N, and $NO_2$-N) in stormwater and a short account of how previous researchers have treated these pollutants. Details are given of a valuable approach which enhances anaerobic denitrification in a submerged anoxic/saturated zone (SAZ) in a filter media by supplementation of an additional carbon source as an electron donor. Sawdust as an agricultural by-product has been chosen to solve the pollutant problem by using the adsorption method. Therefore, this chapter also states the objectives and significance of this research.

**Chapter 2** provides a thorough literature review on this topic. Significant information from previous research is presented. This information includes details of how impervious areas cause increases in pollutants, particularly those of nutrients in stormwater and its source. The impact of excess nutrients in stormwater is also described. Best management practices as new technologies for wastewater treatment are also described in this section which contains details of biofiltration/bioretention methods and how these systems work to remove nutrients from stormwater. The chapter also gives an account of the sorption media used for this treatment, and of sawdust as a low-cost alternative adsorbent for the adsorption process. Finally, this chapter explains the modelling of the adsorption process used in this research.

**Chapter 3** provides details of the materials and experiments used in this research. The chapter begins with the preparation of the sawdust and solution then progresses to the set-up the experiments for the batch and column tests. It also provides the physical and chemical properties of the sawdust.

**Chapter 4** presents the data analysis from batch experiments and provides details of the results and the discussion. The chapter examines the effects of several parameters concerned in the batch experiments such as the effect of the initial nutrient concentrations, sawdust dosage, and sawdust particle size, effect of pH and contact time. The adsorption isotherm models of Langmuir and Freundlich, which are based

on solution concentration and sawdust dosage tests are also clarified here. Finally, the kinetic and sorption mechanism models are evaluated using the intraparticle diffusion model, the liquid film diffusion model, a pseudo-first order model, and pseudo-second order model.

**Chapter 5** gives details of the data analysis obtained from column experiments and provides the results and discussion. The effects of several parameters such as flow rate, influent concentration, and bed-depth are examined in this chapter. This chapter also elucidates the appropriate models (Clark and Yoon-Nelson models) for describing the mechanism of nutrient removal in dynamic conditions using sawdust.

**Chapter 6** discusses and presents the analysis of the mass transfer of nutrient adsorption. This includes the determination of different parameters for mass transfer such as axial dispersion, external fluid-phase mass transfer resistance, and the internal solid-phase mass transfer resistance. A liquid-solid mass transfer correlation is developed for nutrient removal and compared with other available similar mass transfer correlations.

**Chapter 7** summarises the achievements of this research and provides recommendations for further work on this theme.

# CHAPTER 2
# LITERATURE REVIEW

## 2.1. Nutrients in Stormwater

### 2.1.1. Stormwater

Generally, normal rainfall on natural ground or undeveloped catchment areas is totally infiltrated or absorbed into the ground. Development in urban areas, along with rural residential, commercial and industrial areas has resulted in an increase in structures that are impervious to water. These include roads, paved areas, parking lots, and roofs of buildings. Rainfall runoff over impervious structures is known as stormwater. Undeveloped catchments can absorb or be infiltrated by up to 90% of precipitation, whereas in a built environment the amount of infiltration can be as little as 10% of precipitation (Dept. of Environment, Government of Western Australia, 2004). With impervious surfaces in urbanised catchment areas, the increase in the total volume of rainfall is relatively high. Pollutants that have built up on surfaces are dislodged and carried to waterways during typical rainfall events. The resultant stormwater often contains many pollutants and this has become a major cause of surface water degradation (Baker, 1992).

Fig. 2.1 illustrates the changes in water cycles as a result of urbanisation, and demonstrates that infiltration is greatly limited in urban, industrial, commercial and residential catchments, and that runoff has greatly increased (Dept. of Environment, Government of Western Australia, 2004).

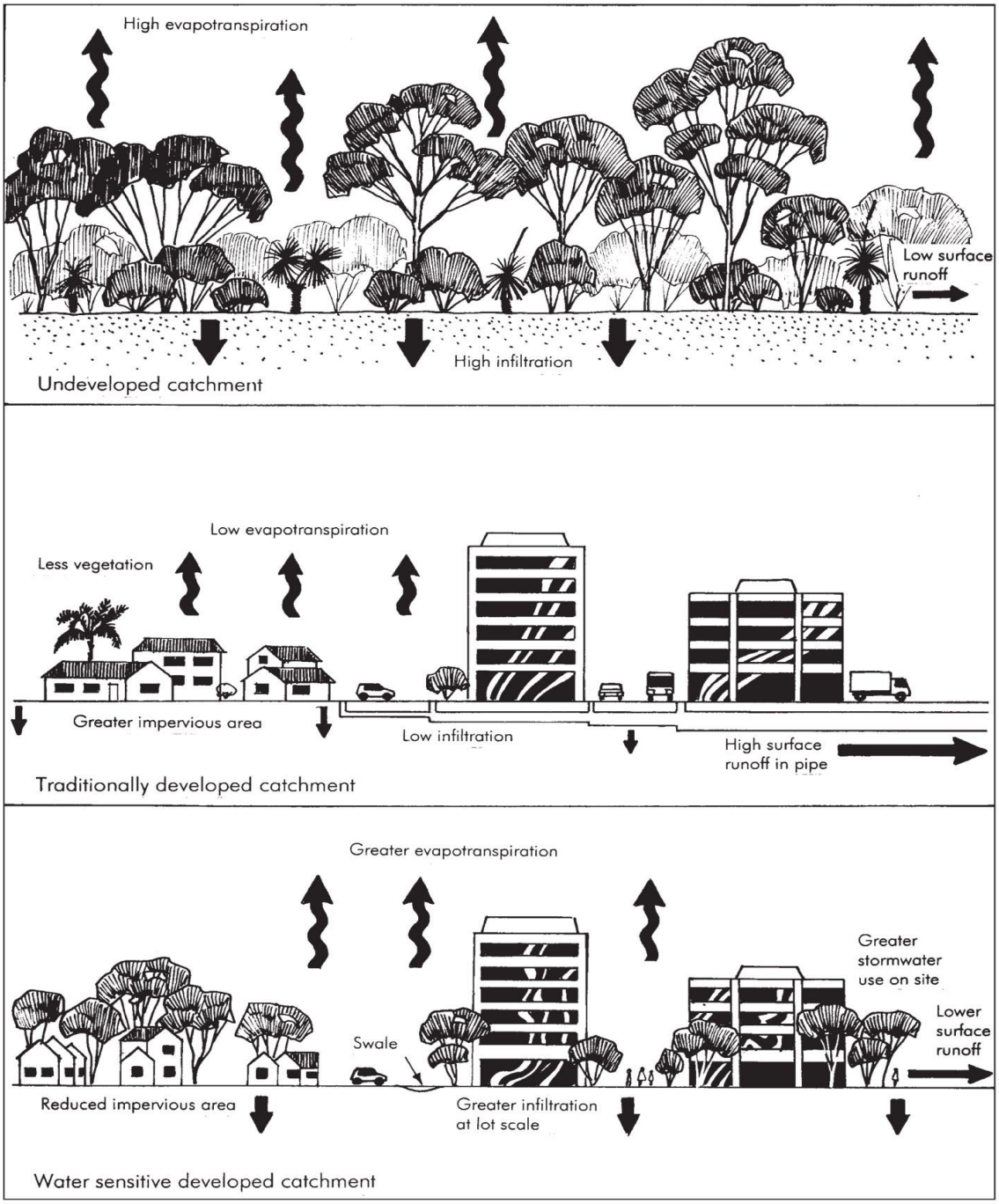


Figure 2.1 Effect of development on the catchment hydrology for low intensity rainfall events (Dept. of Environment, Government of Western Australia, 2004)

### 2.1.2. Pollutants in Stormwater

Major pollutants which are commonly found in urban stormwater runoff include solids, oxygen-demanding substances and dissolved oxygen, nitrogen and phosphorus, pathogens such as faecal coliform, petroleum hydrocarbons including oil and grease, metals e.g. lead, zinc, and copper, synthetic organic compounds. temperature, and pH (U.S.EPA, 1999). Solids, the most common contaminants found in urban stormwater, originate from many sources, they are the result of the erosion of pervious surfaces, or they may come from dust, litter and other particles deposited on impervious surfaces. The oxygen-demanding substances in urban stormwater can be measured by Biochemical Oxygen Demand (BOD), Chemical Oxygen Demand (COD), and Total Organic Carbon (TOC). Maintaining appropriate levels of dissolved oxygen in receiving waters is one of the most important considerations for the protection of fish and aquatic life (U.S.EPA, 1999).

Nitrogen and phosphorus are the principal nutrients of concern in urban stormwater. There are a number of parameters used to measure the various forms of nitrogen and phosphorus found in stormwater runoff. Fig. 2.2 shows the individual constituents of Total Nitrogen (TN), and their named combinations. Particulate nitrogen in urban runoff enters receiving waters predominantly in organic form. However, it cannot be assumed that all organic nitrogen (Org-N) is particulate (Taylor et al., 2005). Dissolved inorganic nitrogen (DIN) includes ammonia ($NH_3$), nitrite ($NO_2^-$), and nitrate ($NO_3^-$). These constituents have the greatest impact on water bodies as they are readily available for uptake by simple organisms (Taylor et al., 2005; U.S.EPA, 1999). Total Kjeldahl nitrogen (TKN) is a measurement of both organic and ammonia nitrogen forms. Total phosphorus (TP) is a measurement of the total amount of phosphorus in both organic and inorganic forms. Ortho-phosphates can be measured in terms of the amount of phosphorus that is readily biologically available. Most of the soluble phosphorus in stormwater is usually present in ortho-phosphate form (U.S.EPA, 1999).

Table 2.1 shows a comparison between the typical pollutant concentrations found in Australian urban catchments and those found globally. It can be noticed that for Australian TP, the concentrations are between 0.12 - 1.6 mg/L and for TN, between

0.6 - 8.6 mg/L. These values are as much as 20 times above the ambient Australian Water Quality Guidelines for the protection of ecosystems in rivers and streams (Australian Water Quality Guidelines for Fresh and Marine Waters, Australia and New Zealand Environment and Conservation Council (ANZECC), 1992), (Wong et al., 2000).

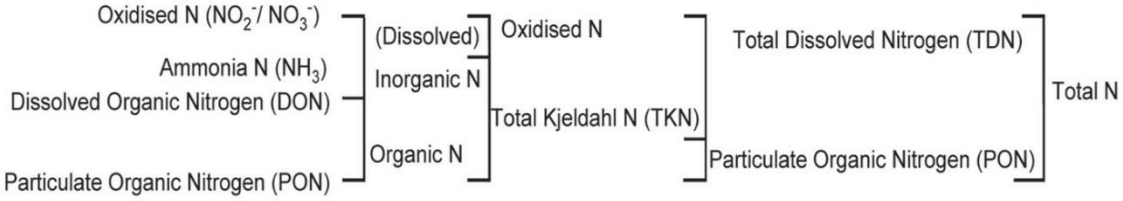


Figure 2.2 Individual constituents of total nitrogen, and their named combinations (Taylor, 2005)

Table 2.1 Comparison between the quality of Australian urban runoff and global runoff (mg/L). (Adapted from Wong et al., 2000)

| **Pollutant** | **Australian range of pollutant concentration (mg/L)** | **Global range of pollutant concentration (mg/L)** | **Australian standards (mg/L)** |
|---|---|---|---|
| TSS | 20-1,000 | 50-800 | <10% change |
| Cd | 0.01-0.09 | 0.001-0.01 | 0.0002-0.002 |
| Cr | 0.006-0.025 | 0.004-0.06 | 0.01 |
| Cu | 0.027-0.094 | 0.01-0.15 | 0.002-0.005 |
| Pb | 0.19-0.53 | 0.05-0.45 | 0.001-0.005 |
| Ni | 0.014-0.025 | - | 0.015-0.15 |
| Zn | 0.27-1.10 | 0.1 | 0.005-0.05 |
| Faecal Coliform | 4,000-200,000 | 1,000-100,000 | 150cfu/100ml (PR)* 1000cfu/100ml (SR)* |
| TP | 0.12-1.6 | 0.1-3 | <0.01-0.1 |
| TN | 0.6-8.6 | 2-6 | <0.1-0.75 |
| $NH_4$-N | 0.01-9.8 | 0.1-2.5 | <0.02-0.03 |
| $NO_x$-N | 0.07-2.8 | 0.4-5 | - |
| Temp ($^0$C) | 1-5 | - | <2$^0$C increase |

### 2.1.3. Source and Impact of Excess Nutrients in Stormwater

The nutrients and pollutants transported by stormwater are the result of a number of processes including: the weathering of bedrock, the erosion of soils containing adsorbed nutrients and the release of sediments as a result of decomposition of organic material. Other causes of the unwanted content in stormwater include fertiliser washoff, sewer overflows/septic tank leaks, animal/bird faeces emissions and washoff, detergent from car washing, spillage/illegal discharge, atmospheric deposition, algae and plant decomposition, and leaching of excessive nutrients from agricultural and horticultural landuses (Dept. of Environment, Government of Western Australia, 2004).

As pollutants, nutrients impact heavily upon the health of receiving water bodies. Excessive nutrients in the stormwater that enters lakes, results in nutrient enrichment (eutrophication), reduced water quality and the increased presence of undesirable blue-green algae. Eutrophication caused by nutrients in stormwater often impairs municipal drinking water supplies. The high nitrate content in drinking water often causes methemoglobinemia in infants**.** Methemoglobinemia is a result of the interaction of nitrite with hemoglobin, the nitrite being formed from nitrate reduction in the digestive system (Sawyer et al., 2003). Due to the dangers of the nitrite, the U.S. EPA has set a maximum contaminant level requiring that nitrate-nitrogen concentration does not exceed 10 mg/L and that nitrite-nitrogen concentration not exceed 1 mg/L in public water supplies (U.S.EPA, 2003). Nutrients can also stimulate the growth of undesirable rooted aquatic plants in streams. In some states, limitations on ammonia-nitrogen have been imposed due to their suspected toxic effect upon fish life. Free ammonia in concentrations above about 0.2 mg/L can cause fatalities in several species of fish (Sawyer et al., 2003).

## 2.2. Technologies Used for Stormwater Treatment

### 2.2.1. Best Management Practices (BMPs)

It is only recently that awareness of the damaging effects stormwater runoff has come about. Traditionally, stormwater management was a flood-control issue, rather than a quality control program. The principles in stormwater control are to use best management practices (BMPs) to manage rainwater at its source, instead of discharging it into conventional, combined or separated sewer systems. A stormwater BMP is a technique, measure or structural control that is used for a given set of conditions to manage the quantity and improve the quality of stormwater runoff in the most cost-effective manner. BMPs can be implemented to address three main factors: flow control, pollutant removal, and pollutant source reduction (U.S.EPA, 1999).

BMPs can be classified into two groups: structural and non-structural BMPs. Structural BMPs include engineered and built systems designed to manage water quantity and/or quality control; these are based on either rainwater retention or infiltration into the soil. Non-structural BMPs include a range of practices such as pollution prevention, education, management and development, all of which are designed to limit the conversion of rainfall into runoff (Martin et al., 2007).

Structural BMPs can be grouped into several general systems according to the U.S.EPA (1999):

- Infiltration systems. These capture a volume of runoff and filtrate it into the ground. These include infiltration basins and porous pavement, infiltration trenches and wells.
- Detention systems capture a volume of runoff and temporarily retain that volume for subsequent release. Detention systems are designed to completely empty out between runoff events; they mainly provide water quantity control in terms of detention basins and underground vaults, pipe and tanks.
- Retention systems capture a volume of runoff and retain that volume until it is displaced in part or in total by the next runoff event. Retention systems therefore maintain a significant permanent pool volume of water between runoff events. Retention systems can provide both quantity and quality control in terms of retention ponds or wet ponds, retention tanks, tunnels, vaults, and pipes.

- Constructed wetland systems are similar to retention and detention systems, except that a major portion of the BMP water surface area (in pond systems) or the bottom (in meadow-type systems) contains wetland vegetation.
- Filtration systems use a granular filtration media with either a membrane or a combination of materials such as sand, soil, organic material and carbon to remove constituents found in runoff. This system includes media filter and biofiltration/bioretention systems.
- Vegetated systems such as grass filter strips and vegetated swales are designed to convey and treat stormwater flows.
- Minimising directly connected impervious surfaces
- Miscellaneous and vendor-supplied systems such as oil/water separators and hydrodynamic devices.

### 2.2.2. Pollutant Removal Process in Stormwater

BMP pollutant removal in stormwater can be accomplished through a number of physical and biochemical processes. In the hierarchy of stormwater treatment, there are three stages of treatment similar to sewage treatment (NSW EPA, 1997). The first stage is physical screening and rapid sedimentation and this removes the inflow litter and coarse sediment. The second stage is sedimentation and filtration which removes suspended solids, nutrients and metals. The third stage of the process includes sedimentation, filtration and biological uptake and adsorption to remove the nutrients and heavy metals (NSW EPA, 1997).

Sedimentation is the removal of suspended particulates from the water column by gravitational settling. Sedimentation is an effective mechanism for BMP pollutant removal in ponds and constructed wetlands. Filtration is the removal of particulates from water by passing the water through a porous media. Materials commonly used in stormwater BMPs include soil, sand, gravel, peat, compost, and various combinations such as peat/sand and sand/gravel. The biological uptake of nutrients is an important mechanism for nutrient control in stormwater BMPs. Ponds and wetlands can be useful for removing these nutrients through biological uptake. Adsorption can occur in infiltration systems where the underlying soils contain appreciable amounts of clay (U.S.EPA, 1999).

### 2.2.3. Biofiltration/Bioretention Systems

Most researchers in recent times have applied biofiltration and bioretention to remove pollutants in stormwater (Hsieh and Davis, 2005; Hatt et al., 2007; Trowsdale and Simcock, 2011). A biofiltration system is one example of a source control method that can be integrated into the streetscape design to treat road and roof runoff, prior to discharging to receiving waters. Biofiltration systems combine detention, infiltration and collection systems, and generally integrate a vegetated swale and infiltration trench as part of their design (Lloyd et al., 2001).

A combination natural-engineered system known as biological retention (bioretention) has recently been suggested as a simple but effective strategy to manage stormwater runoff from small (0.1 to 0.8 ha [0.25 to 2 ac]) development areas (Davis et al., 2001). A schematic diagram of a typical biofilter (bioretention) system is shown in Figure 2.3. Bioretention systems are designed to mimic the functions of the natural forest ecosystem for treating stormwater runoff. A bioretention system generally consists of a porous medium supporting a vegetative layer, with a surface layer of hardwood mulch. A ponding area serves as reserve space for runoff storage and provides further time for water to infiltrate the medium during and after rainfall events. Pollutants can be removed by bioretention media from stormwater through a variety of mechanisms including sedimentation, filtration, adsorption, volatilisation, ion exchange, and decomposition (U.S.EPA, 1999; Hsieh and Davis, 2005).

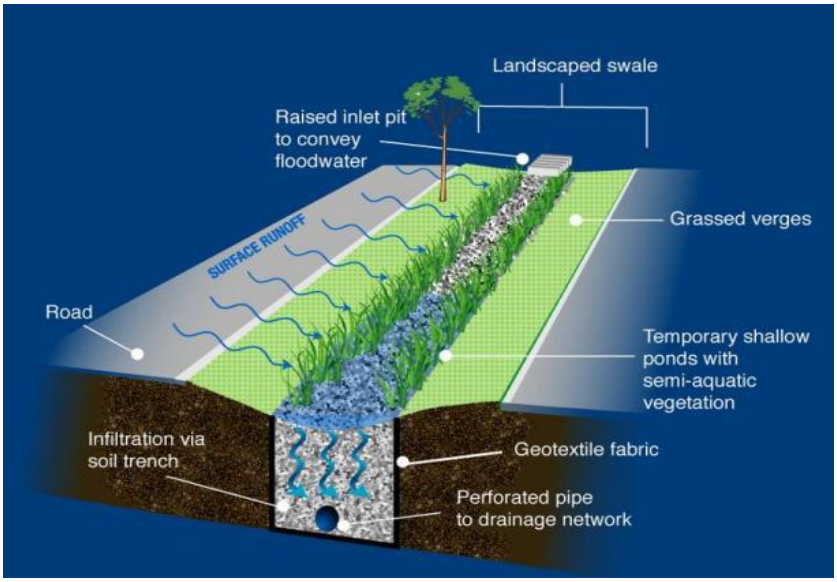


Figure 2.3 Schematic of typical biofilter/bioretention system (Facility for Advancing Water Biofiltration, 2008)

Two main configurations for biofilter systems are recommended by the Facility for Advancing Water Biofiltration (FAWB), depending on the objectives of the system (e.g. targeting pollutants, site opportunities and constraints, etc). They are the standard biofilter design (Figure 2.4) and the biofilter with a submerged zone (Figure 2.5.) (FAWB, 2008).

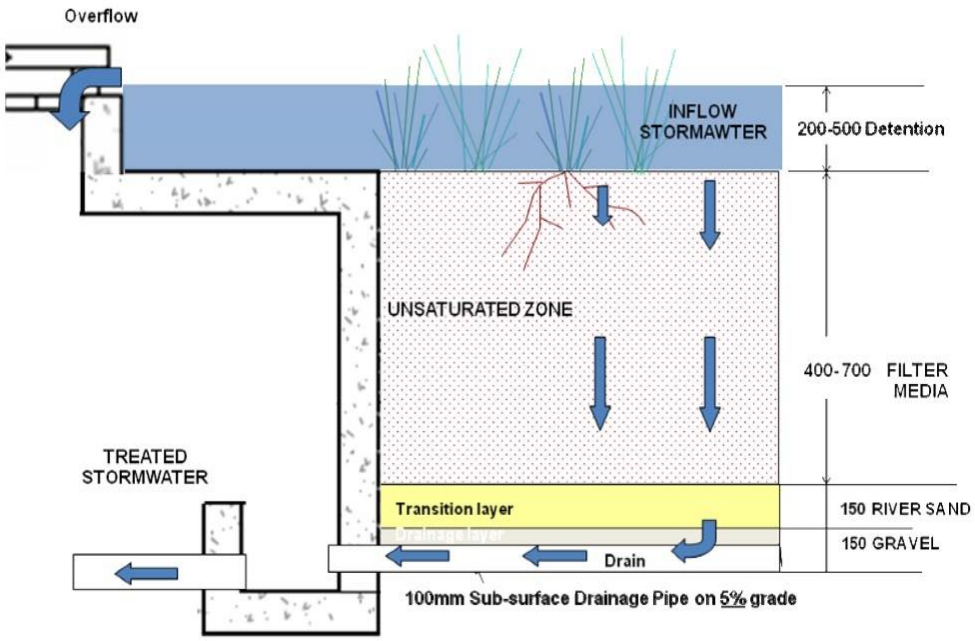


Figure 2.4 Conceptual outline of the design of a standard bioretention system (FAWB, 2008)

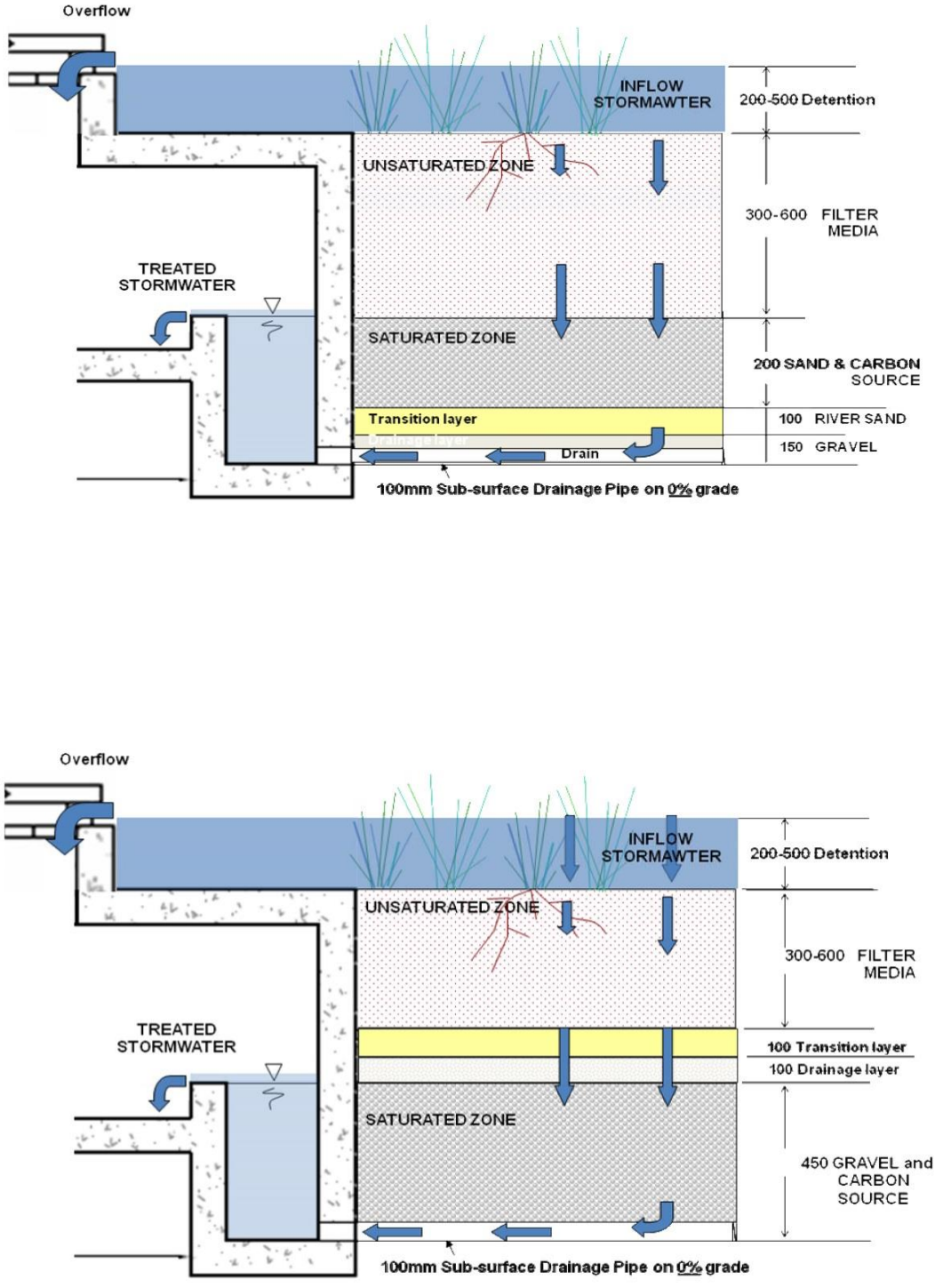


Figure 2.5 Conceptual outline of the design of a bioretention system with a submerged zone (FAWB, 2008)

## 2.3. Nutrient Removal Processes in Bioretention/Biofiltration systems

### 2.3.1. Nitrogen-cycle in Stormwater systems

Stormwater treatment systems must be designed to suit the processes that will take place within the system itself. Nitrogen, for example, can go through many transformations with varying degrees of complexity. Nitrification and denitrification are the two significant processes that assist in the removal of nutrients from stormwater runoff. Nitrification oxidizes ammonia and denitrification reduces nitrate into nitrogen gas before being released into the air. Only the denitrification process under anaerobic conditions can permanently remove nitrate from stormwater runoff (Xuan et al., 2010). In order to understand the nitrogen transformations, it can be grouped into a system called "nitrogen cycle". The nitrogen cycle presented in Fig. 2.6. is appropriate for understanding nutrient removal process in stormwater system.

Nitrogen enters the stormwater system in the form of ammonium-nitrogen ($NH_4^+$), nitrate-nitrogen ($NO_3^-$), and nitrite-nitrogen ($NO_2^-$), dissolved organic N, and particulate organic N. In an aerobic environment, $NH_4^+$ can be nitrified to $NO_3^-$ in a two step microbial process. Organic N can also undergo ammonification to $NH_4^+$ and nitrification to $NO_3^-$. These microbial processes transform N but do not remove it (Collins et al., 2010).

Three main processes must take place before N removal can occur: assimilation (also referred to as N uptake), adsorption, and denitrification. Nitrogen assimilation is the process by which inorganic N ($NH_4^+$, $NO_3^-$, and $NO_2^-$) is transformed into microbial or plant biomass and temporarily stored as organic N. Due to its greatly reduced N state, $NH_4^+$ is most commonly assimilated by microorganisms, although $NO_3^-$ is sometimes used. $NH_4^+$ can also be removed through adsorption onto negatively charged soil particles. The uptake of N via assimilation by plants and microbes, or by adsorption, results in the temporary removal of N, whereas microbal denitrification results in the permanent removal of nitrate in gaseous form from the system. Inorganic N can be permanently removed from the system via volatilisation of ammonium ($NH_4^+$) to ammonia gas ($NH_3$) (Collins et al., 2010).

Under anaerobic conditions, nitrate and nitrite are both reduced by denitrification (Sawyer et al., 2003). Denitrification is a dissimulator microbial process that transforms $NO_3^-$ to $N_2O$ or $N_2$ gas which is released to the atmosphere. Denitrification can involve the following reaction sequence, in which $NO_3^-$ is used as a terminal electron acceptor: $NO_3^- \rightarrow NO_2^- \rightarrow NO \rightarrow N_2O \rightarrow N_2$. Denitrification can be driven by carbon, iron, or sulfur as the electron donor. It is thought that carbon-driven denitrification is a common occurrence in stormwater systems (Collins et al., 2010).

There are also some biological nutrient-reduction processes embedded in the system, such as the anaerobic ammonia oxidation (Annamox) process. The biological nutrient-reduction is a biological heterotropic process and the anaerobic ammonia oxidation is a biological autotropic process in which ammonia is converted to nitrogen gas in the presence of nitrite under anoxic conditions using special microbes. In annamox, nitrite acts as an electron acceptor and no external carbon source is needed for denitrification as the bacteria are autotrophs (Chang et al., 2010).

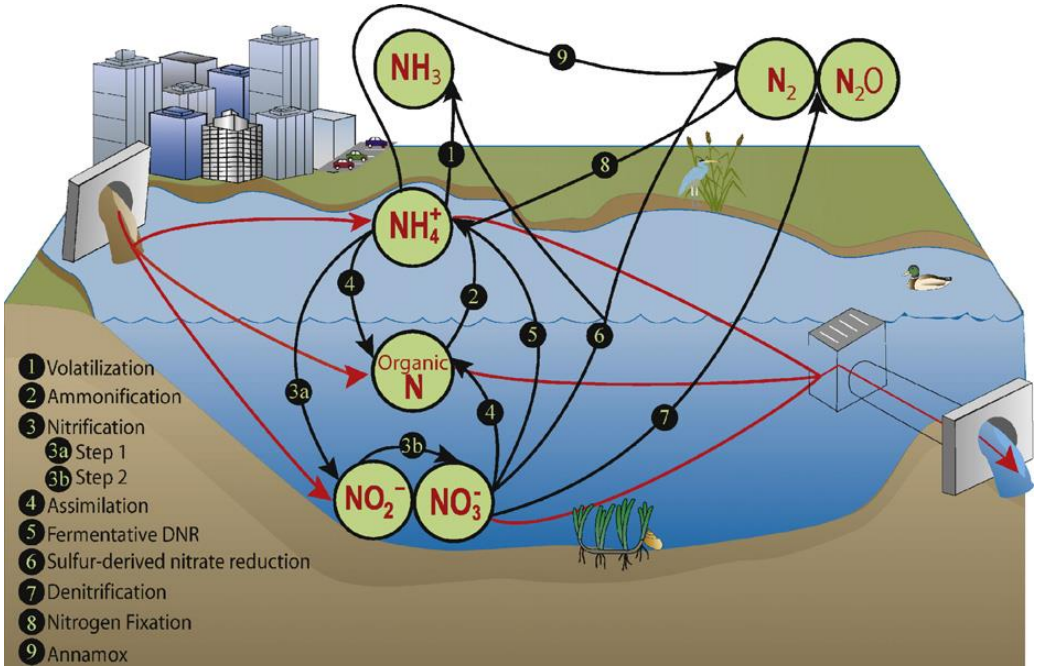


Figure 2.6 Stormwater system N cycle (Collins et al., 2010)

### 2.3.2. Nutrient Removal Processes in Saturated Zone (SAZ) in Biofiltration/Bioretention Systems

With regard to nitrogen removal in biofiltration/bioretention systems, the higher surface area of clay in natural soil may be able to provide more contact area for the solid to adsorb and more space for bacterial colonies to develop. Most filter media may improve solid-liquid contact with a higher surface area, prevent channeling with a better particle distribution, and provide a better ion exchange capacity to support absorption/adsorption, a better retaining capability for adsorbed nutrient, and more surface area for the bacterial colony to develop. Thus filter media can support both physical and biological processes simultaneously (Chang et al., 2010).

The introduction of a saturated zone (SAZ) to enhance anaerobic denitrification in the filter media, combined with a carbon source (acting as an electron donor to facilitate denitrification) has been suggested and successfully tested (Kim et al., 2003; Zinger et al., 2013). However, since the SAZ has been developed relatively recently, its design and function is not yet included in many design guidelines such as the U.S. EPA, 2004 and Melbourne Water, 2005 (Zinger et al., 2013). Hence, the vast majority of existing stormwater biofilters lack SAZs, and thus they may have relatively poor nitrogen removal capability (Zinger et al., 2013).

Where nitrogen removal is of concern, one strategy to overcome the environmental threat is to retrofit SAZs to existing biofilter systems, simply by elevating the outlet, thus maintaining a permanent water level in the base of the biofilter (Zinger et al., 2013). However, if a biofilter is initially designed with SAZs, an additional carbon source is usually included in the SAZ as an electron donor to facilitate denitrification (Kim et al., 2003; Zinger et al., 2007; Xuan et al., 2010; Zinger et al., 2013).

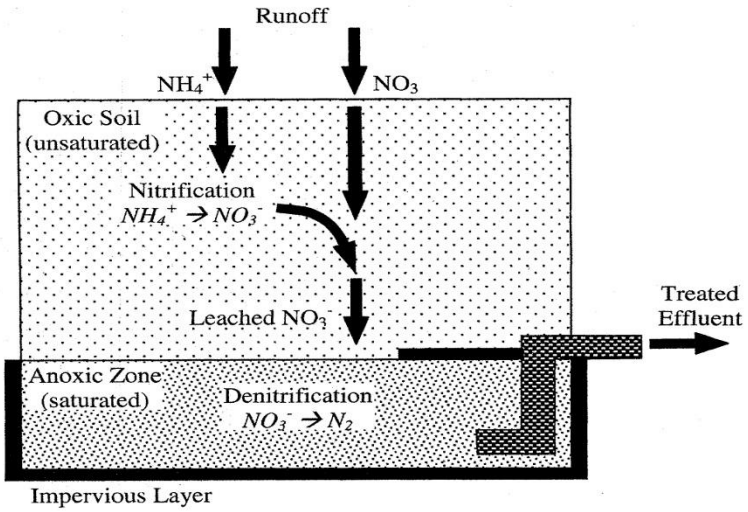


Figure 2.7 Diagram of modified bioretention cell with anoxic zone for denitrification (Kim et al., 2003)

Figure 2.7 shows a range of interacting processes determining N behaviour in an engineered bioretention cell with a SAZ. Ammonification converts organic N (from stormwater and dead organic matter) to $NH_4$. Together with the ammonium entering the filter with the stormwater, it is effectively converted to $NO_x$ by aerobic nitrification processes or sorbed by (negatively charged) soil particles and soil organic matter. $NH_4$ removal in biofilters is usually very effective since oxic conditions are present in the filter material between storm events, and likely to exist at all times in the upper layers of the filter. However, these oxic conditions inhibit anaerobic denitrification and thus $NO_x$ removal. In contrast to $NH_4$, negatively charged $NO_x$ is very mobile and thus poorly adsorbed by the filter media. Hence, $NO_x$ can be readily washed out at the next storm event leading to poor net N removal or even N leaching (Zinger et al., 2013).

Providing anoxic conditions in the biofilter material, together with a carbon source (cellulose based electron donor) will facilitate denitrification and as a result, effective N removal. Thus, biofilters with a SAZ and embedded carbon source have been successfully demonstrated to significantly enhance N removal (Kim et al., 2003; Zinger et al., 2013).

## 2.4. Previous Research into Sorption Media for Stormwater Treatment

Initially, biofiltration and bioretention systems for stormwater treatment generally used gravel or sand as a filter (Hsieh and Davis, 2005; Hatt et al., 2007; Cho et al., 2009). Some research was conducted into the performance of sand and gravel infiltration for stormwater (Hsieh and Davis 2005; Hatt et al., 2007), whilst Hatt et al., (2007) simulated the behaviour of sand and gravel columns over long-term period. The gravel (length 90 cm) was placed above a 70 cm layer of very fine sand and semi-synthetic stormwater was then introduced to the filter medium. Water quality parameters measured were Total Suspended Solid (TSS), Total Nitrogen (TN), Total Phosphorus (TP), Filterable Reactive Phosphorus (FRP), ammonium ($NH_4^+$), nitrate/nitrite (NOx), Dissolved Organic Nitrogen (DON), and heavy metals (Cu, Pb, and Zn). The research concluded that gravel filters are an effective treatment option for stormwater runoff, where treatment of sediment and heavy metals are of major concern. However, when nutrients are the major pollutants, infiltration systems may not be an appropriate treatment option (Hatt at al., 2007).

Table 2.2 shows previous studies that used sorption media for stormwater treatment. Hsieh and Davis (2005) studied the characteristics of the filter medium that controls the bioretention process. They evaluated eighteen bioretention columns with different porous media mixtures. Two types of sand and three types of soil with various physical and chemical properties were used in the laboratory studies. Six onsite experiments were conducted on six existing bioretention facilities to evaluate their performance with respect to pollutant removal. A synthetic runoff solution was used in these experiments. Extremely efficient TSS removal was noted in most of the native-media bioretention columns (96%). The results showed significant removal for oil/grease (96%) and total lead (66% - 98%). Due to special flow patterns, the removal efficiency of total phosphorus ranged widely (4% - 99%). However, for nitrate and ammonium, the removal percentages were 1% - 43% and 2% - 49% respectively. Similar results were found for onsite experiments. The researchers recommended two different designs for the bioretention media depending on the bulk filtration layer. The first design contained only the filtration layer and the second contained separate vegetation layers and filtration layers. Long-term evaluation of the designs has yet to be undertaken (Hsieh and Davis 2005).

In another study, Waldrop et al. (2009) investigated coal combustion products (CCPs) in an efficient filtration system. Three different coal ashes were used in the study: (i) Hopewell - coarser textured and black material (ii) Medium Carbon - fine textured and gray material), and (iii) High Carbon-fine textured and dark black material. The results indicated that the High Carbon and Medium Carbon ashes were very effective at removing $NH_4$-N (almost 100%), with Hopewell removing approximately 90%. All ashes showed a removal efficiency of 75% - 85 % for ortho-P. Despite this, all three ashes had a low adsorption capacity for $NO_3$-N. The Hopewell was eventually suggested as the most suitable ash for use as filtration/sorbent material (Waldrop et al. 2009).

Zinger et al. (2007) explored nitrogen transformation in a biofilter and optimised its design to maximise N removal. They constructed 20 columns to test a range of submerged anoxic zone (SAZ) depths to maximise denitrification and test the effects of adding a carbon source as an electron donor supplement in the filter media. The most effective combination of carbon and SAZ was achieved by placement of SAZ levels at 450 mm, removing approximately 99% of nitrate, whilst a non-carbon column showed an average 50% nitrate removal. The use of a carbon/electron donor was found to be the critical limiting factor for denitrification (Zinger et al., 2007).

Furthermore, Saliling et al. (2007) compared wood chips and wheat straw with an expensive Kaldnes plastic media to treat high nitrate content waters. Upflow bioreactors were loaded at a constant flow rate with three different influent concentrations of $NO_3$-N. The experiments showed that both wood chips and wheat straw produced comparable denitrification rates to the Kaldnes plastic media. Almost 99% of nitrate was removed from wastewater of 200 mg $NO_3$-N/L influent concentration (Saliling et al., 2007).

Recently, Xuan et al. (2010) developed a new mix material to remove nutrients from stormwater which included ammonia-N, nitrate-N, nitrite-N, and ortho-phosphorus. They designed a laboratory-scale microcosm model. A rectangular plastic container was used consisting of a treatment and a collection zone. The bottom of the treatment zone was filled with a porous mix of 68% fine sand, 25% tyre fragments, and 7% sawdust while the remaining space in the container was packed with Astatula sand. This model was able to remove 58% of nitrate-N and 89% of orthophosphorus respectively (Xuan et al. 2010). Similar experiments were conducted by Kim et al.

(2003) where newspaper was selected as a solid-phase electron donor substrate for denitrification of a variety of materials. These materials were alfalfa, newspaper, leaf-mulch compost, sawdust, wood chips, wheat straw, small sulfur-limestone, large sulfur-limestone and large sulfur-only particles. Nitrate and nitrite mass were removed by up to 80% in the pilot-scale bioretention study by Kim et al. (2003).

Greenway and Lucas (2010), investigated the performance efficiency of six different media types and eight different plant species for enhanced phosphorus and nitrogen adsorption in stormwater. Total phosphorus removal reached 99% in sand media, followed by loam at 92%, sand with red mud at 89% and the lowest, sand-gravel at 44%. While total nitrogen removal for all sandy media types only reached around 50%, loam removal measured 79% (Greenway and Lucas 2010).

Table 2.2 Methods and mediums used for stormwater treatment

| Media | Method | Measure | Reference |
|---|---|---|---|
| Mixed newspaper and dried sand, loamy sand | Pilot-scale bioretention | Nitrate and nitrite (removal >80%) | Kim et al., 2003 |
| Mulch, sand, silt, and clay | Bioretention: Column experiments | Oil/grease (removal >96%), Total lead (removal from 66% to >98%), total phosphorus (removal 4%–99%), nitrate (removal 1% to 43%), ammonium (removal 2% to 49%) | Hsieh and Davis, 2005 |
| Gravel and sand | Column infiltration | TSS, TN, TP, filterable reactive phosphorus (FRP), ammonium ($NH_4^+$), nitrate/nitrite (NOx), dissolved organic nitrogen (DON), and heavy metals (Cu, Pb, and Zn). | Hatt et al., 2007 |
| Column consists of 4 main layers:<br>-sandy loam, at the top planted with tall sedge; *carex appressa*<br>-fine sand mixed with wood chips<br>-river sand<br>-small gravel | biofilter | 99% nitrate removed | Zinger et al., 2007 |

| | | | |
|---|---|---|---|
| - Hard wood chips<br>- Wheat straw | biofilter | Nitrate-nitrogen (99% removed) | Saliling et al., 2007 |
| Coal Combustion Products (CCPs) | Batch and Column filtration | Oxalate (TOC), $NH_4$-N, $NO_3$-N, P | Waldrop et al., 2009 |
| Mixed media of 68% fine sand, 25% tyre fragments, and 7% sawdust | A laboratory-scale microcosm model | Ammonia-N, nitrate-N (removed 58%), nitrite-N, and orthophosphorus-phosphorus (removed 89%) | Xuan et al., 2010 |
| - loam<br>- sand<br>- sand with red mud<br>- sand gravel | bioretention | Total Nitrogen<br>(79% removed by loam)<br>(50% removed by all sandy media types) | Greenway and Lucas, 2010 |
| Compost | As sediment retention | Total Solid and petroleum hydrocarbon (95% reduction),<br>total P, and nitrate-N. | Faucette et al., 2012 |

## 2.5. Sawdust as a Low-cost Alternative Adsorbent for Adsorption Process

The adsorption technique is one of the preferred and proven methods for efficient and cost effective removal of toxic contaminants from water (Acar and Eren, 2006; Gupta and Babu, 2009; Bhatnagar and Sillanpaa, 2010). A number of materials have been extensively investigated as adsorbents in water pollution control. Some of the more significant ones include silica gel, activated alumina, zeolites and activated carbon.

The most popular and widely used adsorbent in water treatment around the world is activated carbon. Activated carbon is produced by a process consisting of raw material dehydration and carbonisation followed by activation (Bhatnagar and Sillanpaa, 2010). It has been recognised that many types of pollutants are removed by activated carbon such as metal ions (Memon et al., 2007; Zaini et al., 2009; Prado et al., 2010; Albarelli et al., 2011; Bozic et al., 2013; Chong et al., 2013), anions (Lach et al., 2007; Lemus et al., 2012), dyes (Noonpui et al., 2010; Amel et al., 2012; Ahmad et al., 2012; Politi and Sidiras, 2012; Ates and Un, 2013), phenols (Achak et al., 2009; Larous and Meniai, 2012; Lorenc-Grabowska et al., 2012; Zhong et al. 2012), detergents (Me´ndez-Dı´az, 2009), pesticides (Ignatowicz, 2009; Foo and Hameed, 2010; Ignatowicz, 2011; Jusoh et al., 2011), humic substances (Daifullah, 2004;

Khraisheh, 2010), chlorinated hydrocarbons (Pelech et al., 2006; Klasson et al., 2009; Petrova et al., 2012) and many other chemicals (Bhatnagar and Sillanpaa, 2010). However, activated carbon is expensive, scarce in terms of availability and contributes to the high costs of regeneration processes from chemical and thermal procedures (Bhatnagar and Sillanpaa, 2010; Wahab et al., 2010).

Efforts have been made to develop inexpensive adsorbents, utilising numerous agro-industrial and municipal waste materials. Use of waste materials as low-cost adsorbents is attractive due to their contribution in reducing costs for waste disposal, and the resultant contribution to environmental protection. Some of the waste material that has been applied as a low-cost adsorbent includes agricultural waste such as rice and wheat waste (Daifullah et al., 2004; Han et al., 2010; Wang et al., 2011), tea and coffee waste (Mondal, 2009; Reffas, 2010; Madrakian et al., 2012), coconut waste (Bhatnagar et al., 2010; Ashish et al., 2012), peanut or groundnut waste (Shukla and Pai, 2005; Ozer et al., 2007; Runping et al., 2008), peel from different agricultural waste (orange peel (Chen and Chen, 2009; Khaled et al., 2009; Lugo-Lugo et al., 2009; Liang et al., 2010) and banana peel (Achak et al., 2009; Albarelli et al., 2011; Amel et al., 2012), shells of different agricultural waste and seeds (Ashish et al., 2012; Chong et al., 2013), seed coat (Hameed and Daud, 2008; Petrova et al., 2010), and stems and stalks of different agricultural products (Escudero et al., 2008; El-Hendawy et al., 2008; Chen et al., 2011). Industrial and municipal waste also can be a low-cost adsorbent such as fly ash (Lu et al., 2009), steel industry wastes (blast furnace slag (Korkusuz et al., 2007; Nehrenheim and Gustafsson, 2008), sludge and dust (Kayranli, 2011)), aluminium industry waste (red mud) (Chang-jun et al., 2007), fertilizer industry waste (Gupta et al., 2010), leather industry waste (Kantarli and Yanik, 2010; Oliveira et al., 2011), industrial sludge and waste (Bhatnagar and Sillanpaa, 2010).

Among the economical adsorbents explored by researchers, sawdust is a potential adsorbent and agricultural byproduct. Several studies have suggested that its main biosorption mechanism involves ion exchanges and hydrogen bonding due to the main constituents of sawdust being polymeric materials such as cellulose, lignin, and tannins or other phenolic compounds that are exchangers (Shukla et al., 2002; Wahab et al., 2010). Lignin is a hydrophobic polymer which is generally recognised as the principal wood sorbent (Boving and Neary, 2007).

A wood-based filter medium such as sawdust is considered as a waste material and it is usually found in large quantities. Sawdust may be sourced from many different types of wood. Varieties of wood that have been investigated are meranti wood, a common tree present all in tropical countries such as Malaysia and Indonesia (Ahmad et al., 2009), poplar wood (Samsun Clone) which is solely grown in Samsun, Turkey (Acar and Eren, 2006), eucalyptus globules from a sawmill in Beja, North West of Tunisia (Wahab et al., 2010), and yellow brownish wood from Pilani India (Gupta and Babu, 2009). Details of varieties of wood used as sawdust for adsorption both in batches and in continuous fixed-bed experiments can be seen in Table 2.3.

Some researchers have used treated sawdust as an adsorbent. Treated or modified sawdust means that the sawdust has been treated or mixed with some other chemicals or materials before use. However, untreated sawdust does not automatically mean that the sawdust is used directly without any cleaning, size reduction or mechanical preparation. They claim that through modification techniques, the adsorption capacities of, and the feasible nutrient removal rates by sawdust can be significantly boosted. Moreover, the removal mechanism also changes when the adsorbates are immobilised at the surface of activated carbon. The contamination is not only removed by adsorption on the surface of the untreated carbon but it also could be removed by a surface attraction chemical bonding phenomenon on the newly added chemicals (Sukla et al., 2002; Acar and Eren, 2006).

It has been shown that treated sawdust can be significantly effective in the removal of some pollutants from aqueous solutions, for example sawdust from a poplar tree was used in the adsorption of Cu (II). The sawdust was treated with 1 N $H_2$ $SO_4$ in the ratio of 1:2 (sawdust/$H_2SO_4$; w/v) at 150°C for 24 h. The adsorption capacity increased to13.495 mg/g, while untreated poplar sawdust obtained 5.432 mg/g (Acar and Eren, 2006). Untreated sawdust from a beech tree was compared with sawdust treated with salts for removing methylene blue (Basic dye). The adsorption capacity of the salt treated sawdust increased up to 98%, 87%, 90%, and 100% when treated with $CaCl_2$, $ZnCl_2$, $MgCl_2$, NaCl respectively, in comparison to untreated beech sawdust (Batzias and Sidiras, 2007). Another investigation of the effect of treated sawdust was undertaken by Memon et al. (2007). Cedrus deodar wood from Hyderabad, Sindh, Pakistan was used for this batch of experiments. The results show

that the treated sawdust, which was mixed with 5 grams of sawdust treated with 50 mL of 1 mol/L NaOH for 2 hours, then dried at 100°C for 8 hours, obtained a 1.9 mg/g Cd (II) uptake, while untreated Cedrus sawdust could uptake Cd (II) of 0.6 mg/g (Memon et al., 2007).

Table 2.3 Adsorption of sawdust from different kinds of wood for the removal of various pollutants in water

| **Wood Origin** | **Treated or Untreated** | **Experiment Method** | **Adsorbate** | **Result** | **Reference** |
|---|---|---|---|---|---|
| Monterey pine, *Pinus radiata* D. Don from New Zeland | - Untreated and mixed with soil | Construction of denitrification wall in field | Nitrate | Nitrate ($NO_3$) removal estimated from the nitrate to bromide ratio method: 1.4 g $N/m^3$ of wall/d. | Schipper et al., 2005 |
| Poplar tree (Samsun Clone) from Turkey | - Untreated and<br>- Treated with 1N $H_2SO_4$ in the ratio of 1:2 (sawdust/$H_2SO_4$; w/v) at 150°C for 24 h. | Batch | Cu(II) | Adsorption capacity:<br>- 5.432 mg/g (Untreated)<br>- 13.495 mg/g (Treated) | Acar and Eren, 2006 |
| Cedar wood from Annaba, Algeria | - Untreated | Fixed-bed | Methylene blue | Adsorption capacity: 142.36 mg/g | Hamdaoui, 2006 |
| Beech tree from Greece | - Untreated<br>- Treated with salts ($CaCl_2$, $ZnCl_2$, $MgCl_2$, NaCl) | Batch and Fixed-bed | Methylene blue (Basic dye) | Batch, adsorption capacity of treated sawdust increased up to 98% ($CaCl_2$), 87% ($ZnCl_2$), 90% ($MgCl_2$), 100% (NaCl) compared with untreated sawdust | Batzias and Sidiras, 2007 |
| Cedrus deodar wood from Hyderabad, Sindh, Pakistan | - Untreated and<br>- Treated mixed with 5 g of sawdust with 50 mL of 1 mol/L NaOH for 2 hrs then dried at 100°C for 8 h. | Batch | Cd(II) | Cd (II) uptake: 0.6 mg/g for untreated and 1.9 mg/g for treated sawdust | Memon et al., 2007 |

| | | | | | |
|---|---|---|---|---|---|
| Oak tree (Quercus coccifera) from Turkey | Treated with HCl | Batch | - Cu<br>- Ni<br>- Cr | Removal:<br>- 93% for Cu(II) at pH 4<br>- 82% for Ni(II) at pH 8<br>- 84% for Cr(VI) at pH 3 | Argun et al., 2007 |
| Walnut tree from Turkey | Untretaed | Batch | - Lead (Pb)<br>- Cadmium (Cd)<br>- Nicel (Ni) | Removal:<br>- 75% for Pb<br>- 60% for Cd<br>- 30% for Ni | Yasemin and Zeki, 2007 |
| Meranti wood from tropical countries such as Malaysia and Indonesia | Treated with 0.5 M HCl | Batch | Methylene blue (Basic dye) | Adsorption capacity: 120.48, 117.64, 149.25, and 158.73 mg/g at 30, 40, 50, and 60°C, respectively | Ahmad et al., 2009 |
| Yellow brownish from Pilani India | Untreated | Fixed-bed | Cr(VI) | Removal: 74.6 % | Gupta and Babu, 2009 |
| Brazilian sawdust (Caryocar spp., Manilkara spp., Tabebuia spp.) from Brazilian Santarem city | Untreated | Batch | Pb | Adsorption: 89.10±8.28; 145.04±12.43; 95.31±8.28 mg/g for Caryocar spp., Manilkara spp., Tabebuia spp. respectively | Prado et al., 2010 |
| Eucalyptus Globules from Beja, North West of Tunisia | Untreated | Batch | Ammonium ($NH_4^-$) | Adsorption capacity: 1.7 mg/g | Wahab et al., 2010 |
| Finland wood | Treated with 1N $H_2SO_4$ in the ratio of 1:10 (sawdust/$H_2SO_4$; w/v) at 150°C for 24 h. | Batch | Phenol | Adsorption capacity: 1.477 mg/g at pH 4.13 | Larous and Meniai, 2012 |

| | | | | | |
|---|---|---|---|---|---|
| Mango wood (Mangifera indica) from India | Treated with 0.1N NaOH followed by 0.1 N $H_2SO_4$ | Batch | Cr (VI) | Adsorption capacity: 10.86 mg/g | Kapur and Mondal, 2013 |

## 2.6.Adsorption Modelling

Adsorption may be defined as selective concentration or retention of one or more components of a mixture on a solid surface. The solid that adsorbs a component is called the adsorbent, and the component adsorbed is called the adsorbate. The adsorption process is a result of interaction between the adsorbate molecules and the surface (or pore wall) of the adsorbent by physical/chemical forces (Dutta, 2007).

### 2.6.1. Adsorption Isotherm Models

The analysis of adsorption is not strictly reliable and is rarely made without experiment (Cussler, 2009). Initial experiments, being made on a small scale, lead to the fundamental question regarding adsorption on a bigger scale: how will a large bed behave? This question can be answered by examining current knowledge on adsorbents and isotherm (Cussler, 2009). The equilibrium sorption isotherm is fundamentally important in the design of sorption systems. Equilibrium relationships between sorbent and sorbate are described by sorption isotherms; usually the ratio between the quantity sorbed and the remaining solution at a fixed pH and temperature at equilibrium (Ho, 2004).

The isotherm for various materials is shown schematically in Figure 2.8. Any isotherm with a downward curvature is referred to as favourable, and any isotherm with an upward curvature is referred as unfavourable (Cussler, 2009).

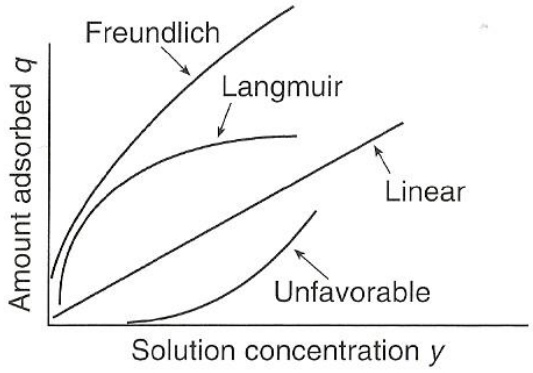


Figure 2.8 Typical schematic isotherms (adapted from Cussler, 2009)

Over the years, a wide variety of equilibrium isotherm models have been formulated in terms of three fundamental approaches. First, kinetic considerations where adsorption equilibrium is defined as being a state of dynamic equilibrium, where both adsorption and desorption rates are equal. In the second approach, thermodynamics can provide a framework for deriving numerous forms of adsorption isotherm models. Potential theory, as the third approach, usually expresses the main idea in the generation of a characteristic curve (Tien, 1994; Foo and Hameed, 2010). However, an interesting trend in isotherm modeling is the derivation of more than one approach, leading to the physical interpretation of the model parameters (Ruthven, 1984; Foo and Hameed, 2010). The equilibrium isotherm models are attributed to Langmuir, Freundlich, Brunauer-Emmett-Teller, Redlich-Peterson, Dubinin-Radushkevich, Temkin, Toth, Koble-Corrigan, Sips, Khan, Hill, Flory-Huggins, and Radke-Prausnitz (Foo and Hameed, 2010). The most widely used among them are the Freundlich and Langmuir equations (Cussler, 2009; Febrianto, et al., 2009).

Freundlich presented a sorption isotherm equation in 1906 (Ho et al., 2002). It is capable of describing the adsorption of organic and inorganic compounds on a wide variety of adsorbents including biosorbents (Febrianto, et al., 2009). The mathematical expression of the Freundlich isotherm is shown in the analysis data for batch and column experiments. This earliest known description of non-ideal and reversible adsorption is not restricted to the formation of a monolayer; the empirical model can be applied to multilayer adsorption with non-uniform distribution of adsorption heat and affinities over the heterogeneous surface (Foo and Hameed, 2010). The slope ranges of between 0 and 1 are a measure of adsorption intensity or surface

heterogeneity. It becomes more heterogeneous as its value gets closer to zero. Whilst a value below unity implies a chemisorptions process, where 1/n above one is indicative of cooperative adsorption (Foo and Hameed, 2010), 1/n equal to 1 indicates linear adsorption, leading to identical adsorption energies for all sites (Febrianto, et al., 2009). However, Freundlich's isotherm is often criticised as lacking a fundamental thermodynamic basis, since it does not reduce to Henry's law at low concentrations (Ho et al., 2002; Foo and Hameed, 2010).

In 1918, Langmuir developed a theoretical equilibrium isotherm relating the amount of gas sorbed on a surface to the pressure from the gas (Langmuir, 1918). In its formulation (Chapters IV and V for batch and column experiments, respectively), this empirical model has four important assumptions. Firstly, it is assumes that adsorption occurs at definite localised sites on the surface. Secondly, it is assumed that each side can bind only one molecule of the adsorbing species. Thirdly, it is assumed that the energy of adsorption is the same for all sites. Fourthly, it is assumed that there are no forces of interaction between adjacently adsorbed molecules (Cooney, 1998).

### 2.6.2. Kinetic Adsorption Models in Batch Systems

There are two important physicochemical aspects for the evaluation of a sorption process as a unit operation: the equilibrium of the sorption and the sorption kinetics (Ho et al., 2000). Adsorption kinetics is expressed as the solute removal rate that controls the residence time of the sorbate in the solid-solution interface (Febrianto, et al., 2009). In technological processes, a sorbent and a solution are brought into contact for a limited period of time which means that the rate of transport of solute molecules from the bulk to the adsorbed phase is of primary importance (Rudzinski and Plazinski, 2007).

The uptake of adsorbates from adsorption-treated solutions by adsorbent particles involves several steps that transfer the adsorbate from the bulk of the fluid phase to the specific sites within the interior of the particle and there are also steps in the adsorption process itself (Tien, 1994). According to the present state of knowledge, the sorption process can be described in following consecutive steps:

1. Transport of solute in the bulk of the solution
2. Diffusion of solute across the so-called liquid film surrounding sorbent particles
3. Diffusion of solute in the liquid contained in the pores of the sorbent particle and along the pore walls (intraparticle diffusion)
4. Adsorption and desorption of solute molecules on/from the sorbent surface viewed as a kind of chemical reaction.

The overall sorption rate may be controlled mainly by any of these steps although the combination of a few steps is also possible (Ho et al., 2000; Rudzinski and Plazinski, 2007). However, in many experimental sorption systems, step 1 which is the movement of pollutant molecules from the bulk liquid to the liquid film is eliminated by rapid mechanical mixing. Thus, it is not assumed to be involved in the controlling of the overall sorption rate and can be ignored (Aksu, 2005; Plazinski et al., 2009). Therefore, the sequence of steps above can be resumed as: transport of solute molecules from the boundary film to the external surface of the sorbent (film diffusion), transfer of molecules from the surface to the intraparticular active sites, and uptake the molecule by the active sites of the sorbent (Aksu, 2005), as shown in Figure 2.9.

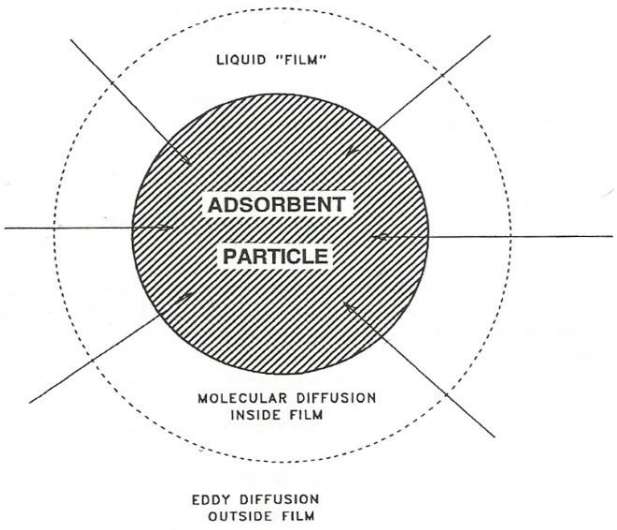


Figure 2.9 Schematic of an adsorbent particle depicting the surrounding stagnant fluid film (Adapted from Cooney, 1998)

To determine the contribution of the remaining steps, numerous kinetic models have been compared in order to predict the behavior of the experimental data. In the first step which is transport of solute molecules from the boundary film to the external surface of the sorbent, the film diffusion is an important rate-controlling step, and external mass transfer or boundary layer diffusion can be characterised by the initial rate of solute sorption. The mathematical expressions of this rate controlling are described in detail in chapter IV.

The last step, uptake the molecule by the active sites of the sorbent, is assumed as making the most significant contribution in the kinetics process as it is the most widely used among researchers (Plazinski et al., 2009). This step is referred to as the surface reaction. In the "surface reaction", not only is there a chemical reaction occurring on the adsorbent surface which involves the formation of chemical bond, interactions of a physical nature may also play a role (Plazinski et al., 2009). The rate of the transfer of solute molecules from the solution to the adsorbed phase is the significant factor behind this model. The rate either governs the overall rate of the sorption process or at the very least, it is partially involved (Plazinski et al., 2009).

In recent years, numerous kinetic models have described the reaction order of adsorption systems based on solution concentrations. These include first-order and second-order reversible systems, first-order and second-order irreversible systems, and pseudo-first-order and pseudo-second-order systems based on the solution concentration (Ho, 2006; Plazinski et al., 2009). In addition to these models, reaction orders based on the capacity of the adsorbent have also been presented, such as Lagergren's first-order equation, Zeldowitsch's model, and Ho's second-order expression (Ho, 2006). In Chapter IV of this paper, two expressions of adsorption rates based on solid capacity will be analysed and discussed. They are Lagergren's first-order equation and Ho's second-order expression.

### 2.6.3. Adsorption Models in Column Experiments

Generally adsorption is carried out in a packed bed. An influent of fluid solution is forced into one end of the bed, passes through the bed, the solute is adsorbed out of the solution and an effluent with very little remaining solute flows out of the

other end of the bed. Adsorption in a packed bed usually produces a more effective separation than adsorption in a stirred tank (Cussler 2009).

As shown in Figure 2.10, in a fixed-bed adsorption, diffusion and mixing of adsorbates in fluid occur as a result of the adsorbate concentration gradients and the uniformity of fluid flow. This effect gives rise to the dispersion of adsorbates, which takes place along the direction of the main fluid flow (*axial dispersion*) and the direction transverse to the main flow direction (*radial dispersion*) (Tien, 1984). Intraparticle mass transfer may become significant in a fixed-bed as the solution is in contact with the adsorbent particle in the movement process. If the intraparticle mass transfer is only due to the diffusion of adsorbate molecules through the pore fluid, it is operated by pore diffusion. If the intraparticle mass transfer is affected through the diffusion of the adsorbed molecules, it is called surface diffusion. However, for a more general description of intraparticle mass transfer, in analysis, it is appropriate to assume that both pore and surface diffusion are operative (Tien, 1984).

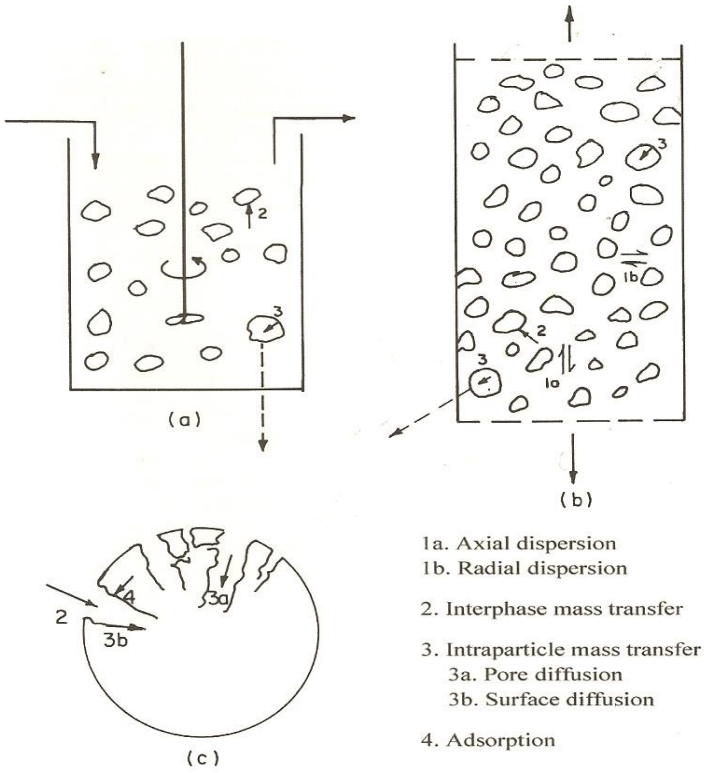


Figure 2.10 Mass transfer in adsorption processes. (a) Batch or continuous-flow tanks, (b) fixed or fluidised beds, and (c) intraparticle mass transfer (Adapted from Tien, 1994)

In physical adsorption, adsorption of adsorbate from the solution phase onto the adsorption sites occurs because of the difference between the adsorbate's chemical potential in the solution and adsorbed phases. At the beginning of the sorbing operation, when the sorbent material is still unused, the exit concentration is actually lower than the permitted one. As sorption proceeds and the sorbent materials are being gradually saturated, the effluent concentration increases and reaches the so-called 'breakthrough' point (Deliyani et al., 2009).

The breakthrough curve is a step towards favourable separation, that is, there would be an instantaneous jump in the effluent concentration from zero to the feed concentration at the moment the column's capacity is reached (Aksu and Gonen, 2004). The breakthrough curves show the loading behaviour of pollutants to be removed from solution in a fixed-bed. This is usually expressed in term of normalised concentration, defined as the ratio of effluent pollutant concentration to inlet pollutant concentration ($C/C_0$) as a function of time or volume of effluent ($V_{eff}$) for a given bed height (Aksu, 2005).

The effects of mass transfer on the breakthrough curves are complicated due to the unsteady-state process (Cussler 2009). Developing a model to accurately describe the dynamic behavior of adsorption in a fixed-bed system is inherently difficult (Aksu and Gonen, 2004), moreover, it usually requires complex numerical methods to solve fundamental transport equations. The numerical solution is in fact not that difficult, however, it often does not fit the experimental data well (Aksu, 2005). Due to this, various simple mathematical models have been developed to predict the dynamic behaviour of the column, for example the Adam-Bohart, Wolborska, Thomas, Yoon and Nelson, and Clark models.

The Adam-Bohart model used to predict the initial part of the breakthrough curve assumes that the adsorption rate is proportional to both the residual capacity of the activated carbon and the concentration of the sorbing species (Bohart and Adam, 1920). The Wolborska model is also used for the description of the adsorption dynamic using mass transfer equations for diffusion mechanisms in the range of the low-concentration breakthrough curve (Wolborska, 1989). The Thomas model can be use to predict the concentration-time profile or breakthrough curve for the effluent, and the maximum adsorption capacity of the adsorbent (Thomas, 1944). Clark's model defined a new simulation of breakthrough curves, and this model combines the

Freundlich equation and the mass transfer concept (Clark, 1987). The Yoon and Nelson model is based on the assumption that the rate of decrease of the probability of adsorption for each adsorbate molecule is proportional to the probability of adsorbate adsorption and the probability of adsorbate breakthrough on the adsorbent (Yoon and Nelson, 1984). In chapter V, two of these relatively new models, (Clark, and Yoon and Nelson) will be analysed for breakthrough curves in the data.

## 2.7.Concluding Remarks

Development in urban areas has increased the number of areas impervious to water. Consequently, the total volume of rainfall and attendant pollutants has increased. This has become the major cause of impairment to surface waters. Biofitration/bioretention is one BMP which may be used for managing stormwater runoff. Due to improve nitrogen removal, biofitration/bioretention with a SAZ with a carbon source is recommended.

Some investigation has previously been carried out to obtain the right sorption medium for stormwater treatment. Initially, many researchers used gravel or sand as a filter. More recently, a new material mix has been developed to remove nutrients from stormwater. The mix can consist of materials such as fine sand, tyre fragments, sawdust, newspaper, compost, wood chips, and wheat straw. Where the adsorption process is used, activated carbon is preferred.

In the adsorption process, there are two important physicochemical aspects requiring evaluation. These are the equilibrium of the sorption and sorption kinetics. Based on adsorption capacity, the Langmuir and Freundlich equations are favored for modelling equilibrium isotherms. The sorption kinetics which has three segments in overall process can be modelled by film diffusion, intraparticle diffusion, pseudo-first-order and pseudo-second-order models based on its solid capacity. In column experiment, the dynamic behaviour is modelled by Clark, and Yoon and Nelson models.

# CHAPTER 3
# MATERIALS AND EXPERIMENTS

## 3.1 Materials

### 3.1.1. Sawdust

As detailed in the literature review (Chapter 2), sawdust has a great deal of potential as an adsorbent for removing nutrients from aqueous solutions. Sawdust is one carbon source which is low cost and easy available. In this research, sawdust from Radiata Pines (*Pinus radiata)* was used for removing dissolved nutrients from stormwater.

Radiata pine is grown on a large scale in Australia for the pulp and paper industry. The wood from Radiata pines is also used for engineering applications, and in the furniture and construction industries, producing a substantial amount of sawdust as waste material (Radiata pine, 2013).

#### 3.1.1.1. Chemical Composition of Sawdust

The cell walls of sawdust mainly consist of cellulose, lignin, and many hydroxyl groups or other phenolic compounds. All these components are active ion exchange compounds. Lignin, the third main component of the wood cell wall, is a polymer material. A lignin molecule is made up of a phenylpropane nucleus, which is an aromatic ring with three carbon sides, along with vanillin and syringaldehyde (Shukla et al., 2002).

The estimates of chemical composition of Radiata pine sawdust are shown in Table 3.1. The data are presented in two forms, one expressing the composition in terms of cellulose, lignin, and hemicelluloses (arabinan, mannan, and galactan), and the other terms of cellulose and the principal polysaccharides of Radiata pine (Uprichard, 2002)

Table 3.1 Chemical composition of the Radiata pine (adapted from Uprichard, 2002)

| Components | % Composition |
|---|---|
| Lignin | 26.0 |
| Anhydro Sugar Arabinan | 1.0 |
| Xylan | 5.2 |
| Mannan | 12.4 |
| Galactan | 3.1 |
| Glucan | 47.3 |
| Uranic acid, acetyl, etc | 5.0 |
| **Total** | 100.0 |
| | |
| Lignin | 26 |
| Arabinogalactan | 4.0 |
| Cellulose | 43.9 |
| Glucomanan | 15.8 |
| Arabinoglucuronoxylan | 6.9 |
| Acetyl, etc | 3.4 |
| **Total** | 100.0 |

### 3.1.1.2. Sawdust Treatment

The sawdust from Radiata pines was obtained from Stokic Nominees, a wood processor and supplier in Maddington, Western Australia. The supplier confirmed that the sawdust had not been chemically treated.

The sawdust was sieved into 5 particle sizes of < 300 µm, 300-600µm, 600µm -1.18mm, 1.18-2.36mm, and >2.36 mm respectively. To remove the soil particles and any possible nutrients, the sawdust was washed with distilled water. After each washing, 2 ml of washed water was taken from the effluent and filtered for nutrient analysis. After 6 to 7 washes, the nutrient content in the sawdust was reduced to nil. The rinsed sawdust was then placed into separate metal trays according to particle size, and dried in an oven at $105^0$C for 24 hours. The dried sawdust was then placed in an air-tight container at room temperature ($22\pm2^0$C) (Fig. 3.1.).

Figure 3.1 Dried sawdust from Radiata Pines

### 3.1.1.3. Particle Size of Sawdust

A sieve analysis was performed to determine particle size distribution. This was determined by placing 495 grams of sawdust into a stacked set of U.S. Standard sieves which was mechanically shaken for 10 minutes. The sieves were then separated, and the weight of sawdust in each sieve determined. The weights of the sieved sawdust were then converted to percentages of the total retained on each sieve.

Fig. 3.2 presents the gradation curves of the sawdust particles. The particle size of the sawdust was deemed to be well-graded. The percentage of finer sawdust particle size was determined from the particle distribution curve. The median diameter of the particle, used for calculating the size, was $d_{50}$. The sawdust size, $d_{50}$, was defined as the sawdust diameter. The effective size ($d_{10}$) of sawdust was therefore 0.6 mm and the $d_{60}$ of sawdust was 1.05. The uniformity coefficient ($U$) of sawdust was determined at 1.75. $U = 1$ indicated that all the particles were almost equal in size, and $U > 1$ indicated that particles were not the same size. Therefore it can be stated that sawdust has a non-uniform particle size.

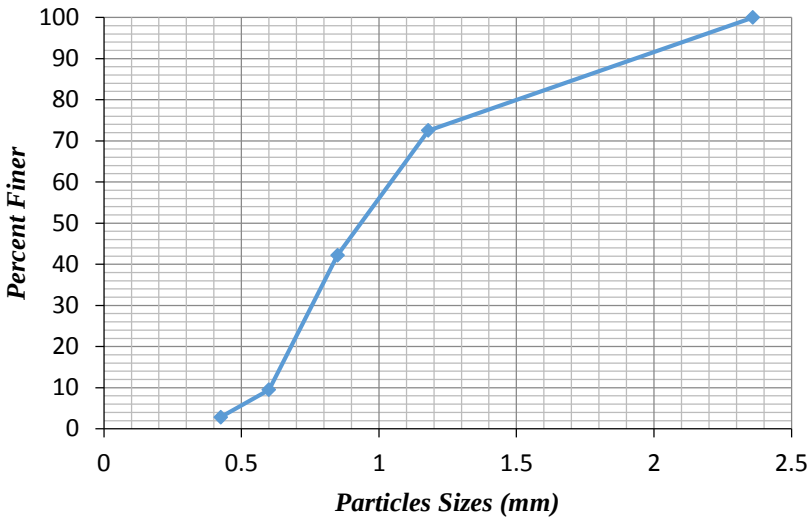


Figure 3.2 Sawdust Particle Size

### 3.1.2. Preparation of Stock Solution

All chemicals used in the experiments were of analytical grade and were purchased from Thermo Fisher Scientific, Sydney Australia. Solutions were prepared with deionised water (DI). The stock solution of ammonia–nitrogen ($NH_3$-N), nitrate-nitrogen ($NO_3$-N), and nitrite-nitrogen ($NO_2$-N) was prepared from $NH_4Cl$, $NaNO_3$, and $NaNO_2$ respectively. The standard solution for each nutrient is prepared by diluting a known mass of the required chemical using deionised water to make up a 1g/L concentration. These standard solutions are then kept in a laboratory refrigerator in sterilised plastic bottles and labelled for later use.

New solutions were prepared by diluting the standard solution with deionised water before each experiment, to avoid any possible deterioration in concentration or any other possible contamination. The pH of the solution was adjusted with small amounts of 1 mol/L NaOH and HCl respectively. The pH measurement was performed using an HACH portable pH/temp meter (accuracy ±0.1).

## 3.2. Experiments

Two sets of experiments were conducted to investigate the adsorption characteristic of nutrient using sawdust of Radiata pine. They are batch and column experiments. Batch experiment was done in order to determine the percentage removal, adsorption capacity, isotherm and kinetics of nutrient adsorption onto sawdust. The dynamic characteristics was investigated by column experiments.

### 3.2.1. Batch Experiments

A series of batch experiments (Table 3.2) was carried out for different initial concentrations (0.5-5mg/l), dosages (2-20gm), particle sizes (< 300µm, 300-600µm, 600-1.18mm, 1.18-2.36mm, and >2.36 mm), pH (4-9), and contact time (until equilibrium). The equilibrium state was characterized by a certain nutrient concentration in the adsorbent and an associated final nutrient concentration in the liquid phase.

In each case, sawdust of selected dosage and particle sizes was poured into an Erlenmeyer flask and a 200 ml of aqueous solution of desired concentration and pH was added into the flask. The top of each flask was wrapped with parafilm to eliminate any possible evaporation. Erlenmeyer flasks were kept on a shaking platform of 16-flask capacity (Innova 2100, New Brunswick Scientific) at 100 rpm at room temperature ($22\pm2^0$C).

Table 3.2 Spesific experimental conditions for each batch

| Batch test based on | Initial Concentration | Dosage | Particle Size | pH |
|---|---|---|---|---|
| Initial concentration | 0.5-5 mg/L | 20 g | 300-600 µm | 6.5 ±0.5 |
| Sawdust dosage | 1 mg/L | 2-20 g | 300-600 µm | 6.5 ±0.5 |
| Particle size | 0.5 mg/L | 10 g | <300µm, 300-600µm, 600µm1.18mm, 1.18-2.36mm, >2.36 mm | 6.5 ±0.5 |
| pH | 0.5 mg/L | 10 g | <300µm | 4-9 |


Figure 3.3 Shaking Platform (Innova 2100, New Brunswick Scientific)

At every sampling time point, a 2mL sample was taken from each flask containing the different concentrations, using a piston-operated pipette (Transferpette). A new pipette tip was used each time to avoid contamination. Each sample taken from the flask was filtered through a filter syringe of 0.45µm and placed into a 2mL sample cup. The first sample was immediately transferred into the sample cup from the filtered syringe. The filtered syringe was reused for the subsequent samples due to the low availability of filters. Each time the filtered syringe was reused, it was first rinsed with the sample solution two or three times before filtering it into the sample cup for analysis. Each sample cup was then placed on a sample tray to be analyzed using the Aquakem 200 Photometric Analyzer machine from Thermo Scientific, Sydney (Fig. 3.4). The accuracy of these analyses was ±0.015, ±0.02, and ±0.015 for $NH_3$-N, $NO_3$-N, and $NO_2$-N respectively.

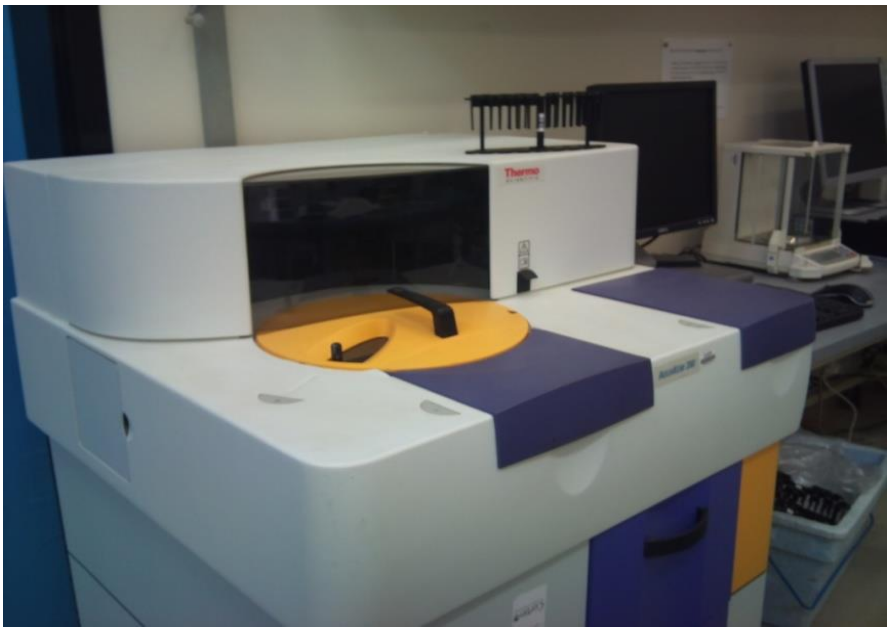

Figure 3.4 Aquakem 200 water analyzer

For the dosage test, dosages ranging between 2-20 grams with a particle size range of 300-600µm were poured into the Erlenmeyer flask. A 1 mg/L concentration of adsorbate solution (pH 6-7) was prepared from stock solution. Two hundred milliliters of this solution was transferred into each flask and then covered with Parafilm to begin the experiment. The next step was the same as the concentration test, where a sample was taken at each retention time and analysed until the equilibrium concentration pattern was reached.

Another parameter tested was the effect of particle sizes on adsorption. The batch experiments were repeated for different particle sizes of < 300µm, 300-600µm, 600-1.18mm, 1.18-2.36mm, and >2.36 mm respectively. A 200 mL solution of 0.5 mg/L concentration (pH 6-7) for each nutrient to be immediately used was deposited into five separate Erlenmeyer flasks or beaker that were already labelled. Each beaker then was added to with 10 grams of sawdust and then covered with parafilm. The same method used for the concentration and dosage tests was used to obtain and analyse the samples at different retention times until an equilibrium concentration was reached.

Finally, the effects of the pH levels were checked using sawdust with a particle size of <300µm. The pH of 200 mL of aqueous solution (0.5 mg/L) was adjusted to 4,

5, 6, 7, 8, and 9 respectively for each different experiment. The pH value for each solution was measured using the HACH pH meter. Sodium Hydroxide (NaOH) was added into the solution using a piston pipette to increase the pH value, and Hydrochloric Acid (HCl) was added to lower the pH value until the desired pH value was reached. A 10 gram measure of sawdust was put into each flask for the batch experiments. To examine contact time, samples were taken at different predetermined times. The shaker machine was set at 100 rpm throughout the experiment and the same analysis method used in previous experiments was used to take and measure each sample at each retention time.

### 3.2.2. Column Experiments Procedure

A column experimental unit was designed in the laboratory. A schematic diagram of the experimental unit set-up is shown in Figure 3.5. The column experimental unit consisted of a fixed-bed adsorption column, a peristaltic pump, a feed tank, and an effluent tank.

The fixed-bed adsorption column was made of polypropylene cylinder with a height of 30 cm and an internal diameter of 3.8 cm. However, the effective length of the column depended upon the experimental conditions. Stainless steel mesh was placed in the upper and lower parts of the column to retain the adsorbent. The column was connected to a peristaltic pump to maintain the flow rates. The solution contaminated by nutrients was placed in the feed tank and injected through the column in the up-flow mode, and the effluent was collected in the effluent tank. The effluent sample was collected using a two-way valve.

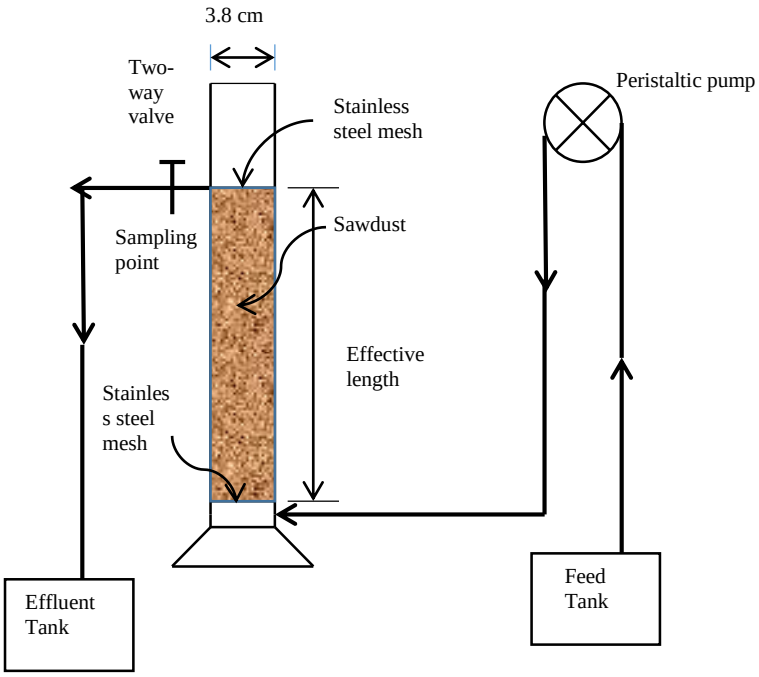


Figure 3.5 Schematic diagram of experimental set-up

A series of column experiments (Fig. 3.6.) was carried out using different flow rates, concentrations, and different heights of sawdust columns.

Initially, column experiments were carried out for different flow rate tests. A 37 gram measure of sawdust was gradually poured into the column. The effective bed length for this experiment was 19 cm. The column was connected to a peristaltic pump and saturated with deionised water prior to filtration. A 0.5 mg/L concentration of solution was brought into the column in an up-flow mode at three different flow rates (ranging between 9-23 mL/min). An effluent sample was collected at predetermined times until the effluent concentration became the same as the influent concentration. Every time the collected sample was obtained, it was filtered through a filter syringe of 0.45µm. The solution that passed through the filter was placed into a 2 mL sample cup and then put on a sample tray to be analysed, using the Aquakem 200.

Following this, the fixed-bed column was used for the concentration test, at a fixed flow rate in up-flow mode. As with the flow rate test, 37 grams of sawdust was poured into the column and the effective bed length was 19 cm. Deionised water was run into the column to obtain saturated sawdust before the adsorption tests

commenced. Three different concentrations (ranging between 0.5-5 mg/L) of nutrient solutions were checked in this experiment. The next procedure used was the same as that used in the flow rates test.

The last test was a test of different column heights. In this test, three different column heights were investigated. The bed-depths were: 11 cm with 18 gram of sawdust, 15 cm with 26 gram of sawdust, and 19 cm with 37 gram of sawdust. A nutrients solution (of approximately 1 mg/L) was brought in to the column in up-flow mode at a fixed flow rate. Samples were taken at predetermined times using the same method as the flow rate and concentration tests.

Figure 3.6 Column experiments

### 3.3. Concluding Remarks

Untreated sawdust from Radiata Pine wood was used for removing dissolved nutrients ($NH_3$-N, $NO_3$-N, and $NO_2$-N) from aqueous solutions. Both batch and column experiments were conducted at room temperature ($22\pm2^0$C). The investigation focused on different initial concentrations, dosages, particle sizes, contact time and pH for batch experiments, and different flow rates, concentrations, and heights of sawdust column for column experiments.

All experiments were conducted in order to identify the mechanism of sawdust as an adsorbent for removing $NH_3$-N, $NO_3$-N, and $NO_2$-N from aqueous solutions and to better understand the adsorption characteristics of sawdust.

# CHAPTER 4

# ADSORPTION CHARACTERISTICS IN BATCH: DATA ANALYSIS AND DISCUSSION

## 4.1. Analysis of Batch Data

There are two important physicochemical processes involved in liquid-solid adsorption include equilibrium and kinetics sorption (Ho et al., 2000). Equilibrium relationships between sorbent and sorbate are described by sorption isotherms; usually the ratio between the quantity sorbed and the remaining solution at a fixed pH and temperature at equilibrium. Adsorption kinetics is expressed as the solute removal rate that controls the residence time of the sorbate in the solid-solution interface. Three sequences of steps can take palce in the adsorption process of a porous adsorbent. Firstly, transport of solute molecules from the boundary film to the external surface of the sorbent can be modelled by film diffusion model. Secondly, transfer of molecules from the surface to the intraparticular active sites which is modelled by intraparticle diffusion model. The last step, uptake the molecule by the active sites of the sorbent can be modelled by pseudo-first order and pseudo-second order models (Aksu, 2005).

In this chapter, the adsorption characteristics of Radiata pine sawdust was analyzed with several parameters including initial concentration, sawdust dosage, pH, particle sizes, and contact time. Adsorption favorability, adsorption isotherms and adsorption kinetics are presented.

### 4.1.1. The Amount of Nutrients Adsorbed

The amount of adsorption at equilibrium, $q_e$ (mg/g), was calculated by:

$$q_e = \left(\frac{C_0 - C_e}{W}\right) V \quad (4.1)$$

where $C_0$ and $C_e$ are the initial and equilibrium concentration (mg/L) of dissolved nutrient respectively. $V$ is volume of aqueous solution (mL), and $W$ is the weight of dry sawdust (g).

However, for analyzing batch kinetic experiments, the amount of adsorption at any time *t*, $q_t$ (mg/g) was calculated by:

$$q_t = \left(\frac{C_0 - C_t}{W}\right) V \quad (4.2)$$

where $C_0$ and $C_t$ (mg/L) are liquid-phase concentration of nutrient at initial and any time *t* respectively, *V* is volume of the solution (mL), and *W* is the weight of dry sawdust (g).

### 4.1.2. Percentage Removal

The percent of adsorption of nutrients was calculated using the following equation (Sari et al. 2007):

$$Removal\ (\%) = \left(\frac{C_0 - C_e}{C_0}\right) \times 100 \quad (4.3)$$

### 4.1.3. Adsorption isotherm

The results of the batch experiment were used for the isotherm study. Adsorption isotherms explain the relationship between the amount of solute adsorbed and the concentration of solute in the fluid phase at a given constant temperature. The Langmuir and Freundlich models were used to fit the experimental data.

#### 4.1.3.1. Langmuir Isotherm

The Langmuir model is used to illustrate the equilibrium between surface and solution as a reversible chemical equilibrium between species (Crittenden et al., 2005). This model can be written as (Hossain et al., 2009):

$$\frac{1}{q_e} = \frac{1}{q_m K_{ads}} \left(\frac{1}{C_e}\right) + \frac{1}{qm} \quad (4.4)$$

where $C_e$ (mg/L) and $q_e$ (mg/g) are the liquid phase concentration and solid phase concentration of sorbet at equilibrium, respectively; $q_m$ (mg/g) is the maximum capacity constant of adsorbent for adsorbate; and $K_{ads}$ ( L/mg) is the measure of affinity of adsorbate with adsorbent known as Langmuir constant. The Langmuir isotherm can be obtained by plotting a graph between 1/*q* and 1/*C*. Based on the additional analysis

of the Langmuir equation, the dimensionless parameter of equilibrium or adsorption intensity ($R_L$) can be expressed by (Sari et al., 2007):

$$R_L = \frac{1}{1+ K_{ads}C_0} \quad (4.5)$$

where $C_0$ (mg/L) is the initial quantity of adsorbate. The $R_L$ parameter is considered a more reliable indicator of adsorption:

$R_L$=0 indicates irreversible

0< $R_L$ <1indicates favorable

$R_L$=1 indicates linear

$R_L$>1 indicates unfavorable

#### 4.1.3.2. Freundlich Isotherm

The adsorption data were then fitted with the Freundlich model. The Freundlich adsorption isotherm is expressed in a linear form which can be applied for non-ideal sorption on heterogeneous surfaces and multilayer sorption (Crittenden et al., 2005; Hossain et al., 2009):

$$\log q_e = \log K + \frac{1}{n} log C_e \quad (4.6)$$

where $K$ and n are constants involving adsorption capacity and adsorption intensity, respectively. These constants are determined from the intercept and slope of the linear plot of log $q_e$ versus log $C_e$, respectively.

### 4.1.4. Sorption Mechanism Models

Kinetic models have been proposed to elucidate the mechanism. The mechanism of adsorption depends on the physical and/or chemical characteristics of the adsorbent, as well as on the mass transport process. In order to investigate the correct mechanism of nutrient adsorption onto sawdust, kinetic models were selected based on their adsorption capacity and tested over the entire contact time used in varying concentration experiment.

The adsorption process can follow either or both the kinetic sorption and diffusion models. The regression coefficient between experimental and theoretical

data is the indicator for an appropriate model. The difference between these two processes is difficult to characterize. A general guideline regarding this is to identify the time when equilibrium is reached. If equilibrium is reached within three hours, the adsorption process is usually kinetically controlled (Ho et al., 2000). If equilibrium is achieved above twenty-four hours, it is diffusion controlled (Ho et al., 2000). In transition zone of 3-24 hours of contact time, the adsorption process might be either or both kinetically controlled and sorption processes may be rate controlling if equilibrium is achieved between three to twenty-four hours (Ho et al., 2000).

However, there is an appropriate quantitative approach to distinguishing between the kinetic and the diffusion rate control. It is a straight line plot of slope $k_{d,}$ yielded by plotting the amount of nutrients adsorbed ($q_t$) against the square root of contact time ($t^{0.5}$), according to equation (4.7). If the straight line passes through the origin, it indicates intraparticle diffusion control (Ho et al., 2000). Therefore, this intraparticle diffusion model will be analyzed first, followed by the pseudo-first order and pseudo-second order kinetic models.

#### 4.1.4.1. Intraparticle Diffusion Model

The intraparticle diffusion model, based on the theory proposed by Weber and Morris (Weber and Morris, 1963), was tested to identify the diffusion mechanism. It is an empirically established functional relationship, common to most adsorption processes, where uptake varies almost proportionally with $t^{0.5,}$ rather than with the contact time *t*.

$$q_t = k_{di} t^{1/2} + M_i \quad (4.7)$$

Where $k_{di}$ (mg/g $h^{1/2}$) is the intraparticle diffusion rate constant of stage *i* which can be found from the slope of the linear plot of $q_t$ versus $t^{1/2}$. The $M_i$ is the intercept of stage *i* provides an idea about the thickness of boundary layer. Larger intercept will provide higher boundary layer effect. If the plot passes through the origin, the rate limiting process is only due to intraparticle diffusion. Otherwise, some other mechanism may take place such as, liquid film diffusion.

#### 4.1.4.2. The Liquid Film Diffusion Model

The liquid film diffusion model proposed by Boyd et al (Boyd et al., 1947) is applicable when the flow of reactant from the bulk liquid to the surface of adsorbent determines the rate constant. It is expressed as:

$$\ln(1 - F) = -k_{fd}t \tag{4.8}$$

where F (=$q_t/q_t^{'}$) is the fractional attainment of equilibrium, and $k_{fd}$ is the adsorption rate constant of the liquid film diffusion model (1/min).

#### 4.1.4.3. Pseudo-First Order Kinetic Model

The pseudo-first order rate expression of Lagergren (Lagergren, 1898), based on the adsorption capacity of an adsorbent, is generally expressed as follows:

$$\frac{dq}{dt} = k_1(q_e - q_t) \tag{4.9}$$

The integrated form of the differential equation becomes

$$ln(q_e - q_t) = lnq_e - k_1 t \tag{4.10}$$

where $q_e$ and $q_t$ are the amounts of nutrients adsorbed (mg/g) at equilibrium and at time $t$ (minutes/hours) respectively, and where $k_1$ is the rate of constant adsorption (1/min). The values of $k_1$ and $q_e$ (cal) were calculated from the slope ($-k_1$) and the intercepts (ln $q_e$) of the plots of ln ($q_e$-$q_t$) vs $t$.

According to Azizian (2004), the rate constant ($k_1$) is a combination of adsorption ($k_a$) and desorption ($k_{ds}$) rate constants, as shown below:

$$k_1 = k_a C_o + k_{ds} \tag{4.11}$$

Thus, the addition of this pseudo-first-order model is to achieve a constant rate of adsorption ($k_a$) and desorption ($k_{ds}$) from the plot of the rate constant, $k_1$ vs various initial concentrations $C_o$ (mg/L), by using Eq. (4.11).

#### 4.1.4.4. Pseudo-Second Order Kinetic Model

Adsorption kinetics may also be described by a pseudo-second order equation, which is based on the adsorption capacity of the solid phase (Ho and McKay, 1998). The equation is expressed as

$$\frac{dq}{dt} = k_2(q_e - q_t)^2 \tag{4.12}$$

Integrating Eq. (4.12) for the boundary condition $q = 0$ to $q = q_t$ at $t = 0$ to $t = t$ is simplified as:

$$\frac{t}{q_t} = \frac{1}{k_2 q_e^2} + \frac{1}{q_e} t \tag{4.13}$$

where $k_2$ (g/mg min) is the rate constant of second-order adsorption. If the second-order kinetic equation is applicable, the plot of $t/q$ against $t$ of Eq. (4.13) should give a linear relationship. The $q_e$ and $k_2$ can be determined from the slope and intercept of the plot (Dursun et al., 2005).

The initial adsorption rate $h$ (mg/g min) can be calculated from the pseudo-second order by the following equation (Ho, 2006):

$$h = k_2 q_e^2 \tag{4.14}$$

### 4.1.5. Validity of Kinetic Models

The applicability of the kinetic model to describe the adsorption process was further validated by the normalised standard deviation, $\Delta q$ (%), which is defined as:

$$\Delta q(\%) = 100\sqrt{\frac{\sum[(q_e(exp) - q_e(cal))/q_e(exp)]^2}{N-1}} \tag{4.15}$$

where $N$ is the number of data points, $q_e$(exp) and $q_e$(cal) (mg/g) are the experimental and calculated adsorption capacity, respectively.

## 4.2. Results and Discussions

### 4.2.1. Effect of Concentration

The effect of concentrations on the removal of different nutrients using sawdust is shown in Fig. 4.1 (a-c). The percentage removal of $NH_3$-N was found to be higher in lower concentrations. Due to the less ability of sawdust to uptake more concentration of $NH_3$-N, the adsorption rate was found to gradually decrease with increasing concentration. The maximum removal (≈55%) (Fig. 4.1a) was obtained within 15 minutes with an initial concentration of 1 mg/L. The lowest removal percentage for $NH_3$-N was found to be 34% with 5 mg/L concentration. As $NH_3$-N concentration in stormwater is usually found to be very low (0.17mg/L) (Taylor et al., 2005), the results revealed that sawdust may be considered as an effective medium in removing $NH_3$-N from stormwater.

The removal percentage of NO3-N decreased with increased concentration (Fig. 4.1b). The removal percentage of $NO_3$-N was found varying 92-99% for a concentration range of 0.5-5 mg/L. A similar pattern of $NO_2$-N removal was also observed, as shown in Fig. 4.1c. The maximum removal of $NO_2$-N was obtained, at almost 100%, for the whole range of initial concentrations, but equilibrium was reached in the early hours for lower initial concentration. The removal percentage of $NO_2$-N shows a gradual decreasing trend with concentrations increasing from 0.5mg/L to 5mg/L. These results reveal that $NO_3$-N and $NO_2$-N are well adsorbed onto sawdust at lower concentrations in a relatively shorter period of time.

The results revealed that the rate of adsorption was very rapid in the early stages of contact time for all adsorbates, but after that, it decreased gradually with time until adsorption was reached at the point of equilibrium. This trend of adsorption kinetics provides the information that external diffusion is rate-controlling at the initial period of contact time (Hamdaoui, 2006; Gupta et al., 2012). When the adsorption on the exterior surface reached saturation point, nutrients diffused into the pores of the sawdust and were adsorbed by its interior surface. The equilibrium time for $NH_3$-N was obtained within 15 minutes for the complete range of concentrations. The concentration of $NO_3$-N and $NO_2$-N reached their equilibrium within 30 minutes and 50 hours, respectively, for initial concentrations of less than 2 mg/L. However, it took longer for the initial concentration range of 2-5 mg/L to reach equilibrium. The average

equilibrium time was found to be 240 minutes and 70 hours for $NO_3$-N and $NO_2$-N, respectively. However, the variation in equilibrium time refers to the dissimilar behaviour of the adsorption mechanism of nutrients onto sawdust. $NH_3$-N and $NO_3$-N reach equilibrium faster, suggesting that the adsorption mechanism depends on the chemical character of the sawdust. The $NO_2$-N needs longer to reach equilibrium, suggesting rate controlled diffusion (Ho et al., 2000).

Nutrient adsorption with different initial concentrations is shown in Figure 4.2. Results show that nutrient adsorption increases linearly with increasing initial concentration. However, $NH_3$-N shows a lower rate of adsorption, but the other two nutrients ($NO_3$-N and $NO_2$-N) show a higher rate with a similar trend of adsorption. The increase in the adsorption capacity of the sawdust with the increase of initial nutrients concentration is due to the higher availability of nutrient ions in the solution. It provides an important driving force to overcome all of the mass transfer resistance of the nutrient ions between the aqueous and the solid phase, resulting in a higher probability of collision between nutrient ions and sawdust. Hence, a higher initial concentration of nutrients tends to enhance the adsorption process. This phenomenon also occurred in other research, such as: adsorption of chromium (VI) on pomace (Malkoc et al. 2006); methylene blue adsorption on wheat shells (Bulut and Aydin, 2006); and basic dye adsorption on banana stalk waste (Hameed et al., 2008).

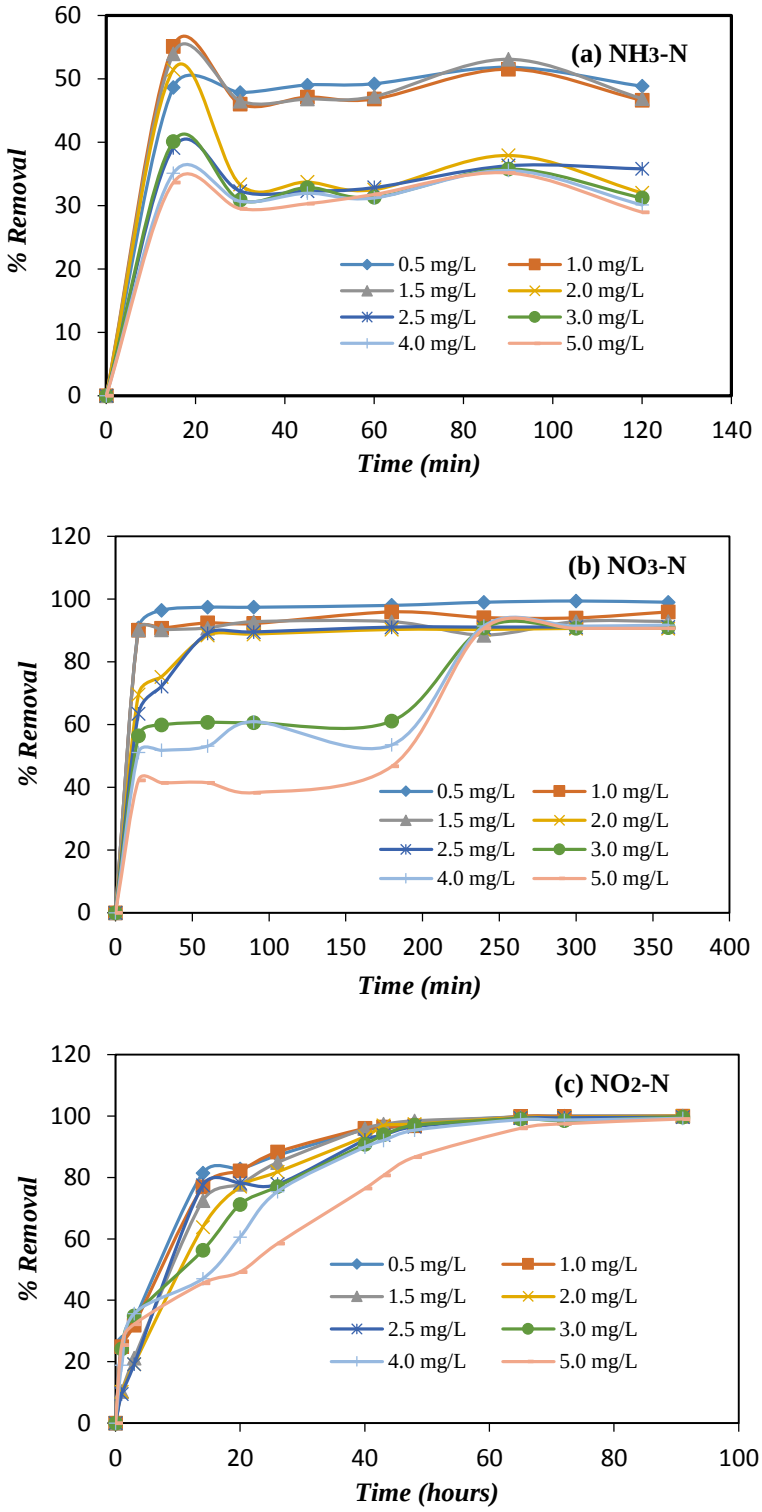


Figure 4.1 The effect of initial concentration and contact time on the removal of (a) $NH_3$-N, (b) $NO_3$-N, and (c) $NO_2$-N respectively using sawdust (sawdust dosage: 20 g; particle size: 300-600µm; pH 6-7)

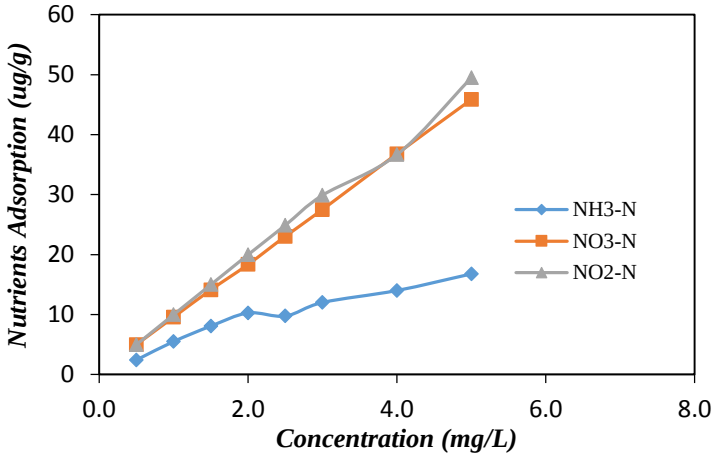


Figure 4.2 Nutrients adsorption (µg/g) for different initial concentrations on the removal of nutrients using sawdust (sawdust dosage: 20 g; particle size: 300-600µm; pH 6-7)

### 4.2.2. The Dosage Test Effect

The removal of nutrients with varying dosages was investigated with an initial concentration of 1mg/L. The nutrient removal obtained with time is shown in Fig. 4.3 (a-c). The addition of an adsorbent dosage increased with the amount of nutrient removal due to the increased surface area. For all nutrients, it appears that removal efficiency increases significantly until it reaches the dosage of 12 grams of sawdust, after this, the percentage removal is insignificant. However, this result is clearly in agreement with the research of Ozturk and Bektas (2004).

The adsorption capacity (Fig. 4.4) for all nutrients showed a decreasing trend with increasing sawdust dosage. When the amount of sawdust is increased by keeping the initial nutrient concentration constant, the amount of nutrients adsorbed per unit mass shows a decrease due to the availability of less nutrient ions per unit mass of sawdust. The adsorption capacity of nutrients dropped by 55% for $NH_3$-N, 78% for $NO_3$-N and 64% for $NO_2$-N with the dosage of sawdust increasing from 2-5grams. This drop may be due to the sites remaining unsaturated during the adsorption process. Similar results have been reported for adsorption of Cr (VI) using activated neem leaves (Babu and Gupta, 2008), adsorption of methylene blue on wheat shells (Bulut and Aydin, 2006), and adsorption of Ni (II) on clays (Gupta and Bhattacharyya, 2006).

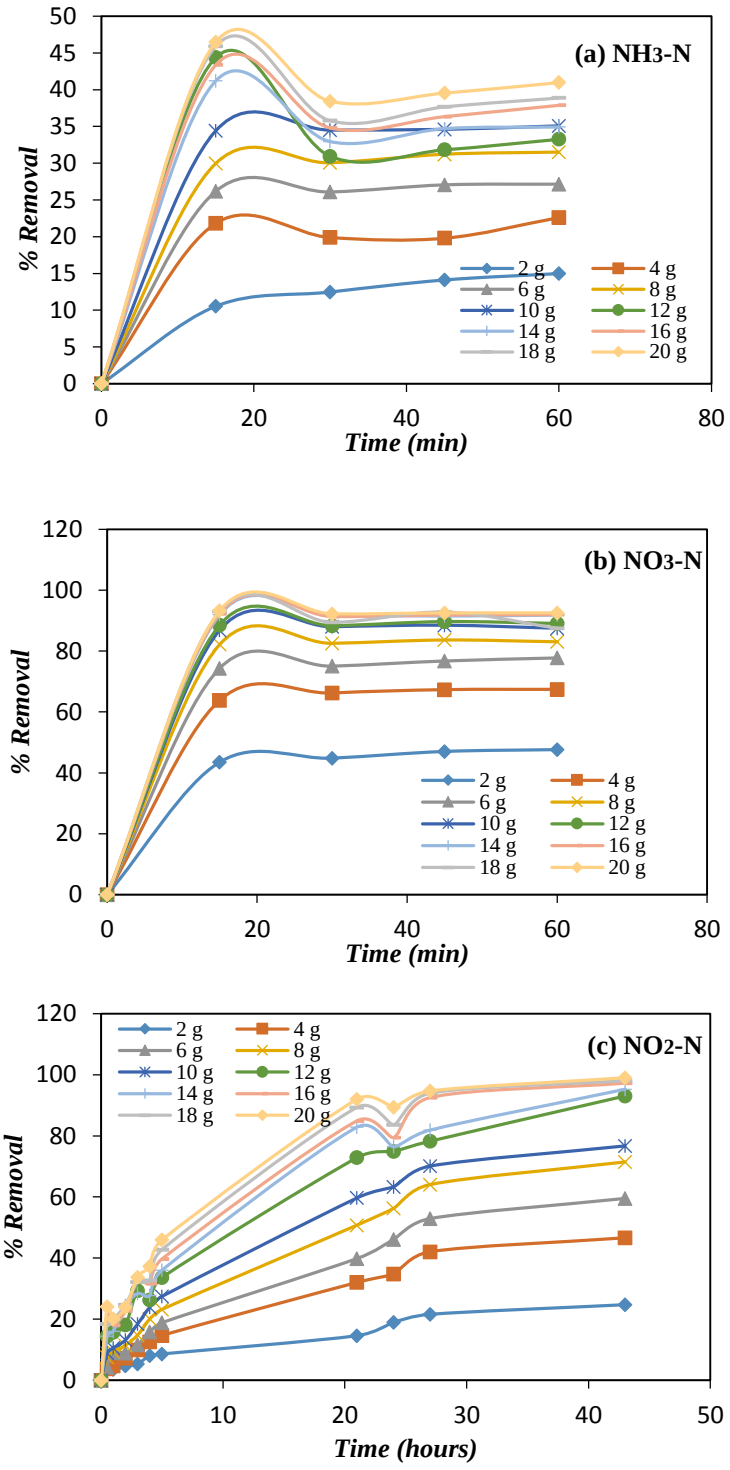


Figure 4.3 The effect of dosage of sawdust and contact time on the removal of a) $NH_3$-N, (b) $NO_3$-N, and (c) $NO_2$-N respectively (initial concentration: 1 mg/L; particle size: 300-600µm; pH 6-7)

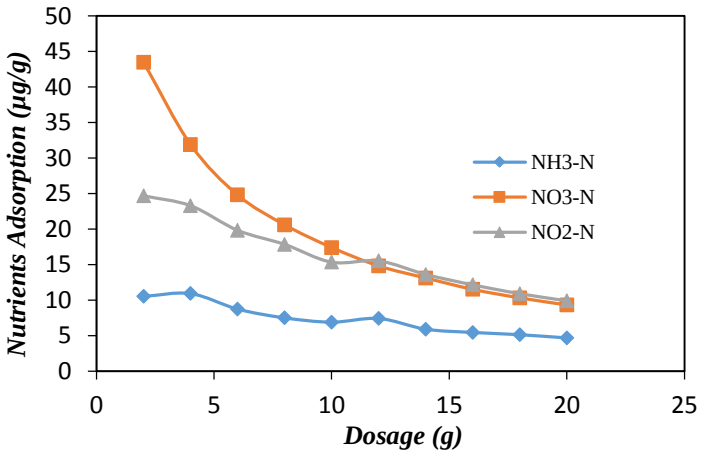


Figure 4.4 Nutrients adsorption (µg/g) for different dosage of sawdust on the removal of nutrients (initial concentration: 1 mg/L; particle size: 300-600µm; pH 6-7)

### 4.2.3. Effect of Sawdust Particle Sizes

The effect of particle sizes on the removal of nutrients is shown in Fig. 4.5 (a-c). The removal of $NH_3$-N (Fig. 4.5(a)) was found to increase with decreasing particle sizes Sawdust particle sizes of <300 µm could remove 40% nutrients within 15 minutes and decreased to 35% of removal with a sawdust particle size of >2.36mm.

In Fig. 4.5(b), it is clearly indicated that a particle of <300µm in size is able to adsorb the most $NO_3$-N, i.e., up to >98%. The removal capacity of sawdust decreases with increasing particle sizes. The particle size of 300-600µm provides 91%, 600 µm-1.18mm provides 90%, 1.18mm-2.36mm provides 88% removal and a particle size of >2.36mm provides 85% of removal, respectively. $NO_3$-N takes only 30 minutes of retention time to reach its equilibrium for all different particle sizes of sawdust.

In the case of $NO_2$-N (Fig. 4.5(c)), the difference in the removal percentage for each particle size does not vary as much, in comparison with the other two nutrients. All particle sizes in contact with $NO_2$-N managed to adsorb up to 98% of the adsorbent within 72 hours. This experiment shows that particle size does affect the removal capacity of sawdust, with smaller sizes having more effective removal capacity. The results support the findings of a previous study showing that a higher rate of removal occurs at a particle size of <2mm (Hossain et al., 2009).

However, overall, the effect of sawdust particle size on nutrient adsorption can be considered insignificant in this study (Fig. 4.6). Independence of sorption capacity

on particle sizes indicate that when the sorbent mass is saturated, the solute is able to diffuse even at the center of the particles (Jansson-Charrier et al., 1996). Moreover, nutrient adsorption onto sawdust might be controlled by ionic exchange. The sawdust might have high porosity and a high quantity of light metals (Ca, K, Mg, and Na) as given in Ragland and Aerts, (1991), which makes it vulnerable to being exchanged. This result supports the findings of chromium (III) biosorption on orange (citrus cinensis) waste (Marin et al., 2009).

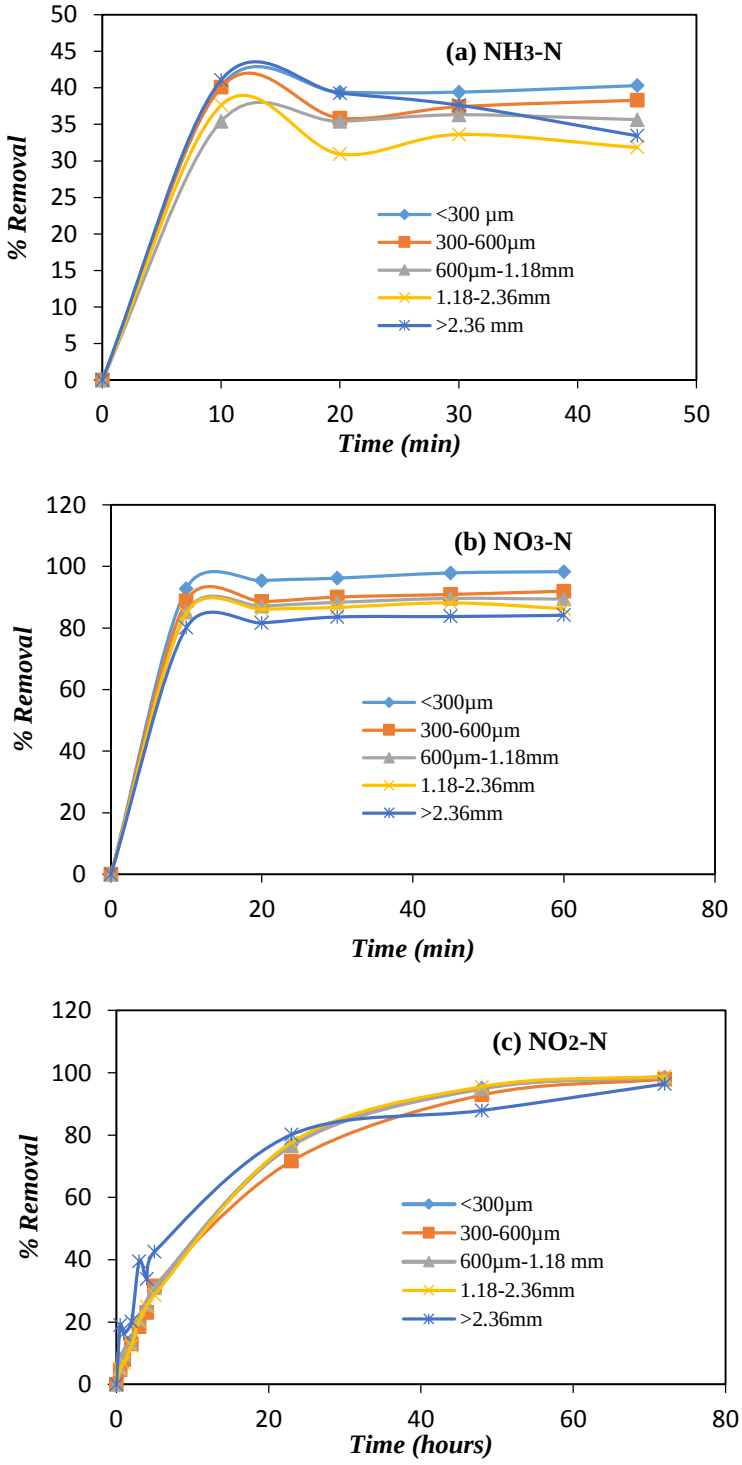


Figure 4.5 The effect of particle sizes and contact time on the removal of (a) $NH_3$-N, (b) $NO_3$-N, and (c) $NO_2$-N respectively using sawdust (initial concentration: 0.5 mg/L solution; dosage of sawdust: 10 g; pH 6-7)

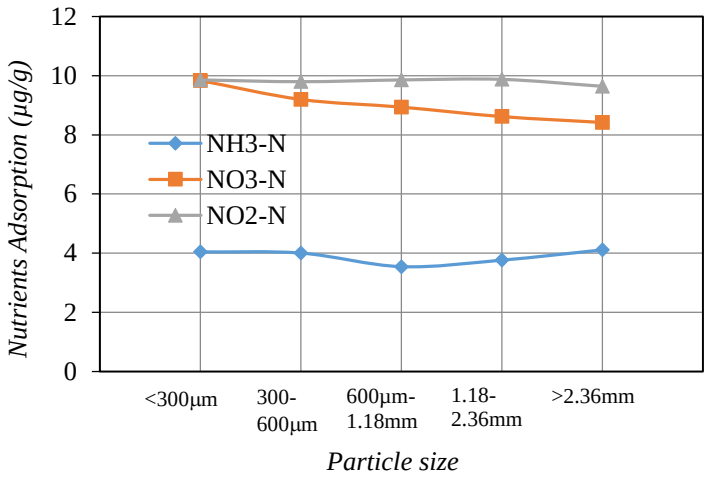


Figure 4.6 Nutrients adsorption effect (µg/g) for different particle sizes of sawdust on the removal of nutrients (initial concentration: 0.5 mg/L solution; dosage of sawdust: 10 g; pH 6-7)

### 4.2.4. Effect of pH

The effect of pH on nutrient adsorption using sawdust was studied and is shown in Figure 4.7(a-c). The pH of solution was controlled by adding NaOH and HCl. The results revealed that pH has mostly insignificant effect on nutrient removal, but the adsorption capacity decreases slightly for $NO_2$-N only with increasing pH, as shown in Figure 4.8. Maximum adsorption at acidic pH indicates that low pH leads to an increase in $H^+$ ions on the carbon surface. As a result, a positively charged surface site on the sawdust favours the adsorption of $NO_2$-N due to the strong electrostatic attraction (Ozturk and Bektas, 2004). The maximum percentage removal of $NO_2$-N reached 98% in 45 hours for pH 4. For a higher value of pH, the interaction between acidic surface groups and nitrite ions becomes weak and adsorption ability decreases.

For the complete range of pH, similar removal and adsorption characteristics are shown for $NH_3$-N and $NO_3$-N. This is because the sawdust shows a positive surface charge in a wide range of pH during the adsorption process (Dobrowolski and Otto, 2010). The maximum removal of 35% and 100% for $NH_3$-N and $NO_3$-N was found within 10 minutes of retention time.

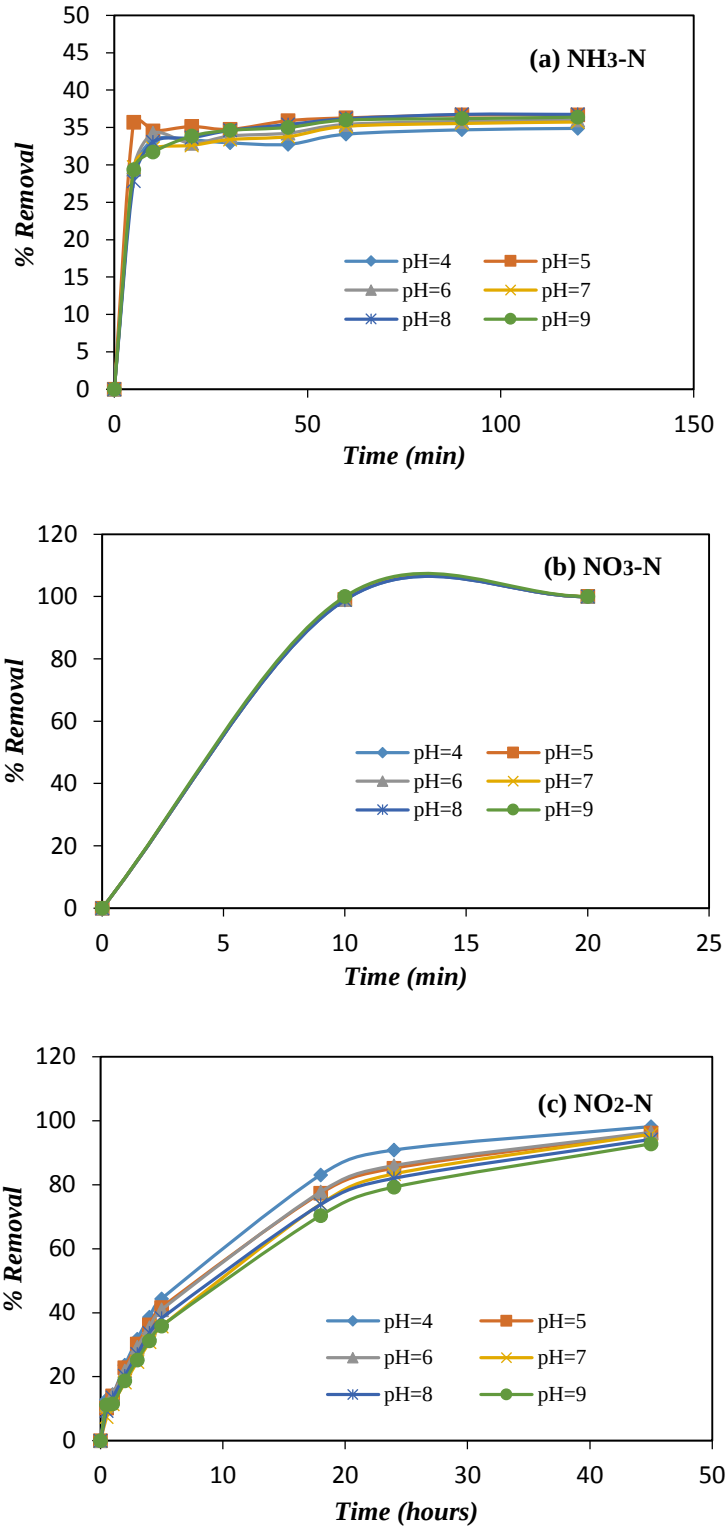


Figure 4.7 Effect of pH and contact time on the removal of (a) $NH_3$-N and (b) $NO_3$-N, and (c) $NO_2$-N respectively using sawdust (initial concentration: 0.5 mg/L; 10 g of sawdust with particle size < 300µm)

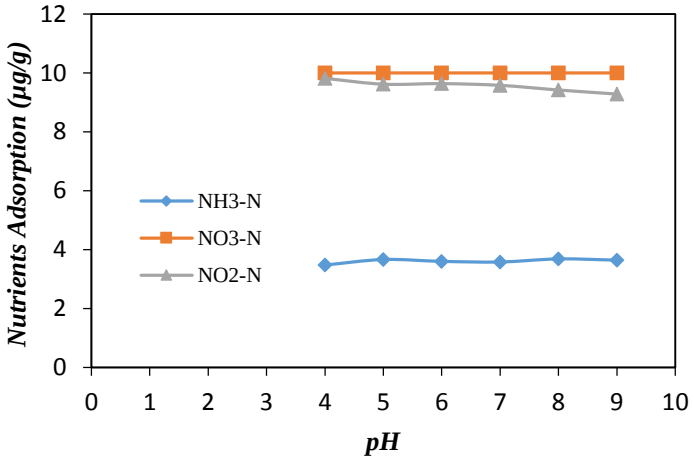


Figure 4.8 Nutrients adsorption (µg/g) for different pH of sawdust on the removal of nutrients (initial concentration: 0.5 mg/L solution; dosage of sawdust: 10 g with particle size < 300µm)

### 4.2.5. Effect of Contact Time

The effect of contact time on nutrient removal is shown in Figures 4.1, 4.3, 4.5, and 4.7. It is evident that contact time has a significant effect on the adsorption of dissolved nutrients onto sawdust. The Figures show that $NH_3$-N and $NO_3$-N follow a similar trend of adsorption characteristics.

In general, it was found that the percentage removal of $NO_2$-N from an aqueous solution increased rapidly and reached up to 80% in the first 20 hours. This was then increased slowly to 45 hours and reached 99% of removal. A further increase in contact time had a negligible effect on the removal process. This trend may be explained by the mechanism of the adsorption process. The mechanism of nutrient transfer to solid surfaces includes diffusion through the fluid film around the sawdust particle and diffusion through the pores to the internal sites. Initially, the concentration slope between the film and solid surface was large, and as a result, the transfer of solute onto the solid surface was faster. The solute therefore takes more time to transfer from the solid surface to the internal adsorption sites through the pores. During this time, the intraparticle diffusion becomes predominant.

However, $NH_3$-N and $NO_3$-N showed rapid adsorption in the first 15 minutes and decreased gradually to reach equilibrium. High removal within a short period of

time indicates a high degree of affinity for $NH_3$-N and $NO_3$-N and this is in agreement with chemisorptions being the rate controlling step (Ho et al., 2000; Hameed et al., 2008).

### 4.2.6. Adsorption Isotherm Models

The adsorption isotherm model was analyzed using two different categories of batch experiments – varying concentrations and dosages. The Langmuir and Freundlich models were analyzed by using Eq. (4.4) and (4.5) respectively. Plots of $1/q$ and $1/C$ for Langmuir model and log $q$ versus log $C$ for Freundlich model are given in appendix A.

#### 4.2.6.1. Langmuir Isotherm Model

- **Based on Concentration Test**

Derived from a concentration test, the Langmuir model using Eq. (4.4) was fitted with experimental data and is shown in Table 4.1. The values of $q_m$ and $K_{ads}$ were calculated from the slope and intercept of the linear plots of the Langmuir adsorption isotherm respectively. The maximum Langmuir adsorption capacity ($q_m$) was found to be 0.048 mg/g, 0.021 mg/g and 0.042 mg/g for $NH_3$-N, $NO_3$-N, and $NO_2$-N respectively. The values of $K_{ads}$ in the Langmuir model for $NO_3$-N, and $NO_2$-N were found to be very high ($K_{ads}$ >1), which indicates that the ions of these nutrients was strongly adsorbed onto the sawdust.

The variation of adsorption intensity ($R_L$) with concentrations of solution is shown in Fig. 4.9. The values of $R_L$ for $NH_3$-N, $NO_3$-N, and $NO_2$-N were found to vary from 0.47-0.9 to 0.002-0.02, and 0.0007-0.007 respectively. The value of $R_L$ in the range of $0 < R_L < 1$ indicates that sawdust can be used as an appropriate adsorbent for the removal of these nutrients from stormwater.

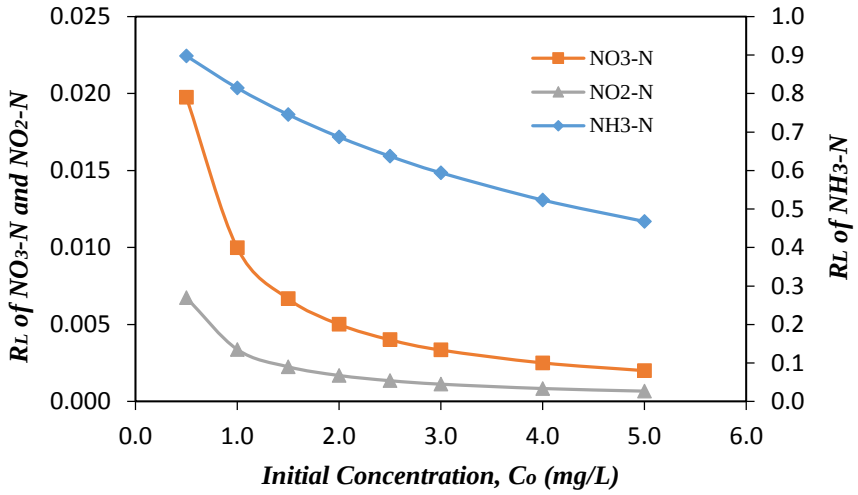


Figure 4.9 Variation of adsorption intensity ($R_L$) for $NH_3$-N, $NO_3$-N, and $NO_2$-N

Table 4.1 Parameters of the Langmuir isotherm for nutrients based on concentration test

| Species | Isotherm equation | $R^2$ | 1/(*q*m *K*ads) | *q*m *K*ads | 1/*q*m | *q*m (mg/g) | *K*ads |
|---|---|---|---|---|---|---|---|
| $NH_3$-N | y = 91.779x + 20.886 | 0.944 | 91.779 | 0.011 | 20.886 | 0.048 | 0.228 |
| $NO_3$-N | y = 0.473x + 46.922 | 0.844 | 0.473 | 2.114 | 46.922 | 0.021 | 99.201 |
| $NO_2$-N | y= 0.0806x + 23.746 | 0.451 | 0.081 | 12.407 | 23.746 | 0.042 | 294.615 |

- **Based on Dosage Test**

Table 4.2 lists the values of $q_m$ and $K_{ads,}$ which were calculated from the slope and intercept of the linear plots of experimental data obtained from the dosage test. The Langmuir adsorption maximum capacity values of $q_{m,}$ were 0.0647 mg/g and 0.0188 mg/g for $NO_3$-N and $NO_2$-N, respectively. The value of Langmuir constants for $NO_3$-N and NO2-N was very high (K>1). This high value indicated that $NO_3$-N and NO2-N were strongly adsorbed onto the sawdust. Negative values for $NH_3$-N indicated the inadequacy of the isotherm model to explain the adsorption process (Ramakrishna and Viraraghavan, 1997).

Table 4.2 Parameters of the Langmuir isotherm for nutrients based on dosage test

| Adsorbate | Isotherm equation | $R^2$ | 1/(*q*m *K*ads) | *q*m *K*ads | 1/*q*m | *q*m | *K*ads |
|---|---|---|---|---|---|---|---|
| $NH_3$-N | y= 164.19x - 103.55 | 0.955 | 164.19 | 0.0061 | -103.550 | -0.0097 | -0.6307 |
| $NO_3$-N | y=5.6327x + 15.445 | 0.975 | 5.6327 | 0.1775 | 15.445 | 0.0647 | 2.7420 |
| $NO_2$-N | y= 0.5736x + 53.162 | 0.805 | 0.5736 | 1.7434 | 53.162 | 0.0188 | 92.6813 |

#### 4.2.6.2. Freundlich Isotherm Model

The Freundlich model is based on the relationship between the adsorbed quantity (*q*) and the remaining solute concentration (*C*). According to the Freundlich equation, the isotherm does not reach a plateau as *C* increases (Limousin et al., 2007).

- **Based on Concentration Test**

The values of *K* and *n* in the Freundlich isotherm (Table 4.3) were calculated from the interception and slope of the linear plot (Eq. 4.6), based on the concentration test. In general, an increase in *K* is followed by an increase in the adsorption capacity of the sawdust. The *K* values show that sawdust is extremely effective in removing $NO_2$-N. The *n* value indicates the favourability of sorption. Generally, *n* values in the range of 2-10 represent effective adsorption characteristics, 1-2 reflect moderate characteristics, and less than 1 indicates poor adsorption characteristics (Hamdaoui, 2006). Moreover, the closer the *n* value of Freundlich is to zero, the more heterogeneous the system is (Aksu and Gonen, 2004). The results reveal that sawdust is an effective adsorbent for $NO_3$-N and NO2-N (n > 2). However, when the *n* value is lower than 2 for $NH_3$-N a complex adsorption characteristic is shown.

Table 4.3 Parameters of the Freundlich isotherm for nutrients based on concentration test

| Species | Isotherm Equation | $R^2$ | 1/*n* | *n* | log *K* | *K* (mg/g) |
|---|---|---|---|---|---|---|
| $NH_3$-N | y = 0.6701x - 2.0791 | 0.907 | 0.670 | 1.492 | -2.079 | 0.008 |
| $NO_3$-N | y =0.4348x - 1.3037 | 0.910 | 0.435 | 2.300 | -1.304 | 0.050 |
| $NO_2$-N | y = 0.3875x - 0.788 | 0.718 | 0.388 | 2.581 | -0.788 | 0.163 |

- **Based on Dosage Test**

The parameters of the Freundlich isotherm are shown in Table 4.4 and these are derived from the dosage test. The values of *K* and *n* were calculated from the intersection and slope. In general, as *K* increases the adsorption capacity of the adsorbent increases. *K* values showed that sawdust was more effective at removing $NO_2$-N. The *n* value indicates the favourability of sorption.

The Freundlich isotherm, based on a dosage test, found that all nutrients have *n* values less than 2, which shows poor adsorption characteristics (Hamdaoui, 2006). Moreover, the *n* values are close to zero, which indicates that the system is more heterogeneous (Aksu and Gonen, 2004).

Table 4.4 Parameters of the Freundlich isotherm for nutrients based on dosage test

| Species | Isotherm equation | $R^2$ | 1/*n* | *n* | log *K* | *K* |
|---|---|---|---|---|---|---|
| $NH_3$-N | y = 1.6927x - 1.8477 | 0.946 | 1.693 | 0.591 | -1.848 | 0.158 |
| $NO_3$-N | y = 0.672 x - 1.193 | 0.986 | 0.672 | 1.488 | -1.193 | 0.303 |
| $NO_2$-N | y = -x | 1.000 | -1.000 | -1.000 | 0.000 | 1.000 |

Comparing the correlation coefficients in both the Langmuir and Freundlich models based on a concentration test, it was found that the Freundlich model ($R^2$ = 0.9098 and 0.7182) proved a more effective fit than the Langmuir model ($R^2$ = 0.8442 and 0.4518) for $NO_3$-N and $NO_2$-N, respectively. But $NH_3$-N fitted with the Langmuir model when $R^2$ = 0.9444, and with the Freundlich model when $R^2$ = 0.9072. It appeared that $NH_3$-N adsorption fitted well with both the Langmuir and Freundlich isotherms, $NO_3$-N adsorption fitted well with the Freundlich isotherm, but only moderately well with the Langmuir isotherm, and $NO_2$-N adsorption followed the Freundlich isotherm with a relatively low degree of regression coefficient.

Based on the dosage test, the correlation coefficient of $NH_3$-N had a slightly bigger value for the Langmuir model ($R^2$ = 0.955) than for the Freundlich model ($R^2$ = 0.946). However, $NO_3$-N and NO2-N had a closer correlation to the Freundlich model ($R^2$ = 0.986 and 1 for $NO_3$-N and $NO_2$-N respectively) than to the Langmuir model ($R^2$ = 0.975 and 0.805 for $NO_3$-N and $NO_2$-N, respectively). Therefore, as the Freundlich-type adsorption isotherm is an indication of the surface heterogeneity of the adsorbent,

this leads to the conclusion that the surface of sawdust is made from small heterogeneous adsorption patches (Ajmal et al., 1997).

### 4.2.7. Kinetic Models

The kinetics of adsorption describe the rate of nutrient ion uptake on sawdust and this rate controls the equilibrium time. The kinetic parameter provides significant information about the mechanism of adsorption for designing and modelling the processes. Thus, the effect of the initial concentration and its contact time were analysed (Fig. 4.10) from the kinetic position.

From Fig. 4.10, it can be seen that the rates of adsorption were very rapid for all adsorbates in the early stages of contact time; after that, the rates decreased gradually with time until adsorption was reached at the point of equilibrium. This trend of adsorption kinetics shows that the external diffusion is rate-controlling at the beginning of contact time (Hamdaoui, 2006; Gupta et al., 2012). When the adsorption on the exterior surface reached saturation point, nutrients diffused into the pores of the sawdust and were adsorbed by the interior surface of the sawdust. The equilibrium time for $NH_3$-N was obtained within 15 minutes for the whole range of concentrations. While $NO_3$-N and $NO_2$-N reached equilibrium time within 30 minutes and 50 hours, respectively, for a concentration of less than 2 mg/L, they took longer for concentrations from 2 to 5 mg/L; the average of their equilibrium time was 240 minutes and 70 hours for $NO_3$-N and $NO_2$-N, respectively.

In order to investigate the experimental data (Fig. 4.10), whether following the kinetic or diffusion rate controlling model, an analysis was conducted with regard to the intraparticle model. The investigation continued using kinetic models such as the pseudo-first-order model, and pseudo-second-order model.

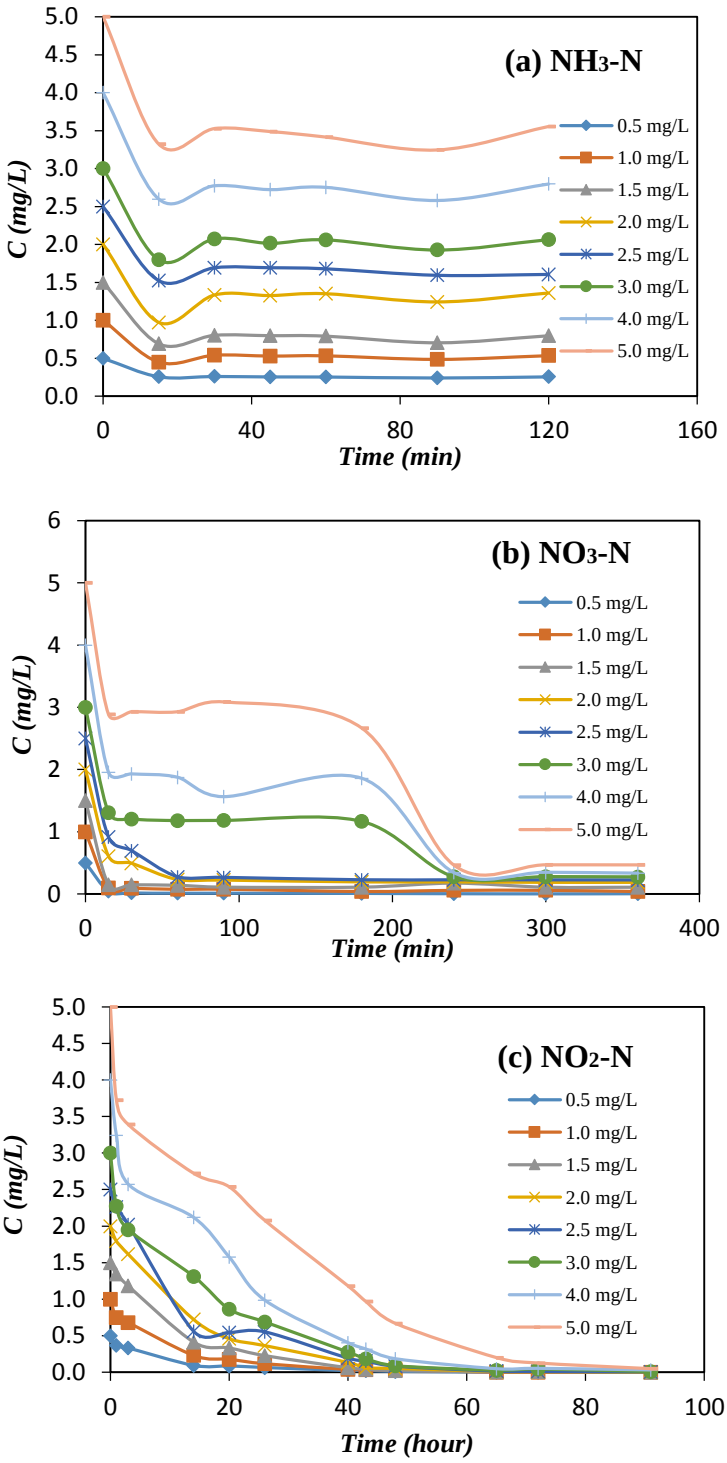


Figure 4.10 Dynamic of nutrients adsorbed onto sawdust (a) $NH_3$-N, (b) $NO_3$-N, and (c) $NO_2$-N.

#### 4.2.7.1. Intraparticle Diffusion Model

From the general guidelines, in order to identify the nutrient sorption process mechanism, the experimental data was identified by checking the adsorption equilibrium time. It is known that $NH_3$-N and $NO_3$-N, reach equilibrium time very rapidly, within 15 and 30 minutes respectively, while $NO_2$-N achieved the point of equilibrium at 70 hours. As equilibrium was reached before 3 hours, it can be said that $NH_3$-N and $NO_3$-N sorption processes are kinetically controlled. However, as $NO_2$-N took more than 3 hours, it is possible that the $NO_2$-N sorption process was either kinetically and diffusion controlled or both.

However, this first statement needs to be verified by analysing the experimental data along with the intraparticle diffusion model. As predicted, $NH_3$-N and $NO_3$-N did not follow this model. The regression coefficient of the linear line that was obtained by plotting $q_t$ against $t^{0.5}$ was very low (0.005 to 0.611 and 0.153 to 0.8 for $NH_3$-N and $NO_3$-N, respectively). So, neither of these nutrients are diffusion rate controlled.

On the other hand, $NO_2$-N adsorption showed intraparticle diffusion. The plot of $q_t$ against $t^{1/2}$ for $NO_2$-N adsorption is shown in Fig. 4.11 which represents two stages of adsorption. The first step represents the adsorption of $NO_2$-N onto the sawdust surface. The second step concerns the diffusion of $NO_2$-N to the adsorption site (Kalavathy et al., 2005; Gupta et al., 2012). A surface adsorption mechanism took place in the first 25 hours of contact time for a $NO_2$-N concentration of 0.5-2.5 mg/L, and 36 hours of contact time for a concentration range of 3.0-5.0 mg/L. Diffusion then became rate controlling. The slope of the second linear portion yields the intraparticle diffusion rate constant $k_{d2}$ (Table 4.5). Results show that higher initial concentration reveals higher diffusion rate. This is due to the higher concentration remaining in the solution phase after surface adsorption, resulting in an increase of the driving force and increasing the diffusion rate. The values of rate constant were found 0.179-4.772 µg/g hours$^{0.5}$ for a $NO_2$-N concentration range of 0.5 - 5 mg/L.

The plotting of the experimental and calculation data of this model can be seen in Fig. 4.12. A fairly positive correlation between the experimental and calculation data was achieved during the whole adsorption process. Some deviations occurring in the final stage might have been due to the difference between the mass transfer rates in the initial and final stages of adsorption.

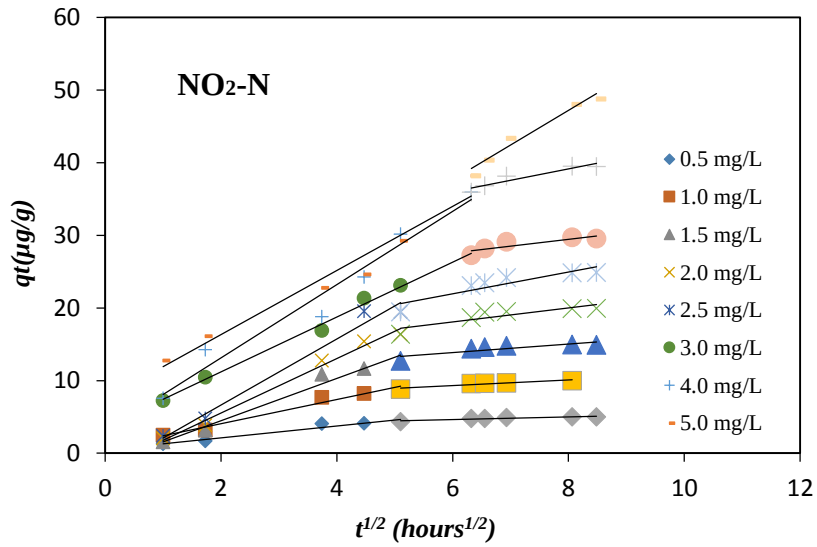


Figure 4.11 Intraparticle diffusion plot of $NO_2$-N adsorbed onto sawdust

Table 4.5 Intraparticle diffusion model constants and correlation coefficient for $NO_2$-N adsorbed onto sawdust.

| Concentration (mg/L) | $M_1$ | $kd_1$ (µg/g hours$^{0.5}$) | $R_1^2$ | $M_2$ | $kd_2$ (µg/g hours$^{0.5}$) | $R_2^2$ |
|---|---|---|---|---|---|---|
| 0.5 | 0.488 | 0.819 | 0.953 | 3.564 | 0.179 | 0.867 |
| 1.0 | 0.709 | 1.675 | 0.976 | 7.025 | 0.383 | 0.904 |
| 1.5 | -1.354 | 2.915 | 0.976 | 10.374 | 0.581 | 0.726 |
| 2.0 | -1.965 | 3.755 | 0.989 | 12.233 | 0.973 | 0.783 |
| 2.5 | -2.437 | 4.546 | 0.981 | 12.986 | 1.494 | 0.828 |
| 3.0 | 3.645 | 3.777 | 0.994 | 21.794 | 0.958 | 0.766 |
| 4.0 | 3.038 | 5.040 | 0.962 | 26.513 | 1.578 | 0.893 |
| 5.0 | 7.484 | 4.415 | 0.957 | 9.023 | 4.772 | 0.960 |

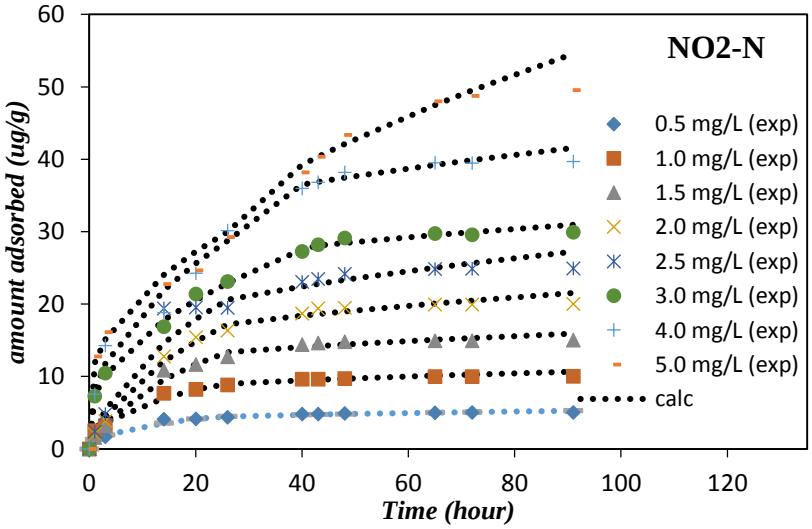


Figure 4.12 Experimental data is fitted with intraparticle diffusion model for $NO_2$-N adsorption

However, the plots (Fig 4.12) do not show zero intercepts but shows two intercepts $M_1$ and $M_2$. In this adsorption process, the higher concentration of solution results in a higher value of intercepts indicating that intraparticle diffusion may not be the sole dominating factor controlling the mechanism of adsorption process (Bhattacharyya and Gupta, 2006). This may be explained by the liquid film diffusion model.

### 4.2.7.2. The Liquid Film Diffusion Model

The plot of $-ln\ (1-F)$ vs t (Fig. 4.13) has a positive linearity with $R^2$ from 0.929 to 0.995 and the intercepts of -0.1937 to 0.081 (Table. 4.6). Even though the linear curves did not pass through the origin as required by the model, all of the intercept values were close to zero. Therefore, the interaction process might be controlled by diffusion from the liquid phase (Bhattacharyya and Gupta, 2006). The film diffusion rate coefficient had values in the range of 0.051 to 0.093 $min^{-1}$ for $NO_2$-N concentrations from 0.5 mg/L to 5 mg/L.

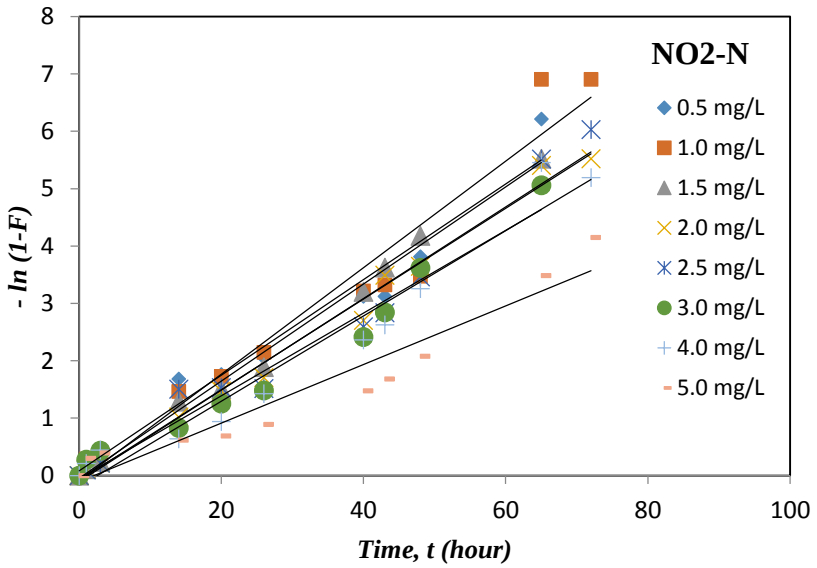


Figure 4.13 Liquid film diffusion plot of $NO_2$-N adsorbed onto sawdust

Table 4.6 Liquid film diffusion model constants and correlation coefficient for $NO_2$-N adsorbed onto sawdust.

| *Concentration (mg/L)* | *equation* | *kfd (1/min)* | *intercepts* | $R^2$ |
|---|---|---|---|---|
| 0.5 | y = 0.0834x + 0.0806 | 0.083 | 0.081 | 0.963 |
| 1.0 | y = 0.0929x - 0.0897 | 0.093 | -0.090 | 0.956 |
| 1.5 | y = 0.0847x - 0.0456 | 0.085 | -0.046 | 0.995 |
| 2.0 | y = 0.0791x - 0.0876 | 0.079 | -0.088 | 0.990 |
| 2.5 | y = 0.0798x - 0.1091 | 0.080 | -0.109 | 0.968 |
| 3.0 | y = 0.0722x - 0.0547 | 0.072 | -0.055 | 0.970 |
| 4.0 | y = 0.0744x - 0.1937 | 0.074 | -0.194 | 0.958 |
| 5.0 | y = 0.051x - 0.1083 | 0.051 | -0.108 | 0.929 |

#### 4.2.7.3. Pseudo-First Order Kinetic Model

The values of the pseudo-first order model are presented in Table 4.7. The regression coefficient ($R^2$) values have a range of 0.741- 0.995. The calculated $q_e$ values obtained for all nutrients from this model did not show a positive relationship to the experimental data. This confirms that the pseudo-first-order model is not suitable for the prediction of the adsorption kinetic of nutrients onto sawdust.

In the case of $NH_3$-N, the adsorption rate, using the pseudo-first model is shown in Table 4.7. The equilibrium was reached at the beginning of the experiments. Thus, in order to avoid a mathematical error caused by the logarithm of negative number in Equation 4.10, the appropriate $q_e$ value was chosen hence the $q_t$ value was still higher than $q_e$. (Ho and McKay, 1998; Plazinski et al., 2009). From Table 4.7, the values of the correlation coefficients were found to be in the range of 0.741 to 0.914. However, the calculated $q_e$ obtained did not correlate with the experimental one, so it can be said that this model is not appropriate for describing the entire process.

In a similar observation, it was demonstrated that for $NO_3$-N, the values of calculated $q_e$ (Table. 4.7) did not to match with the experimental data. This confirms that this adsorption process cannot be explained by the pseudo-first model.

$NO_2$-N was found to fit well with the Lagergren model, especially with regard to low initial concentrations. The calculated $q_e$ (Table. 4.7) was closer to the experimental data and $R^2 > 0.9$. The adsorption first-order rate constants were found in a range of 0.051 to 0.090/min for an initial concentration of 0.5 to 5.0 mg/L. Also,

the normalized standard deviation $\Delta q$ were very small (0.01-0.21 %) provides better goodness of fit.

As an addition to this first-order model, a plot of the rate constant $k_1$ with initial concentration (Fig. 4.14) was examined to obtain the rate of adsorption ($k_a$) and desorption ($k_{ds}$). This plot was only used for $NO_2$-N as the model fitted more effectively than other adsorbates. The Figure shows the regression coefficient as 0.791. The adsorption and desorption rate constants were $k_a$ = 0.007 L/mg min and $k_{ds}$ = 0.094/min, respectively. Thus, based on the Azizian model, where the equilibrium constant is independent of the initial concentration of solute (Azizian, 2004), the equilibrium constant ($K = k_a/k_{ds}$) of this process was equal to 0.074 L/mg.

Overall, the adsorption first-rate constant ($k_1$) decreases with the increasing concentration of nutrient solution. This is understandable, since the $k_1$ parameter is the time-scaling factor which establishes how fast the equilibrium in the system can be achieved (Plazinski et al., 2009).

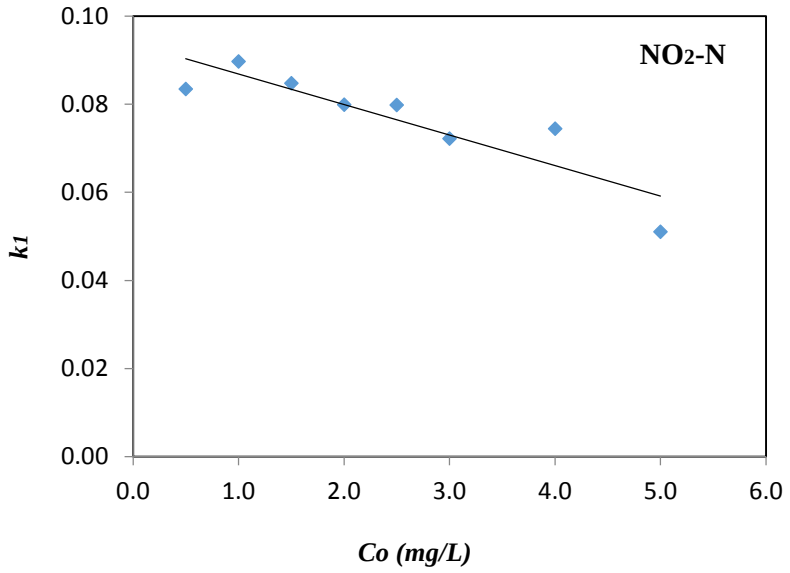


Figure 4.14 Plot of rate constant ($k_1$) of the first order model for adsorption of nutrients on sawdust vs initial concentration $NO_2$-N.

Table 4.7 Kinetic parameters of pseudo-first order plot for nutrients adsorbed onto sawdust.

| Adsorbate | Concentration (mg/L) | $q_e$(exp) (µg/g) | $q_e$(cal) (µg/g) | *k1* (1/min) | $R^2$ | Δ*q*(%) |
|---|---|---|---|---|---|---|
| $NH_3$-N | 0.5 | 2.590 | 1.783 | 0.052 | 0.864 | 0.81 |
| $NH_3$-N | 1.0 | 5.510 | 3.588 | 0.028 | 0.847 | 1.01 |
| $NH_3$-N | 1.5 | 8.090 | 6.839 | 0.042 | 0.914 | 0.20 |
| $NH_3$-N | 2.0 | 10.280 | 8.510 | 0.017 | 0.741 | 0.25 |
| $NH_3$-N | 2.5 | 9.770 | 5.128 | 0.019 | 0.762 | 1.88 |
| $NH_3$-N | 3.0 | 12.030 | 8.266 | 0.022 | 0.821 | 0.82 |
| $NH_3$-N | 4.0 | 14.210 | 10.156 | 0.037 | 0.798 | 0.68 |
| $NH_3$-N | 5.0 | 17.570 | 14.088 | 0.039 | 0.911 | 0.33 |
| $NO_3$-N | 0.5 | 4.970 | 0.280 | 0.010 | 0.827 | 9.86 |
| $NO_3$-N | 1.0 | 9.590 | 0.568 | 0.046 | 0.941 | 7.01 |
| $NO_3$-N | 1.5 | 13.920 | 5.161 | 0.065 | 0.813 | 4.86 |
| $NO_3$-N | 2.0 | 18.200 | 5.222 | 0.022 | 0.837 | 5.17 |
| $NO_3$-N | 2.5 | 22.770 | 7.125 | 0.025 | 0.903 | 5.22 |
| $NO_3$-N | 3.0 | 27.260 | 30.090 | 0.022 | 0.761 | 4.79 |
| $NO_3$-N | 4.0 | 36.680 | 35.945 | 0.020 | 0.937 | 5.09 |
| $NO_3$-N | 5.0 | 45.320 | 57.974 | 0.028 | 0.980 | 5.18 |
| $NO_2$-N | 0.5 | 5.00 | 4.613 | 0.083 | 0.963 | 0.03 |
| $NO_2$-N | 1.0 | 10.00 | 10.386 | 0.090 | 0.938 | 0.01 |
| $NO_2$-N | 1.5 | 15.00 | 15.699 | 0.085 | 0.995 | 0.01 |
| $NO_2$-N | 2.0 | 20.00 | 22.134 | 0.080 | 0.987 | 0.05 |
| $NO_2$-N | 2.5 | 24.93 | 27.805 | 0.080 | 0.968 | 0.06 |
| $NO_2$-N | 3.0 | 29.91 | 31.592 | 0.072 | 0.970 | 0.01 |
| $NO_2$-N | 4.0 | 39.69 | 48.173 | 0.074 | 0.958 | 0.21 |
| $NO_2$-N | 5.0 | 49.53 | 55.197 | 0.051 | 0.929 | 0.06 |

#### 4.2.7.4. Pseudo-Second Order Kinetic Model

The advantage of the pseudo-second order model is in its potential for obtaining all kinetic parameters (the adsorption capacity, the rate constant of pseudo-second order, and the initial adsorption rate), with no need to identify any parameters in advance (Ho, 2006). Due to this advantage, the pseudo-second order expression was applied to investigate the adsorption process. The results are shown in Fig. 4.15 and Table 4.8, respectively. The correlation coefficient ($R^2$) was found to be more than 0.95, except for $NO_3$-N, which, at a higher concentration only reached a value of 0.783. Almost all of the calculated $q_e$ ($q_{e(cal)}$) for nutrients matched with the experimental $q_e$

($q_{e(exp)}$) in this pseudo-second model. The applicability of this model was also validated in relation to the normalized standard deviation. It can be understood that this model was applicable for explaining the whole of the process, as the standard deviation was mostly less than 0.1.

Based on plotting $t/q_t$ against $t$ (Fig. 4.15), the Figure shows that almost all of the nutrients have a linear relationship. This can be proven by the high regression coefficient for most nutrient adsorption. It appears that the correlation coefficient of fitting the pseudo-second order ($R^2$) tends to decrease with an increase in the initial concentration; 0.998 at 0.5 mg/L becomes 0.977 mg/L at 5 mg/L for $NH_3$-N; 1 mg/L at 0.5 mg/L becomes 0.783 at 5 mg/L for $NO_3$-N, and 0.999 at 0.5 mg/L becomes 0.946 at 5 mg/L for $NO_2$-N, respectively. In the pseudo-first order model, the trend of $R^2$ for $NH_3$-N and $NO_3$-N increases with the increase in the concentration of the solution (0.864 and 0.827 at 0.5 mg/L becomes 0.911 and 0.980 at 5 mg/L for $NH_3$-N and $NO_3$-N, respectively). Thus the $NH_3$-N and $NO_3$-N are well in agreement with Azizian (2004) who states that by increasing the initial concentration of the solute, the correlation of experimental data to the pseudo-second order kinetics model decreases, while that to the pseudo-first order model increases.

The rate constants of second-order coefficients tended to decrease as the initial concentration increases. The rate constants of the second order coefficients ($k_2$) were in the range of 0.038-0.539 g/mg min, 0.0003-0.133 g/mg min, and 0.001-0.039 g/mg min for $NH_3$-N, $NO_3$-N, and $NO_2$-N, respectively (Table 4.8).

In case of initial adsorption rates ($h$), differences in the results were found for all of the nutrients. Generally, the initial adsorption rates for $NH_3$-N and $NO_2$-N increased with an increase in the initial concentration of nutrients, which was due to the increase in the driving force at a higher concentration. However, an exception was found at a concentration of 1.5 mg/L for $NH_3$-N. As nitrogen has a very high adsorption rate, this might be the result of both the higher amount of solution adsorbed at equilibrium time, as well as its second-order constant. Against $NH_3$-N, initial adsorption rates for $NO_3$-N decrease with an increase in the solution concentration. However, this results in the same exception at a concentration of 1.5 mg/L and, the same explanation of this phenomenon is as for $NH_3$-N.

Overall, it can be stated that the kinetic is well described by pseudo second order for $NH_3$-N, $NO_3$-N, and $NO_2$-N adsorption onto sawdust.

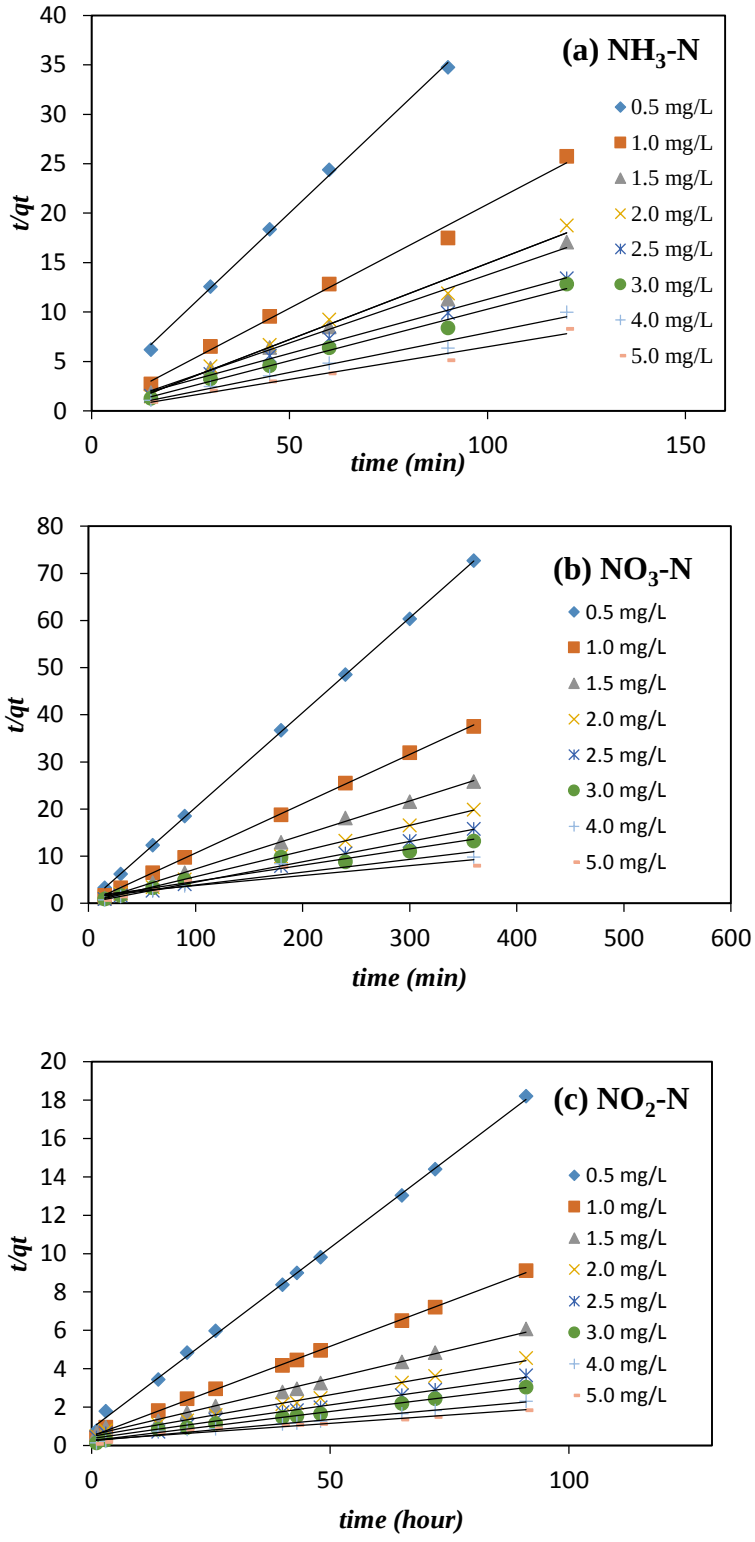


Figure 4.15 Pseudo-second order plots of nutrients adsorbed onto sawdust (a) $NH_3$-N, (b) $NO_3$-N, and (c) $NO_2$-N

Table 4.8 Kinetic parameters of pseudo-second order plot for nutrients adsorbed onto sawdust

| Adsorbate | Concentration (mg/L) | $q_{e(exp)}$ (µg/g) | $q_{e(cal)}$ (µg/g) | $k_2$ (g/mg min) | $h$ (µg/g min) | $R^2$ | $\Delta q$(%) |
|---|---|---|---|---|---|---|---|
| $NH_3$-N | 0.5 | 2.590 | 2.627 | 0.148 | 1.023 | 0.998 | 0.00 |
| $NH_3$-N | 1.0 | 5.510 | 4.757 | 0.324 | 7.326 | 0.993 | 0.16 |
| $NH_3$-N | 1.5 | 8.090 | 7.252 | 0.539 | 28.329 | 0.989 | 0.09 |
| $NH_3$-N | 2.0 | 10.280 | 6.481 | 0.047 | 1.969 | 0.982 | 1.14 |
| $NH_3$-N | 2.5 | 9.770 | 9.132 | 0.035 | 2.945 | 0.994 | 0.04 |
| $NH_3$-N | 3.0 | 12.030 | 9.579 | 0.069 | 6.325 | 0.987 | 0.35 |
| $NH_3$-N | 4.0 | 14.210 | 12.469 | 0.052 | 8.123 | 0.983 | 0.13 |
| $NH_3$-N | 5.0 | 17.570 | 15.129 | 0.038 | 8.673 | 0.977 | 0.16 |
| $NO_3$-N | 0.5 | 4.950 | 4.978 | 0.133 | 3.294 | 1.000 | 0.00 |
| $NO_3$-N | 1.0 | 9.590 | 9.560 | 0.056 | 5.076 | 1.000 | 0.00 |
| $NO_3$-N | 1.5 | 13.920 | 13.850 | 0.074 | 14.245 | 0.999 | 0.00 |
| $NO_3$-N | 2.0 | 18.200 | 18.382 | 0.013 | 4.380 | 1.000 | 0.00 |
| $NO_3$-N | 2.5 | 22.770 | 23.202 | 0.008 | 4.429 | 1.000 | 0.00 |
| $NO_3$-N | 3.0 | 27.260 | 29.070 | 0.001 | 0.813 | 0.946 | 0.03 |
| $NO_3$-N | 4.0 | 36.680 | 36.765 | 0.001 | 0.865 | 0.889 | 0.00 |
| $NO_3$-N | 5.0 | 45.320 | 47.393 | 0.000 | 0.604 | 0.783 | 0.01 |
| $NO_2$-N | 0.5 | 5.000 | 5.308 | 0.039 | 1.111 | 0.999 | 0.02 |
| $NO_2$-N | 1.0 | 10.000 | 10.672 | 0.018 | 2.067 | 0.999 | 0.02 |
| $NO_2$-N | 1.5 | 15.000 | 16.949 | 0.006 | 1.861 | 0.996 | 0.08 |
| $NO_2$-N | 2.0 | 20.000 | 23.041 | 0.004 | 2.142 | 0.995 | 0.11 |
| $NO_2$-N | 2.5 | 24.930 | 28.490 | 0.003 | 2.765 | 0.994 | 0.09 |
| $NO_2$-N | 3.0 | 29.910 | 32.787 | 0.004 | 4.023 | 0.992 | 0.04 |
| $NO_2$-N | 4.0 | 39.690 | 45.045 | 0.002 | 4.098 | 0.979 | 0.08 |
| $NO_2$-N | 5.0 | 49.530 | 57.143 | 0.001 | 3.608 | 0.946 | 0.11 |

### 4.3.Concluding Remarks

The adsorption capability of sawdust was investigated in batches and examined for removal of selected dissolved nutrients ($NH_3$-N, $NO_3$-N, and $NO_2$-N) from stormwater. The results show that sawdust is an effective adsorbent for removing these nutrients from an aqueous solution, especially at lower concentrations. The amount of sawdust dosage showed significant effects on nutrient removal but pH and particle sizes did not show such effect. The hundred percent removals were obtained for $NO_3$-N, and $NO_2$-N but only 55% removal was obtained for $NH_3$-N.The maximum removal of $NO_3$-N and $NH_3$-N was obtained within shorter period of contact time while it took

longer time to reach maximum removal for $NO_2$-N. The isotherm study shows that $NO_3$-N and $NO_2$-N adsorption follow Freundlichmodel fairly better than Langmuir, while $NH_3$-N adsorption follows both Langmuir and Freundlich isotherms.

The kinetics and mechanisms of sawdust were investigated using: the intraparticle diffusion, the liquid film diffusion, the pseudo-first-order, and the pseudo-second-order models. The adsorption kinetic was described well by the pseudo-second-order model for $NH_3$-N, $NO_3$-N and $NO_2$-N. The rate constants of pseudo-second order were found 0.038-0.539 g/mg min, 0.0003-0.133 g/mg min, and 0.001-0.039 g/mg min for $NH_3$-N, $NO_3$-N, and $NO_2$-N respectively. In the adsorption process for $NO_2$-N, the intraparticle diffusion was not the only rate controlling but film liquid diffusion also take part in the overall adsorption process.

# CHAPTER 5
# DYNAMIC ADSORPTION CHARACTERISTICS: DATA ANALYSIS AND DISCUSSION

## 5.1. Dynamic Process in Fixed-Bed

In the large-scale applications, continuous-flow fixed bed columns are often preferred. A large volume of contaminated water can be continuously treated using a defined quantity of sorbent in the column. In this system, the concentration of pollutant in water and adsorbent phases vary in both space and time. Thus, it makes difficult to design and optimization. Therefore a quantitative modelling approach is required.

The history of effluent concentration is the main feature of the dynamic behaviour of fixed-bed adsorption. This concentration-versus-time plot is commonly referred to as a breakthrough curve (BTC). The time taken for the appearance of the breakthrough along with the shape of the BTC are the important characteristics for determining the operation and the dynamic capacity of an adsorption column.

### 5.1.1. Mathematical Description

**Total Removal**

The breakthrough curves show the loading behaviour of nutrient to be removed from solution in fixed-bed column and is usually expressed in terms of normalized concentration defined as the ratio of effluent nutrient concentration to inlet nutrient concentration ($C/C_0$) as a function of time or volume of effluent for a given bed height (Aksu and Gonen, 2004). Effluent volume, $V_{eff}$ (mL) can be calculated as:

$$V_{eff} = Qt_{total} \tag{5.1}$$

where $Q$ and $t_{total}$ are the volumetric flow rate (mL/min) and the total flow time (min), respectively. The total quantity of nutrients adsorbed ($q_{total}$; mg) in the column for a fixed-feed concentration and flow rate of $Q$ is calculated according to Malkoc and Nuhoglu (2006):

$$q_{total} = \frac{QA}{1000} = \frac{Q}{1000}\int_{t=0}^{t=t_{total}} C_{ad}\, dt \tag{5.2}$$

where $A$ ($m^2$) is the area under the BTC which can be calculated by integrating the BTC, $C_{ad}$ (mg/L) is the concentration of nutrients adsorbed, which is taken as influent concentration, $C_o$(mg/L) – effluent concentration, $C$ (mg/L).

The total amount of $NH_3$-N, $NO_3$-N, and $NO_2$-N ions driven to column ($m_{total}$) is calculated as:

$$m_{total} = \frac{C_o Q\, t_{total}}{1000} \tag{5.3}$$

the total removal is calculated as:

$$Total\ removal\ (\%) = \frac{q_{total}}{m_{total}} * 100 \tag{5.4}$$

The maximum capacity of the column ($q_e$) is defined as the total amount of nutrient adsorption ($q_{total}$) per gram of sawdust ($x$) at the end of each experiment:

$$q_e = \frac{q_{total}}{X} \tag{5.5}$$

**The Dynamic Adsorption Capacity**

The dynamic adsorption capacity of sawdust $W_e$ (mg/g) may be calculated using the breakthrough time ($t_{breakthrough}$). The value of -$W_e$ is taken as a milligram of nutrient adsorption per gram of dry sawdust. The amount of nutrients adsorbed onto the sawdust at breakpoint may be calculated as:

$$W_e = \frac{(Co-C)Qt_{breakthrough}}{X} \tag{5.6}$$

where $Q$ is the flow rate of nutrient solution and $x$ is the weight of oven-dried sawdust.

**The Length-of -Unused-Bed Theory**

The fixed-bed column may be designed using various methods, which include the length-of-unused-bed (LUB) theory, the equilibrium theory for convex isotherms, the empty-bed contact-time approach, and the bed-depth service-time design approach (Cooney, 1998). The equivalent length of unused bed is used for preparing the adsorber. This parameter can be determined by analysing the BTC:

$$LUB = \left(1 - \frac{W_e}{q_e}\right) H \tag{5.7}$$

where $H$ is the bed length and $q_e$ is the adsorbed amount of nutrients in the saturated bed (mg/g).

### 5.1.2. Analysis of Adsorption Isotherm

Information relating to the capacity of sawdust or the amount of sawdust required to remove a unit mass of nutrients under the system conditions can be obtained by equilibrium studies. As the adsorption isotherms obtained from sorption data in a batch system are not able to represent the column equilibrium, the experimental data from the column experiments should be used to fit the isotherm models. Theoretically, for a specific ion exchange or adsorption system, the equilibrium isotherm, the capacity, and diffusion coefficient are independent of the experimental method. Also, in column experiments, the operating capacity and diffusion coefficient were expected to be independent of the flow rate (Deliyani et al, 2009). However, according to some references and these experiments, the operating capacity is dependent on the flow rate, and in the experiments, was different from that measured in the batch systems. Consequently, the equilibrium isotherm was likely to be influenced by the type of reactor used for its measurement (fixed-bed and batch reactor). The hydrodynamic differences between the two types of reactors led to a different physicochemical behaviour (Deliyani et al, 2009).

Equilibrium nutrient uptake ($q_e$) (or maximum capacity of the column) in the column is defined by Eq. (5.5) as the total amount of nutrients sorbed ($q_{total}$) per gram of sawdust ($x$) at the end of total flow time. Unadsorbed nutrient concentration at equilibrium in the column ($C_{eq}$; mg $L^{-1}$) can be defined by Eq. (5.8):

$$C_{eq} = \left(\frac{m_{total} - q_{total}}{V_{eff}}\right) 1000 \tag{5.8}$$

The most widely used isotherm equation for modelling the equilibrium is the Langmuir equation, which is valid for a monolayer sorption onto the surface of a finite number of identical sites, as given in Eq. (5.9).

$$q_e = \frac{Q^o b C_{eq}}{1 + b C_{eq}} \tag{5.9}$$

where $Q^\circ$ is the maximum amount of nutrients per unit weight of sawdust required to form a complete monolayer on the surface bound at high $C_{eq}$, and $b$ is a constant, related to the affinity of the binding sites. $Q^\circ$ represents a practical limiting adsorption capacity when the surface is fully covered with nutrients and assists in the comparison of adsorption performance, particularly in cases where the sorbent did not reach its full

saturation in experiments. $Q^{\circ}$ and $b$ can be determined from the linear plot of $C_{eq}/q_e$ versus $C_{eq}$.

The empirical Freundlich equation based on sorption on a heterogeneous surface is given below by Eq. (5.10).

$$q_e = KC_{eq}^{1/n} \tag{5.10}$$

where $K$ and $n$ are the characteristic Freundlich constants in the system. $K$ and $n$ are indicators of adsorption capacity and adsorption intensity, respectively. Eq. (5.11) can be linearised in logarithmic form and the Freundlich constants can be determined.

### 5.1.3. Modelling of Dynamic Adsorption Process

The fundamental transport equations for a fixed-bed are those of material balance between solid and fluid. The next key equation is the mass balance on the adsorbed solute. Also, the mathematical description of adsorption rate must be added to these transport equations given for the fixed bed. The last key equation for mathematical modelling of a fixed bed is the adsorption isotherm (Aksu and Gonen, 2004). These fundamental transport equations derived to model the fixed bed usually require complex numerical methods to solve. Because of this, various simple mathematical models have been developed to predict the dynamic behaviour of the column. In this research, the data from the column experiments was analysed using the Clark Model (Clark, 1987) and the Yoon and Nelson model (Yoon and Nelson, 1984). Both models are quite new and rely on new theoretical concepts.

#### 5.1.3.1. The Clark Model

The Clark model was developed using a mass-transfer concept in combination with the Freundlich isotherm. The reason for this is that, for any given concentration of material in the liquid phase, the capacity of the activated carbon at equilibrium can be determined from the appropriate adsorption isotherm. When the adsorbed material is in equilibrium with the influent concentration, the bed is “loaded” to capacity, and that portion of the bed is “exhausted”. In an ideal “plug flow” situation, the exhausted zone moves downward with time in service until the entire adsorbent bed is exhausted (Clark 1987).

$$K_T(C - C_e) = G_s \frac{dC}{dZ} \tag{5.11}$$

where: $K_T$ = mass-transfer coefficient ($min^{-1}$); $C_e$ = equilibrium value for nutrients at the solid surface (mg of solute/$m^3$); and, $G_s$ = flow rate of solvent per unit of cross-sectional area ($m^3min^{-1}m^{-2}$); $Z$ = column height (cm).

Assuming that all the solvent is removed, an ideal mass balance over the entire column would be:

$$G_s C = L_a q_e \tag{5.12}$$

where: $L_a$ is mass velocity of adsorbent to keep the mass-transfer zone stationary (mg $h^{-1}m^{-2}$); and, $q_e$ is concentration of adsorbed solute per unit weight of adsorbent (mg of solute/mg of adsorbent)

If all the solvent is removed, then:

$$\frac{L_a}{G_s} = \frac{C}{q_e} \tag{5.13}$$

From equation (5.11)

$$\frac{dC}{C - C_e} = \frac{K_T dZ}{G_s} \tag{5.14}$$

Using the Freundlich equation:

$$q_e = K(C_e)^{1/n} \tag{5.15}$$

where: $K$= Freundlich constant; $1/n$ = slope of the isotherm.

From equation (5.15):

$$C_e = (1/K)^n {q_e}^n \tag{5.16}$$

Substituting Eq.5.13 and Eq. 5.16 into Eq. 5.14 yields

$$\frac{C}{C_o} = \frac{1}{(1 + A_C e^{-rt})^{\frac{1}{n}-1}} \tag{5.17}$$

The linearisation of Eq. 5.17 according to Hamdaoui (2006):

$$ln\left[\left(\frac{C_0}{C}\right)^{n-1} - 1\right] = \ln A_C - rt \quad (5.18)$$

Where $A_C$ and $r$ are the Clark constants:

$$A_C = exp\left(\frac{K_C N_0 Z}{U}\right) \quad (5.19)$$

and

$$r = K_C C_0 \quad (5.20)$$

Eq. 5.18 was applied to the effluent data from the fixed bed using linear regression. From a plot of $ln\ [(C_0/C)^{n-1}-1]$ versus time, the values of $r$ ($h^{-1}$) and $A_C$ can be determined from its slope and intercept, respectively. $K_C$ is the sorption rate coefficient (L $mg^{-1}$ $h^{-1}$), $N_O$ is the sorption capacity (mg $L^{-1}$), and $U$ is the linear velocity ($mmh^{-1}$).

### 5.1.3.2. The Yoon and Nelson Model

The Yoon and Nelson (1984) model is based on the assumption that the rate of decrease in the probability of adsorption for each adsorbate molecule is proportional to the probability of adsorbate adsorption and the probability of adsorbate breakthrough on the adsorbent.

The Yoon and Nelson equation with regard to a single-component system is expressed as:

$$ln\frac{C}{C_0 - C} = k_{YN}t - \tau k_{YN} \quad (5.21)$$

where $k_{YN}$ is the rate constant ($min^{-1}$), $\tau$ is the time required for 50% adsorbate breakthrough (min), and $t$ is the breakthrough (sampling) time (min). The calculation of the theoretical breakthrough curves for a single-component system requires the determination of the parameter $k_{YN}$ and $\tau$ for the adsorbate of interest. These values may be determined from available experimental data. The approach involves a plot of ln $C/(C_0-C)$ versus sampling time ($t$) according to Eq. 5.21. If the theoretical model accurately characterises the experimental data, this plot will result in a straight line with a slope of $k_{YN}$ and an intercept of $\tau\ k_{YN}$.

#### 5.1.3.3. The Average Percentage Error (*APE*)

The prediction of the dynamic behaviour of the column was analysed using the above models. The breakthrough curves of the original, and the results of the model were compared. This comparison of the breakthrough curves shows the superposition of the experimental result curve (points) and the theoretical calculated curve (lines). The linear regression coefficient ($R^2$) shows the fit between the experimental data and the linearised forms of the models. The average percentage error (*APE*) that indicated the fit between the experimental and the predicted value of $C/C_o$ used for plotting the breakthrough curve was calculated using the equation below:

$$APE = \frac{\sum_{i=1}^{N} \left| \frac{(C/C_O)_{exp} - (C/C_O)_{theo}}{(C/C_O)_{exp}} \right|}{N} \times 100 \quad (5.22)$$

where the subscripts "*exp*" and "*theo*" show the experimental and calculated values, respectively. *N* is the number of measurements.

## 5.2. Results and Discussions

### 5.2.1. Effect of Flow Rate

Generally, it was found that there was a significant effect of the flow rates on adsorption of $NH_3$-N, $NO_3$-N, and $NO_2$-N solution in the fixed bed column. The influence of flow rates on sorption of $NH_3$-N onto the sawdust was observed by maintaining initial $NH_3$-N concentration at 0.5 mg/L and keeping the bed height constant at 19 cm. The breakthrough curve of adsorption at different flow rates (9.19 mL/min, 16.55 mL/min, and 21.97 mL/min) are shown in Fig. 5.1(a). With the increase in flow rate, the breakthrough curve became steeper but the breakpoint time decreased significantly (from 45 min to 20 min). The breakthrough curve of $NO_3$-N was generated to investigate the effect of the flow rates in the case of three different flow rates (9.58 mL/min, 16.61 mL/min, and 21.95 mL/min), as shown in Fig. 5.1(b). The breakthrough point was achieved faster at a high flow rate. The breakthrough time was attained within 6 minutes at a high flow rate and within 14 minutes at the lowest flow rate. The same result was also obtained for $NO_2$-N at three different flow rates (9.44 mL/min, 12.5 mL/min, and 22.43 mL/min).

The breakthrough curves in Fig. 5.1 show a similar trend for all nutrients. The decreasing flow rate resulted in a longer contact time. This not only increased the breakthrough time, but also broadened the breakthrough curves. At a higher flow rate, the front of the adsorption zone rapidly contacted the top of the column and the column became saturated faster. This resulted in less adsorption uptake of the nutrients. The results indicate that the residence time of the solute inside the column was not long enough to reach adsorption equilibrium at that flow rate. For this reason, the adsorbate solution leaves the column before equilibrium occurs. The contact time for all adsorbate ions onto the sawdust was very short at the higher flow rate, thereby causing a reduction in removal efficiency.

Results revealed that the dynamic adsorption capacity of sawdust does not depend on the flow rate at a lower initial concentration of the selected nutrients. This result was found to be similar to that of other studies (V´azquez et al., 2006; Deliyanni et al., 2009). Generally it is considered that an increase in flow rate is accompanied by a decrease in dynamic capacity. The use of high flow rates automatically reduces the contact time between the solutions and sawdust and thus less time for adsorption is allocated.

When the breakthrough time was achieved for all column experiments, the maximum dynamic capacity of $NH_3$-N, $NO_3$-N and $NO_2$-N adsorption onto the sawdust was calculated as 0.006 mg/g, 0.002 mg/g and 0.002 mg/g at the flow rates of 9.19 mL/min, 9.58 mL/min and 9.44 mL/min, respectively. Nonetheless, the total time was used for calculating the percentage of the total removal of $NH_3$-N, $NO_3$-N and $NO_2$-N by using Eq. 5.4. However, the results of the fixed-bed column experiments were found to be dissimilar to the previous batch experiments. These results support the study of Deliyanni et al (2009). The maximum percentage removal of $NH_3$-N, $NO_3$-N and $NO_2$-N was found to be 38.95%, 33.63% and 13.86%, respectively, at the lowest flow rate. This is because of the fact that the solution was flushed in an up-flow mode and the solution had less contact time than that of the batch experiments. The adsorption onto the sawdust did not reach equilibrium due to its dynamic action. However, the hydrodynamic differences between the two types of reactors (batch and fixed-bed reactor) led to a difference in physicochemical behavior (Deliyanni et al., 2009).

The length of unused bed (*LUB*) was determined using BTC, as given in Eq (5.7). The *LUB* design approach assumes that the system is governed by a convex isotherm and in addition, that the adsorption bed is long enough to produce a constant pattern behaviour (Cooney, 1998). In batch experiments, the experimental equilibrium data for the adsorption of nutrients onto the sawdust was fitted to the Freundlich isotherm, and thus, the validity of this assumption for the design of *LUB* was proven. In this study, the *LUB* was determined from the breakthrough curves; the results are shown in Table 5.1. The results reveal that the best process of the bed (the lower values of *LUB*) was achieved for the experiments performed at a lower flow rate for $NH_3$-N (14.69 cm) and $NO_3$-N (17.10 cm), respectively, but not for $NO_2$-N (7.6 cm), where the best process was found at a higher flow rate. In actual design, this value of *LUB* can be added to the stoichiometric length of bed needed. This makes the actual column longer to account for unused adsorption capacity under actual conditions.

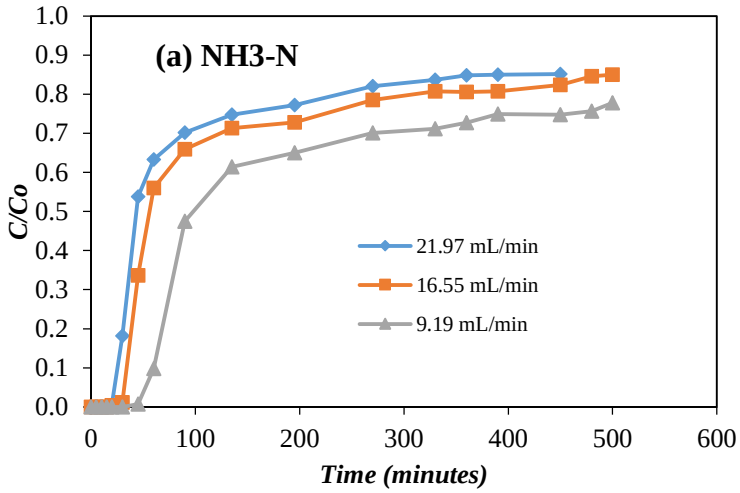


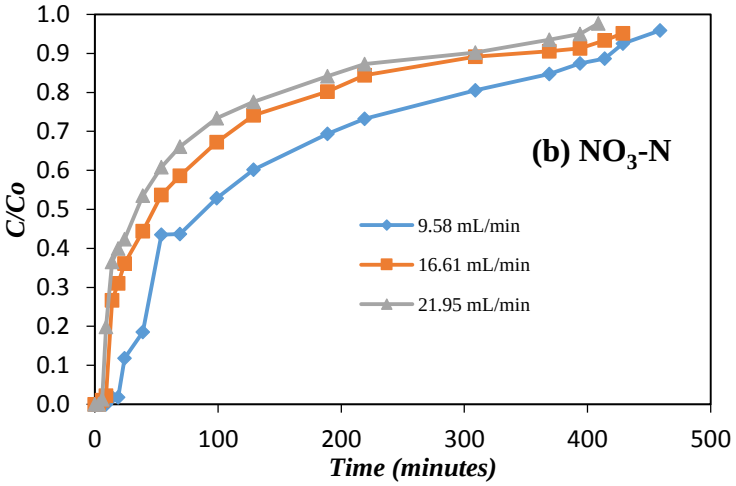


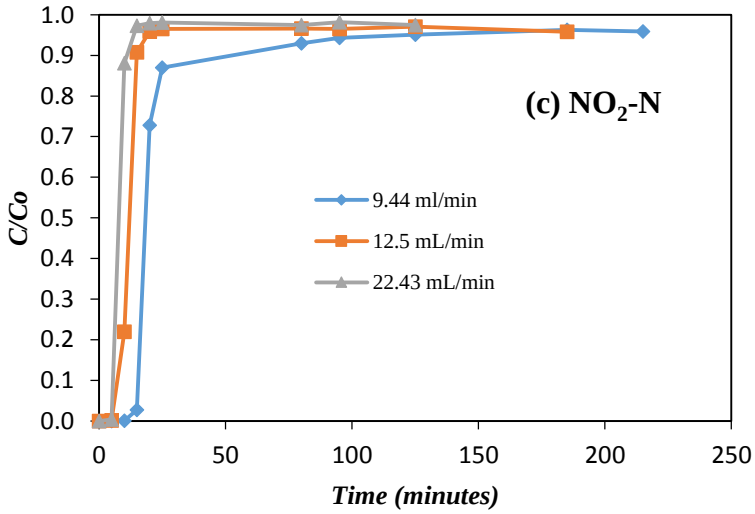


Figure 5.1 Effect of different flow rates on (a) $NH_3$-N, (b) $NO_3$-N, and (c) $NO_2$-N adsorption

Table 5.1 Concentration of solution ($C_b$) at breakthrough time, experimental breakthrough time ($t_b$), dynamic capacity of sawdust at the breakpoint ($W_e$), total adsorbed quantity of nutrients ($q_{total}$), maximum capacity of column ($q_e$), total removal, and equivalent length of unused bed (*LUB*) at the different flow rates for (a) $NH_3$-N, (b) $NO_3$-N, and (c) $NO_2$-N solutions.

(a) $NH_3$-N

| *Q* | Depth | $C_o$ | $C_b$ | $t_b$ | $W_e$ | $q_{total}$ | $q_e$ | Total Removal | *LUB* |
|---|---|---|---|---|---|---|---|---|---|
| (mL/min) | (cm) | (mg/L) | (mg/L) | (min) | (mg/g) | (mg) | (mg/g) | % | (cm) |
| 9.19 | 19 | 0.533 | 0.004 | 45 | 0.006 | 0.954 | 0.026 | 38.949 | 14.69 |
| 16.55 | 19 | 0.542 | 0.002 | 20 | 0.005 | 1.286 | 0.035 | 28.672 | 16.39 |
| 21.97 | 19 | 0.539 | 0.003 | 20 | 0.006 | 1.372 | 0.037 | 25.749 | 15.71 |

(b) $NO_3$-N

| *Q* | Depth | $C_o$ | $C_b$ | $t_b$ | $W_e$ | $q_{total}$ | $q_e$ | Total Removal | *LUB* |
|---|---|---|---|---|---|---|---|---|---|
| (mL/min) | (cm) | (mg/L) | (mg/L) | (min) | (mg/g) | (mg) | (mg/g) | % | (cm) |
| 9.58 | 19 | 0.565 | 0.010 | 14 | 0.002 | 0.754 | 0.020 | 33.626 | 17.10 |
| 16.61 | 19 | 0.544 | 0.006 | 6 | 0.001 | 0.835 | 0.023 | 21.530 | 17.84 |
| 21.95 | 19 | 0.548 | 0.007 | 6 | 0.002 | 0.937 | 0.025 | 19.049 | 17.56 |

(c) $NO_2$-N

| *Q* | Depth | $C_o$ | $C_b$ | $t_b$ | $W_e$ | $q_{total}$ | $q_e$ | Total Removal | *LUB* |
|---|---|---|---|---|---|---|---|---|---|
| (mL/min) | (cm) | (mg/L) | (mg/L) | (min) | (mg/g) | (mg) | (mg/g) | % | cm |
| 9.44 | 19 | 0.537 | 0.015 | 15 | 0.002 | 0.130 | 0.004 | 13.862 | 9.5 |
| 12.50 | 19 | 0.545 | 0.012 | 10 | 0.002 | 0.110 | 0.003 | 12.917 | 7.6 |
| 22.43 | 19 | 0.549 | 0.002 | 5 | 0.002 | 0.100 | 0.003 | 6.497 | 8.23 |

### 5.2.2. Effect of Concentration

The variations of breakthrough curves for all nutrients with respect to feed concentration are shown in Fig. 5.2. The effect of feed concentration under varying conditions, such as: in an experimental breakthrough time ($t_b$); with the dynamic capacity of sawdust at the breakpoint ($W_e$); with the total adsorbed quantity of nutrients ($q_{total}$); with the maximum capacity of the column ($q_e$); with total removal; and with the equivalent length of unused bed (*LUB*), can be seen in Table. 5.2. The sorption breakthrough curves were attained by changing the inlet concentration from 0.5 to 5 mg/L at the same flow rate (9.8 mL/min) and bed height (19 cm). The treated volume was the greatest at the lowest inlet concentration since the lower inlet concentration

gradient caused a slower transport due to a decreased diffusion coefficient or decreased mass transfer coefficient (Aksu and Gonen, 2004). With an increased inlet concentration, the breakthrough curve becomes steeper; in addition, the breakthrough time comes earlier as the binding sites become more quickly saturated in the system.

Overall, the equilibrium nutrient uptake and the total amount of sorbed nutrients increased with increasing inlet concentrations, but the total removal percentage of nutrients showed an opposite trend. The maximum removal percentages were 39.043%, 30.329% for $NH_3$-N and $NO_3$-N at 0.5 mg/L and 14.136% for $NO_2$-N at 5.260 mg/L. The maximum capacities of columns were as follows: 0.052 mg/g for 2.185 mg/L concentration of $NH_3$-N; 0.047 mg/g for 1.060 mg/L concentration of $NO_3$-N; and 0.043 mg/g for 5.260 mg/L concentration of $NO_2$-N. The adsorption capacities were obtained in the column of higher influent concentration, due to the effect of the driving force that occurred in the column. The driving force for adsorption is the concentration difference between the solute on the sorbent and the solute in the solution. A high concentration difference provides a high driving force and enhances the rate of the diffusion of nutrients within the sawdust in the adsorption process. Similar trends were observed by other researchers (Aksu and Gonen, 2004; Expete et al., 2011; Kim et al., 2003).

The best *LUB* for the bed process is the lowest concentration for all nutrients. It was at 14.65 cm, 17.12 cm, and 8.04 cm for ammonia, nitrate and nitrite, respectively.

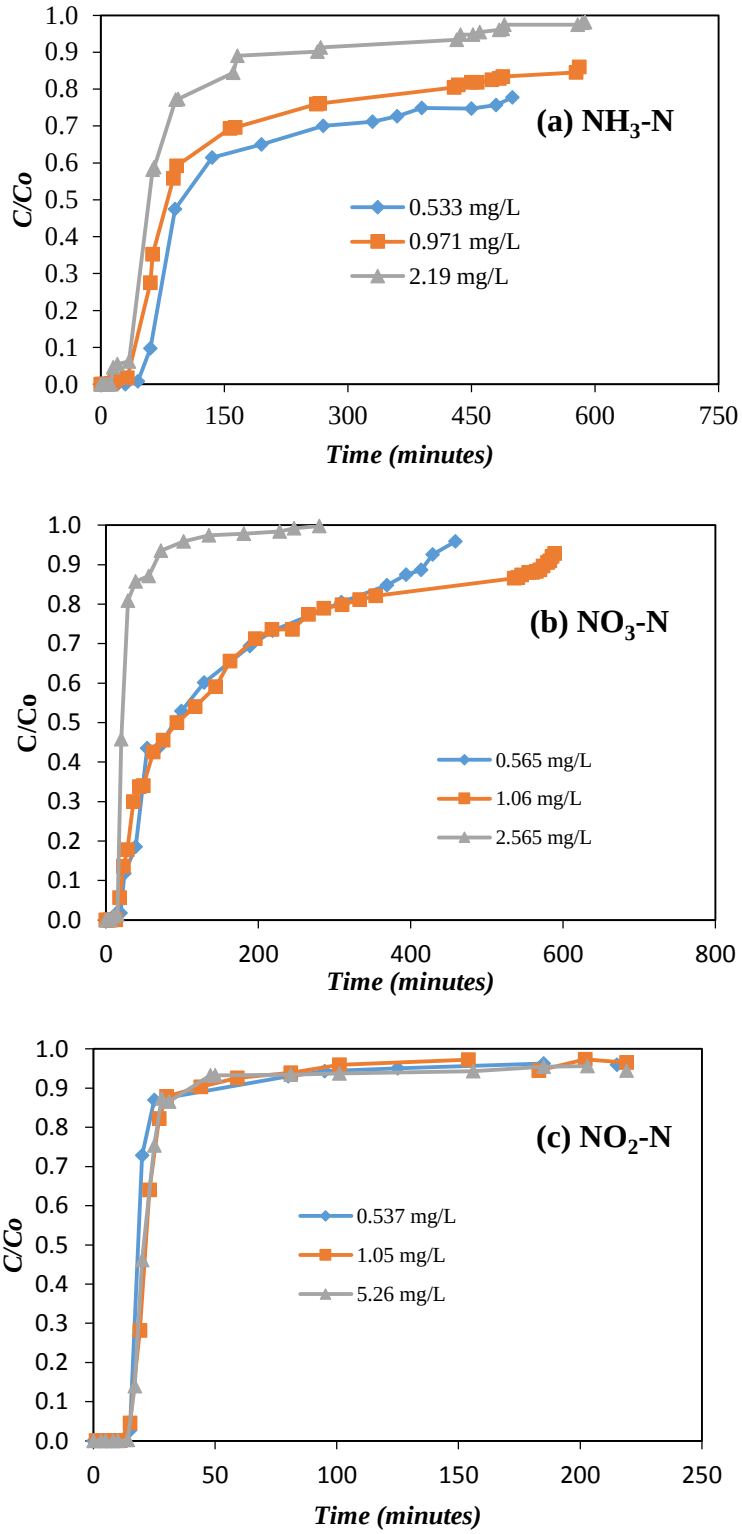


Figure 5.2 Effect of different initial concentrations on (a) $NH_3$-N, (b) $NO_3$-N, and (c) $NO_2$-N adsorption

Table 5.2 Concentration of solution ($C_b$) at breakthrough time, experimental breakthrough time ($t_b$), dynamic capacity of sawdust at the breakpoint ($W_e$), total adsorbed quantity of nutrients ($q_{total}$), maximum capacity of column ($q_e$), total removal, and equivalent length of unused bed (*LUB*) at different solution concentrations of (a) $NH_3$-N, (b) $NO_3$-N, and (c) $NO_2$-N solutions.

(a) $NH_3$-N

| $C_o$ | $Q$ | Depth | $C_b$ | $t_b$ | $W_e$ | $q_{total}$ | $q_e$ | Total Removal | *LUB* |
|---|---|---|---|---|---|---|---|---|---|
| (mg/L) | (mL/min) | (cm) | (mg/L) | (min) | (mg/g) | (mg) | (mg/g) | % | (cm) |
| 0.533 | 9.19 | 19 | 0.004 | 45 | 0.006 | 0.956 | 0.026 | 39.043 | 14.65 |
| 0.971 | 9.84 | 19 | 0.003 | 13 | 0.003 | 1.623 | 0.044 | 29.235 | 17.55 |
| 2.185 | 9.84 | 19 | 0.100 | 7 | 0.004 | 1.916 | 0.052 | 15.154 | 17.58 |

(b) $NO_3$-N

| $C_o$ | $Q$ | Depth | $C_b$ | $t_b$ | $W_e$ | $q_{total}$ | $q_e$ | Total Removal | *LUB* |
|---|---|---|---|---|---|---|---|---|---|
| (mg/L) | (mL/min) | (cm) | (mg/L) | (min) | (mg/g) | (mg) | (mg/g) | % | (cm) |
| 0.565 | 9.58 | 19 | 0.010 | 14 | 0.002 | 0.754 | 0.020 | 30.329 | 17.12 |
| 1.060 | 9.84 | 19 | 0.001 | 13 | 0.004 | 1.742 | 0.047 | 28.361 | 17.52 |
| 2.565 | 9.84 | 19 | 0.001 | 2 | 0.001 | 0.706 | 0.019 | 9.983 | 17.64 |

(c) $NO_2$-N

| $C_o$ | $Q$ | Depth | $C_b$ | $t_b$ | $W_e$ | $q_{total}$ | $q_e$ | Total Removal | *LUB* |
|---|---|---|---|---|---|---|---|---|---|
| (mg/L) | (mL/min) | (cm) | (mg/L) | (min) | (mg/g) | (mg) | (mg/g) | % | (cm) |
| 0.537 | 9.44 | 19 | 0.015 | 15 | 0.002 | 0.128 | 0.003 | 13.663 | 8.04 |
| 1.050 | 9.96 | 19 | 0.048 | 15 | 0.004 | 0.275 | 0.007 | 13.235 | 8.66 |
| 5.260 | 9.84 | 19 | 0.012 | 14 | 0.020 | 1.602 | 0.043 | 14.136 | 10.43 |

### 5.2.3. Effect of Bed Depth

The sorption breakthrough curves obtained by varying the bed heights, and with 1 mg/l initial nutrient concentration pumped at 9.8 ml/min flow rate, are given in Fig. 5.3. In order to make different bed heights of 11, 15, and 19 cms, 18, 26, and 27g, respectively, of sawdust was added. Results indicate that an increase in bed height increases the breakthrough time, resulting in a longer service time. This is because of the increase in the amount of packed sawdust, and therefore, increasing bed height, in the binding sites. By increasing the height of the column, the adsorbate molecule has

enough time to diffuse through the sawdust. This phenomenon increases the breakthrough time.

The sorption data was evaluated and the dynamic capacity of sawdust under the following conditions is presented in Table 5.3: at the breakpoint ($W_e$); the total adsorbed quantity of nutrients ($q_{total}$); the maximum capacity of the column ($q_e$); the total percentage removal; and the equivalent length of unused bed (*LUB*) with respect to bed height. Concentration of solution ($C_b$) is measured at the effluent concentration at breakthrough time. Total percentage removal was calculated by using Eg. 5.4.

In general, the values of all parameters increased significantly when the height of the bed increased for all nutrients, except in the case of the maximum capacity of column ($q_e$) for ammonia and nitrite. The LUB was the most affected by the bed height: when the bed height was increased from 11 to 19 cm, the increase in LUB was 10.45, 14.23, and 17.55 cm for ammonia; 10.81, 14.35, and 17.52 cm for nitrate; and 4.75, 6.65, and 8.66 cm for nitrite. Similar to the LUB, the percentage removal also demonstrated a considerable change: with the bed depth increasing from 11 to 19 cm, the percentage of nutrients removed was 20.094, 26.105, and 29.235% for $NH_3$-N; 20.503, 14.675, and 28.361 % for $NO_3$-N; and 15.519, 15.659, and 17.075 % for $NO_2$-N.

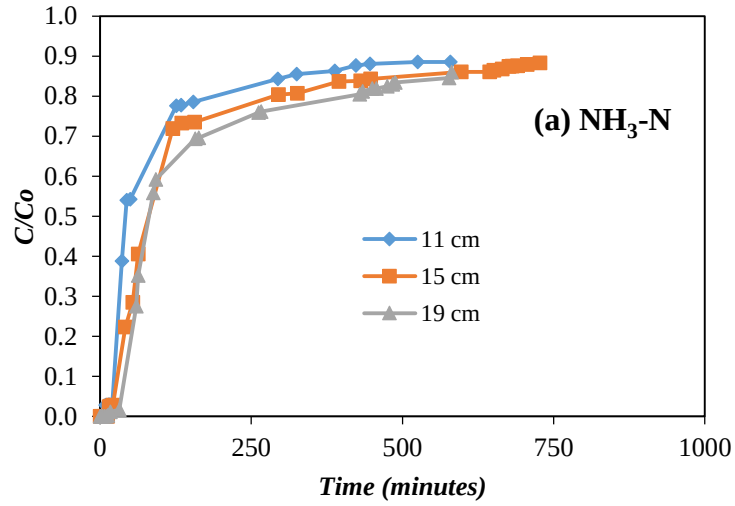


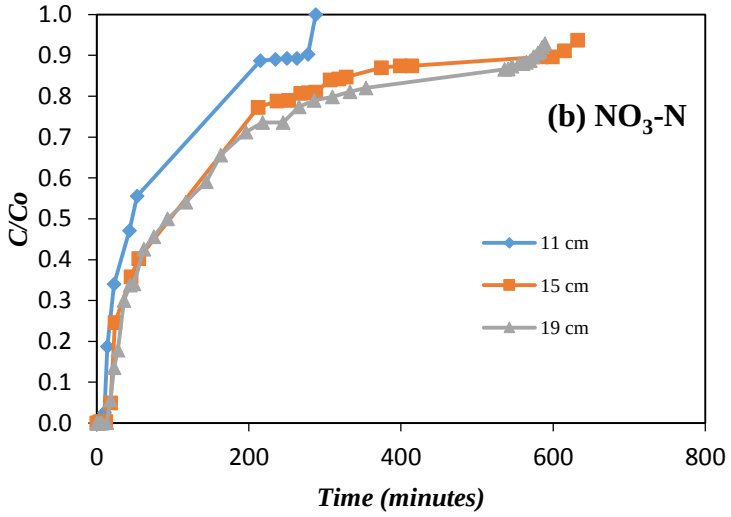


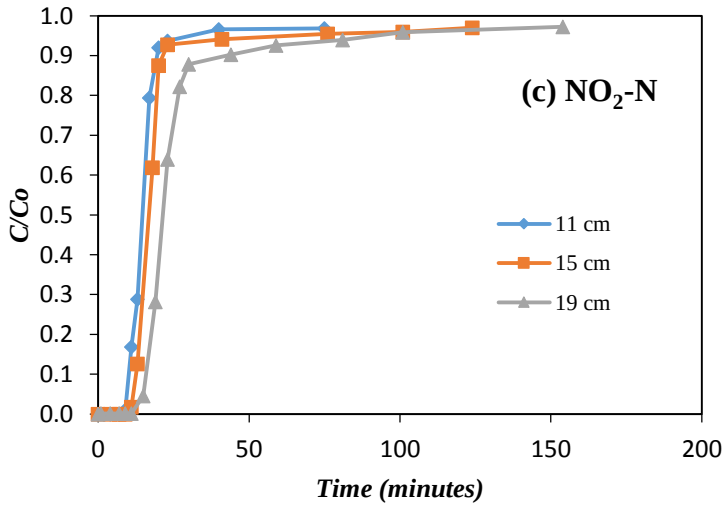


Figure 5.3 Effect of different bed-depths on (a) $NH_3$-N, (b) $NO_3$-N, and (c) $NO_2$-N adsorption

Table 5.3 Concentration of solution ($C_b$) at breakthrough time, experimental breakthrough time ($t_b$), dynamic capacity of sawdust at the breakpoint ($W_e$), total adsorbed quantity of nutrients ($q_{total}$), maximum capacity of column ($q_e$), total removal, and equivalent length of unused bed ($LUB$) at different bed-depths of (a) $NH_3$-N, (b) $NO_3$-N, and (c) $NO_2$-N solutions.

(a) $NH_3$-N

| Depth | $C_o$ | $Q$ | $C_b$ | $t_b$ | $W_e$ | $q_{total}$ | $q_e$ | Total Removal | $LUB$ |
|---|---|---|---|---|---|---|---|---|---|
| (cm) | (mg/L) | (mL/min) | (mg/L) | (min) | (mg/g) | (mg) | (mg/g) | % | (cm) |
| 11 | 1.030 | 9.84 | 0.029 | 6 | 0.003 | 1.179 | 0.066 | 20.094 | 10.45 |
| 15 | 0.999 | 9.84 | 0.024 | 10 | 0.004 | 1.864 | 0.072 | 26.105 | 14.23 |
| 19 | 0.971 | 9.84 | 0.003 | 13 | 0.003 | 1.623 | 0.044 | 29.235 | 17.55 |

(b) $NO_3$-N

| Depth | $C_o$ | $Q$ | $C_b$ | $t_b$ | $W_e$ | $q_{total}$ | $q_e$ | Total Removal | $LUB$ |
|---|---|---|---|---|---|---|---|---|---|
| (cm) | (mg/L) | (mL/min) | (mg/L) | (min) | (mg/g) | (mg) | (mg/g) | % | (cm) |
| 11 | 1.020 | 9.84 | 0.005 | 1 | 0.001 | 0.593 | 0.033 | 20.503 | 10.81 |
| 15 | 1.045 | 9.84 | 0.003 | 4 | 0.002 | 0.954 | 0.037 | 14.675 | 14.35 |
| 19 | 1.060 | 9.84 | 0.001 | 13 | 0.004 | 1.742 | 0.047 | 28.361 | 17.52 |

(c) $NO_2$-N

| Depth | $C_o$ | $Q$ | $C_b$ | $t_b$ | $W_e$ | $q_{total}$ | $q_e$ | Total Removal | $LUB$ |
|---|---|---|---|---|---|---|---|---|---|
| (cm) | (mg/L) | (mL/min) | (mg/L) | (min) | (mg/g) | (mg) | (mg/g) | % | (cm) |
| 11 | 1.044 | 9.84 | 0.011 | 9 | 0.005 | 0.161 | 0.009 | 15.519 | 4.75 |
| 15 | 1.013 | 9.84 | 0.018 | 11 | 0.004 | 0.194 | 0.007 | 15.659 | 6.65 |
| 19 | 1.050 | 9.96 | 0.048 | 15 | 0.004 | 0.275 | 0.007 | 17.075 | 8.66 |

### 5.2.4. Adsorption Isotherm

The distribution of solute between the liquid and solid phases can be expressed by several mathematical equations, such as the standard Langmuir and Freundlich models. These adsorption isotherm models are characterised by certain constants which express the surface properties and affinity of the sawdust and they can also be used to compare the sorption capacity of sawdust for nutrients in the fixed column. The Langmuir constants of $Q^\circ$ and $b$ were determined from the linear plot of $C_{eq}/q_e$ versus $C_{eq}$ for all variations affected in the nutrient adsorption by sawdust. The $Q^\circ$ shows the total capacity of sawdust for nutrients. The Freundlich constants, $K$ and $n$, are indicators of adsorption capacity and adsorption intensity respectively.

The values of the Langmuir and Freundlich parameters are presented in Table 5.4. In general, the correlation coefficients ($R^2$) give different results for different categories. $NH_3$-N and $NO_2$-N provide the best value of Freundlich with the regression coefficient ($R^2$ =0.999) for different flow rates and different inlet concentration respectively. $NO_3$-N follows the Langmuir model, as the regression coefficient presents the 'better' one ($R^2$ = 0.958) for variations in concentration. The applicability of both Langmuir and Freundlich isotherm models to sorbent systems implies that both monolayer adsorption and heterogeneous surface conditions exist under batch and column experimental conditions (Hamdaoui, 2006).

In general, the values of isotherm constants in batch experiments produced the maximum values and were significantly higher than those constant values that were obtained from fixed-bed column experiments. This is deemed reasonable, as the flow rate in batch systems is zero and the contact time between the nutrient solution and sawdust approximates infinity (Aksu and Gonen, 2004; Hamdaoui, 2006). The constant values in batch experiments were then used for the prediction of breakthrough curves in further studies concerning the dynamic adsorption of nutrients in a column. However, it is important to note that the constant adsorption isotherms determined in column experiments should be used mathematically to model a system for evaluating the breakthrough curves and kinetic constants.

Table 5.4 Langmuir and Freundlich isotherm constants of (a) $NH_3$-N, (b) $NO_3$-N, and (c) $NO_2$-N adsorption onto sawdust.

(a) $NH_3$-N

| $Q$ | $C_o$ | Depth | Langmuir | | | Freundlich | | |
|---|---|---|---|---|---|---|---|---|
| (ml/min) | (mg/L) | (cm) | $Q°$ | $b$ | $R^2$ | $K$ | $n$ | $R^2$ |
| 9.19 | 0.533 | 19 | | | | | | |
| 16.55 | 0.542 | 19 | | | | | | |
| 21.97 | 0.539 | 19 | -0.043 | -1.153 | 0.997 | 0.177 | 0.584 | 0.999 |
| 9.19 | 0.533 | 19 | | | | | | |
| 9.84 | 0.971 | 19 | | | | | | |
| 9.84 | 2.185 | 19 | 0.066 | 2.374 | 0.989 | 0.044 | 2.585 | 0.867 |
| 9.84 | 1.030 | 11 | | | | | | |
| 9.84 | 0.999 | 15 | | | | | | |
| 9.84 | 0.971 | 19 | -0.056 | -0.680 | 0.205 | 0.105 | 0.507 | 0.469 |

(b) $NO_3$-N

| $Q$ | $C_o$ | Depth | Langmuir | | | Freundlich | | |
|---|---|---|---|---|---|---|---|---|
| (ml/min) | (mg/L) | (cm) | $Q°$ | $b$ | $R^2$ | $K$ | $n$ | $R^2$ |
| 9.58 | 0.565 | 19 | | | | | | |
| 16.61 | 0.544 | 19 | | | | | | |
| 21.95 | 0.548 | 19 | -0.130 | -0.360 | 0.148 | 0.064 | 0.856 | 0.889 |
| 9.58 | 0.565 | 19 | | | | | | |
| 9.84 | 1.06 | 19 | | | | | | |
| 9.84 | 2.565 | 19 | 0.017 | -4.070 | 0.958 | 0.026 | -8.403 | 0.045 |
| 9.84 | 1.020 | 11 | | | | | | |
| 9.84 | 1.045 | 15 | | | | | | |
| 9.84 | 1.060 | 19 | 0.018 | -2.310 | 0.601 | 0.029 | -0.733 | 0.340 |

(c) $NO_2$-N

| $Q$ | $Co$ | Depth | Langmuir | | | Freundlich | | |
|---|---|---|---|---|---|---|---|---|
| (ml/min) | (mg/L) | (cm) | $Q°$ | $b$ | $R^2$ | $K$ | $n$ | $R^2$ |
| 9.44 | 0.537 | 19 | | | | | | |
| 12.5 | 0.545 | 19 | | | | | | |
| 22.43 | 0.549 | 19 | 0.001 | -3.013 | 0.928 | 0.001 | -0.452 | 0.818 |
| 9.44 | 0.537 | 19 | | | | | | |
| 9.96 | 1.05 | 19 | | | | | | |
| 9.84 | 5.26 | 19 | -0.190 | -0.041 | 0.716 | 0.008 | 0.907 | 0.999 |
| 9.84 | 1.044 | 11 | | | | | | |
| 9.84 | 1.013 | 15 | | | | | | |
| 9.96 | 1.05 | 19 | -0.002 | -0.930 | 0.538 | 0.017 | 0.187 | 0.642 |

### 5.2.5. Modelling of Dynamic Sorption

The dynamic behaviour of the column was modelled using both the Clark and Yoon and the Nelson model. The breakthrough curve showed the superposition of experimental results (points) and the theoretically calculated (points). Linear regression coefficients ($R^2$) illustrated the fit between the experimental data and the linearised form of the Clark and Yoon and the Nelson models, while the average percentage error ($\varepsilon$%) indicated the fit between the experimental and predicted values of $C/C_o$ used for plotting breakthrough curves.

#### 5.2.5.1. The Clark Model

In the section on nutrient adsorption by sawdust, it was found that the Freundlich model was the most valid for the adsorption isotherm. The Freundlich constant *n* obtained was then used to calculate the parameters in the Clark model.

- **Modelling of $NH_3$-N Adsorption**

In general, the adsorption breakthrough curve of $NH_3$-N adsorption onto sawdust could only be effectively described by the Clark model at the ratio *C*/*Co* higher than 0.1, with respect to flow rate, $NH_3$-N concentration, and the height of the bed. Below these levels ($C/Co<0.1$), the model could not be applied to its experimental data due to unable to determine the kinetics coefficients in this system. Only breakthrough curve of concentration at 2.185 mg/L with flowrate of 9.8 mL/min and bed depth at 19 cm can be described at the ratio C/Co higher than 0.046. This concurs with other research which reported that the adsorption breakthrough of phenol by immobilised activated sludge could be well described by the Clark model at the ratio *C*/*Co* higher than 0.08 (Aksu and Gonen, 2004), and at the ratio *C*/*Co* above 0.07 and 0.6 for adsorption of methylene blue by cedar sawdust and crushed brick respectively (Hamdoui, 2006).

The values of $ln\ A_C$ and *r* in the Clark equation were determined (using Eq. 5.19) by linear regression analysis and are shown in Table 5.5. Even though the correlation coefficients for the linear regression ($R^2$) were quite low (0.639 – 0.886), they are still acceptable. Figures 5.4-5.6 show the experimental and model-calculated breakthrough curves obtained at different flow rates, at different $NH_3$-N inlet concentrations, and at different bed-depths. It appears that the whole breakthrough

curve is effective using the Clark model at higher flow rates, at higher inlet concentrations, and at higher bed heights. This result equates well with Aksu and Gonen (2004) and Hamdoui (2006). Where there were lower flow rates, inlet concentrations, and bed-depths, the correlation between the experimental and predicted values using this model deviated significantly.

Table 5.5 Clark models parameters for $NH_3$-N adsorption by sawdust at different flow rates, initial concentrations, and bed heights.

| *Q* | *Co* | *H* | *ln* $A_C$ | *r* | $R^2$ | *APE* |
|---|---|---|---|---|---|---|
| mL/min | (mg/L) | cm | | 1/min | | (%) |
| 9.19 | 0.533 | 19 | 0.215 | 0.004 | 0.639 | 24.2 |
| 16.55 | 0.542 | 19 | 0.930 | 0.003 | 0.799 | 18.4 |
| 21.95 | 0.539 | 19 | 1.239 | 0.003 | 0.886 | 22.7 |
| 9.84 | 0.971 | 19 | 0.566 | 0.006 | 0.642 | 16.3 |
| 9.84 | 2.185 | 19 | 0.121 | 0.009 | 0.832 | 29.7 |
| 9.84 | 1.030 | 11 | 0.775 | 0.011 | 0.665 | 32.2 |
| 9.84 | 0.999 | 15 | 0.715 | 0.008 | 0.688 | 24.7 |

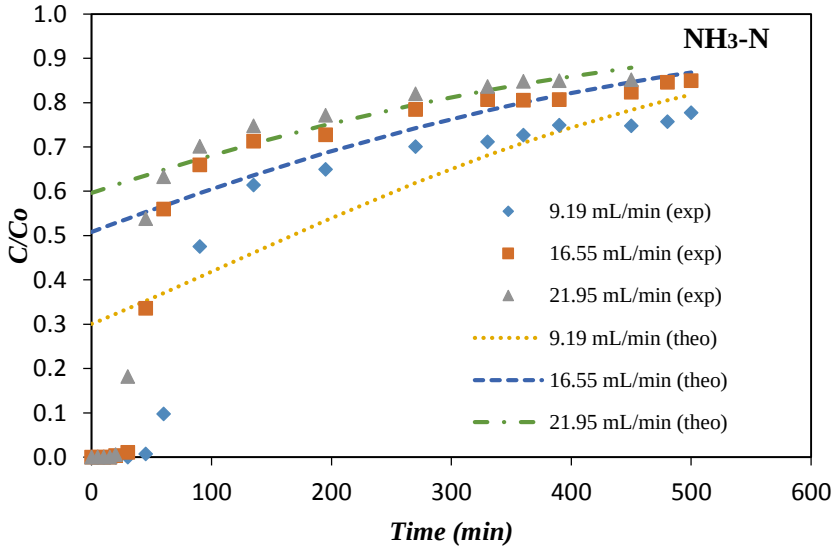


Figure 5.4 Experimental data of $NH_3$-N adsorption fitted with Clark model varying flow rates (Co = 0.5 mg/L; Depth = 19 cm; pH = 6-7)

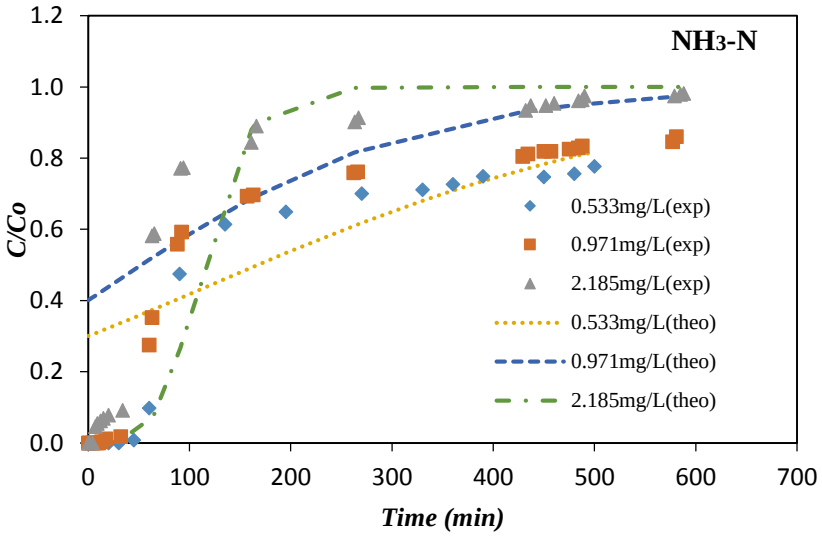


Figure 5.5 Experimental data of $NH_3$-N adsorption fitted with Clark model varying concentrations (Q = 9.8 mL/min; Depth = 19 cm; pH = 6-7)

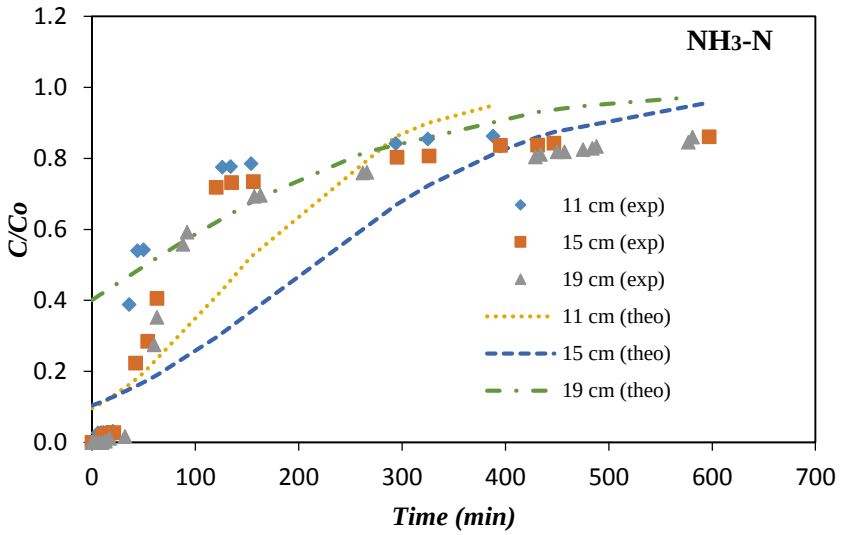


Figure 5.6 Experimental data of $NH_3$-N adsorption fitted with Clark model varying height of beds (Q = 9.8 mL/min; Co = 1 mg/L; pH = 6-7)

- **Modelling of $NO_3$-N Adsorption**

As with $NH_3$-N, the adsorption breakthrough curve of $NO_3$-N adsorption onto sawdust could be described by the Clark model only at a ratio *C*/*Co* higher than 0.1 with respect to flow rate, $NO_3$-N inlet concentration, and height of the bed. Below these levels, it was not suitable to examine the kinetic coefficients in this system, thus the model could not be applied to the experimental data. The linear regression coefficients $R^2$ were 0.565-0.801. Clark model fitted well with breakthrough curves

when it was fitted with the plot of *C*/*Co* against *t* (Figs. 5.7-5.9). It can be observed that at the lower flow rates, at higher inlet concentrations, and at lower bed-depths, there is a good fit with this model.

Table 5.6 Clark models parameters for $NO_3$-N adsorption by sawdust at different flow rates, initial concentrations, and bed heights.

| *Q* | *Co* | *H* | *ln* $A_C$ | *r* | $R^2$ | *APE* |
|---|---|---|---|---|---|---|
| mL/min | (mg/L) | cm | | 1/min | | (%) |
| 9.58 | 0.565 | 19 | 2.805 | 0.013 | 0.738 | 26.3 |
| 16.61 | 0.544 | 19 | 2.010 | 0.012 | 0.639 | 33.2 |
| 21.95 | 0.548 | 19 | 1.429 | 0.012 | 0.657 | 10.5 |
| 9.84 | 1.06 | 19 | 2.018 | 0.008 | 0.565 | 45.6 |
| 9.84 | 2.565 | 19 | 9.050 | 0.247 | 0.801 | 31.3 |
| 9.84 | 1.020 | 11 | 4.478 | 0.026 | 0.707 | 20.8 |
| 9.84 | 1.045 | 15 | 3.916 | 0.013 | 0.618 | 19.8 |

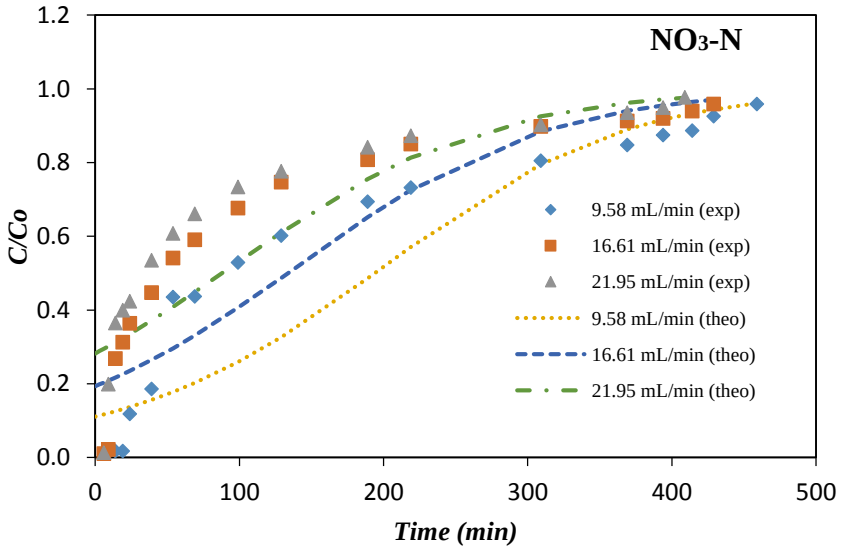


Figure 5.7 Experimental data of $NO_3$-N adsorption fitted with Clark model varying flow rates (Co = 0.5 mg/L; Depth = 19 cm; pH = 6-7)

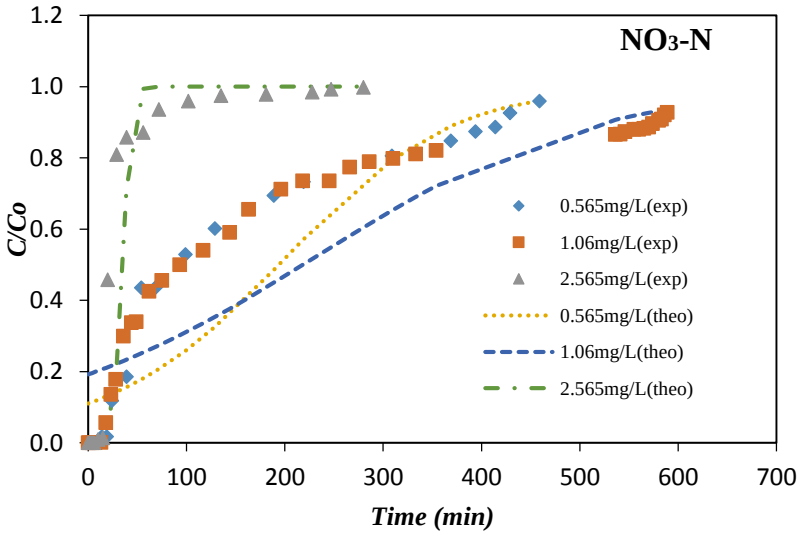


Figure 5.8 Experimental data of $NO_3$-N adsorption fitted with Clark model varying concentrations (Q = 9.8 mL/min; Depth = 19 cm; pH = 6-7)

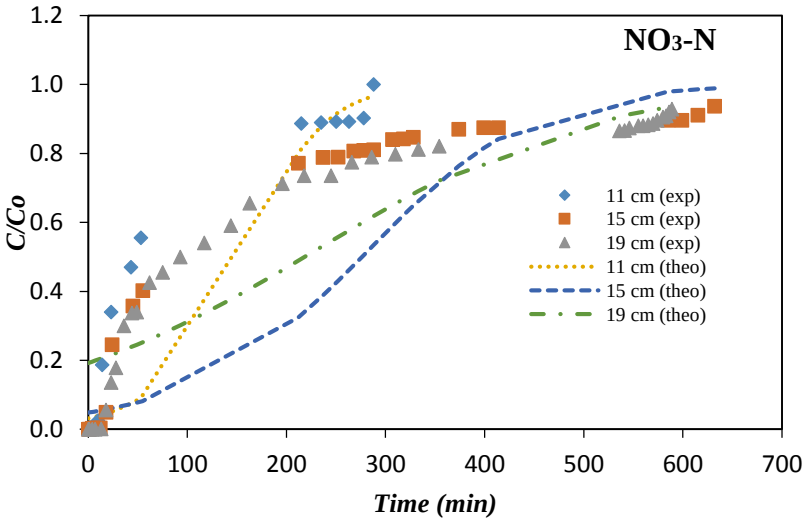


Figure 5.9 Experimental data of $NO_3$-N adsorption fitted with Clark model varying height of beds (Q = 9.8 mL/min; Co = 1 mg/L; pH = 6-7)

- **Modelling of $NO_2$-N Adsorption**

Unlike $NH_3$-N and $NO_3$-N, the application of the Clark model to $NO_2$-N adsorption onto sawdust was very effective. The parameters of the Clark equation and the correlation coefficient ($R^2$) for all flow rates, inlet concentrations, and bed heights are given in Table 5.7. The correlation coefficients for the linear regression were high ($R^2$ = 0.803-0.995), showing good agreement between the Clark model and the experimental data.

Plotting *C/Co* against *t* according to the Clark model equations provided the breakthrough curves predicted by the Clark model (Figs 5.10-5.12). It is clear from the figures and the average percentage error (*APE*) shown in Table 5.7 that the experimental results fit the model very well. The value of the average percentage error was in the range of 2.5-13.3 for all results. The predicted curve deviated slightly from the experimental data at the highest flow rates, at the highest inlet concentration, and at the lowest depth-bed.

Table 5.7 Clark models parameters for $NO_2$-N adsorption by sawdust at different flow rates, initial concentrations, and bed heights.

| $Q$ | $C_o$ | $H$ | $ln\ A_C$ | $r$ | $R^2$ | $APE$ |
|---|---|---|---|---|---|---|
| mL/min | (mg/L) | cm | | 1/min | | (%) |
| 9.44 | 0.537 | 19 | 27.294 | 1.401 | 0.995 | 4.2 |
| 12.5 | 0.545 | 19 | 16.324 | 1.257 | 0.961 | 3.0 |
| 22.43 | 0.549 | 19 | 13.314 | 1.192 | 0.850 | 13.0 |
| 9.96 | 1.050 | 19 | 16.324 | 0.722 | 0.895 | 2.5 |
| 9.84 | 5.260 | 19 | 13.314 | 0.861 | 0.803 | 13.3 |
| 9.84 | 1.044 | 11 | 12.411 | 0.757 | 0.888 | 9.0 |
| 9.84 | 1.013 | 15 | 14.647 | 0.811 | 0.967 | 3.0 |

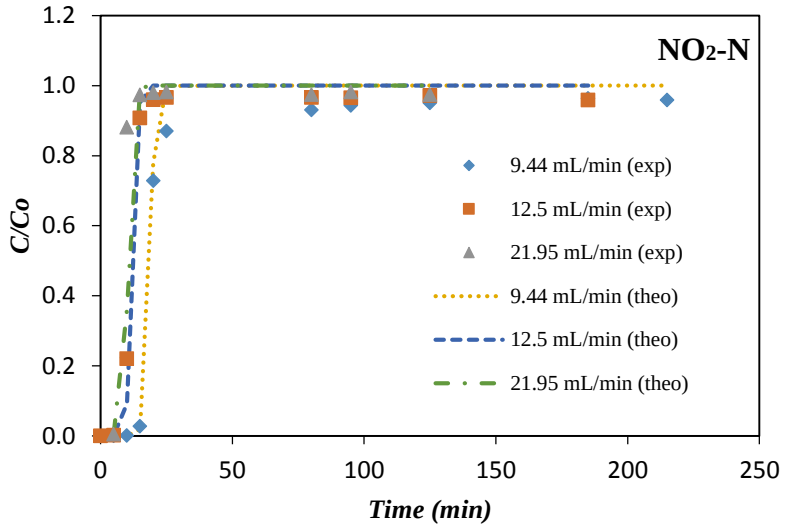


Figure 5.10 Experimental data of $NO_2$-N adsorption fitted with Clark model varying flow rates (Co = 0.5 mg/L; Depth = 19 cm; pH = 6-7)

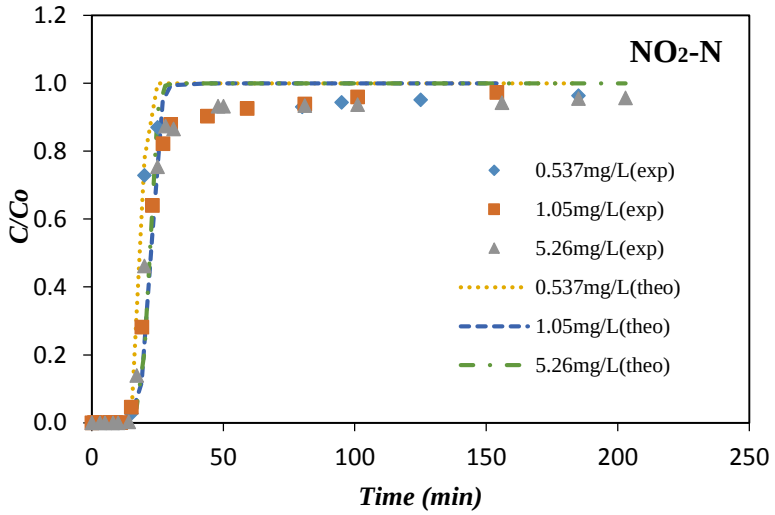


Figure 5.11 Experimental data of $NO_2$-N adsorption fitted with Clark model varying concentrations (Q = 9.8 mL/min; Depth = 19 cm; pH = 6-7)

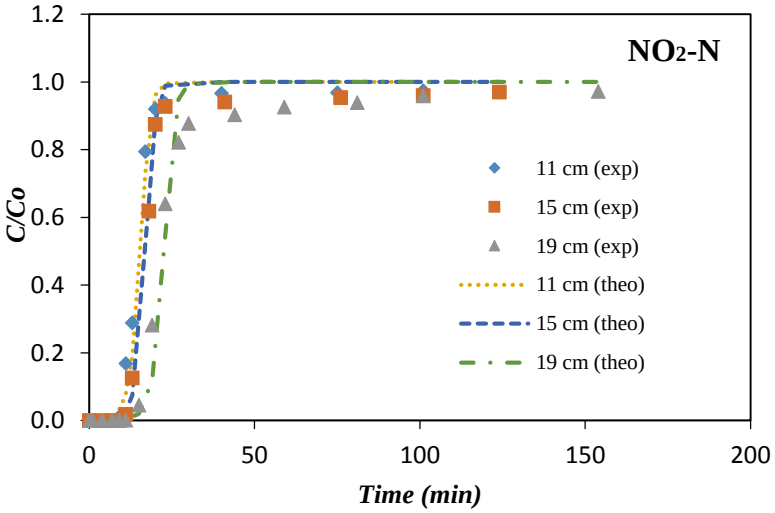


Figure 5.12 Experimental data of $NO_2$-N adsorption fitted with Clark model varying height of beds (Q = 9.8 mL/min; Co = 1 mg/L; pH = 6-7)

### 5.2.5.2. The Yoon and Nelson Model

A simple theoretical model developed by Yoon and Nelson (1984) was applied to investigate the breakthrough behaviour of nutrients onto sawdust. The Yoon and Nelson model is not only less complicated than other models, but it also does not necessitate detailed data concerning the characteristics of adsorbate, the type of adsorbent, and the physical properties of the adsorption bed (Tsai et al, 1999). The values of rate constant ($k_{YN}$) and time required for 50% nutrient breakthrough ($\tau$) were

determined from ln[C/(Co-C)] against *t* plots at different flow rates, different inlet concentrations, and different bed heights, according to Eq. 5.22 These values were used to calculate the breakthrough curve of this model.

- **Modelling of $NH_3$-N Adsorption**

The experimental data obtained from different flow rates (9.19-21.95 mL/min), different inlet concentrations (0.533-2.185 mg/L), and different bed heights (11-15 cm) were applied to the Yoon and Nelson model in $NH_3$-N adsorption onto sawdust. The parameter values of the Yoon and Nelson model are listed in Table 5.8. However, this model was only applied from zero to 0.7 of *C*/*Co* of the experimental data. Above this level, the model could not be applied to the experimental data. Different results at different variations of the parameters can be observed in Table 5.8. The rate constant ($k_{YN}$) increased and the 50% breakthrough time ($\tau$) decreased with increasing flow rates. However, both parameters decreased with an increase in the influent concentration, while the rate constant ($k_{YN}$) decreased and the 50% breakthrough time ($\tau$) increased when the bed heights were increased. The data in Table 5.8 also indicates that 50% breakthrough time ($\tau$) values are almost comparable with the experimental data.

The theoretical curves were compared with the corresponding experimental data, as in Figs. 5.13-5.15. It appears that none of the breakthrough curves were well predicted by the Yoon and Nelson model. However, from initiation until almost 70% of breakthrough curves, the average percentage error for superposition of the experimental data and theoretical calculated points was between 5.68 – 21.43%.

Table 5.8 Yoon and Nelson model parameters for $NH_3$-N adsorption by sawdust at different flow rates, initial concentrations, and bed heights.

| $Q$ | $C_o$ | $H$ | $k_{YN}$ | $\tau_{theo}$ | $\tau_{exp}$ | $R^2$ | $APE$ |
|---|---|---|---|---|---|---|---|
| mL/min | (mg/L) | cm | L/ min | min | min | | (%) |
| 9.19 | 0.533 | 19 | 0.101 | 89 | 98 | 0.937 | 21.43 |
| 16.55 | 0.542 | 19 | 0.158 | 56 | 55 | 0.943 | 17.46 |
| 21.95 | 0.539 | 19 | 0.205 | 43 | 42 | 0.895 | 18.56 |
| 9.84 | 0.971 | 19 | 0.081 | 78 | 81 | 0.950 | 16.12 |
| 9.84 | 2.185 | 19 | 0.058 | 61 | 58 | 0.953 | 5.68 |
| 9.84 | 1.030 | 11 | 0.111 | 44 | 42 | 0.911 | 14.45 |
| 9.84 | 0.999 | 15 | 0.049 | 85 | 80 | 0.904 | 12.40 |

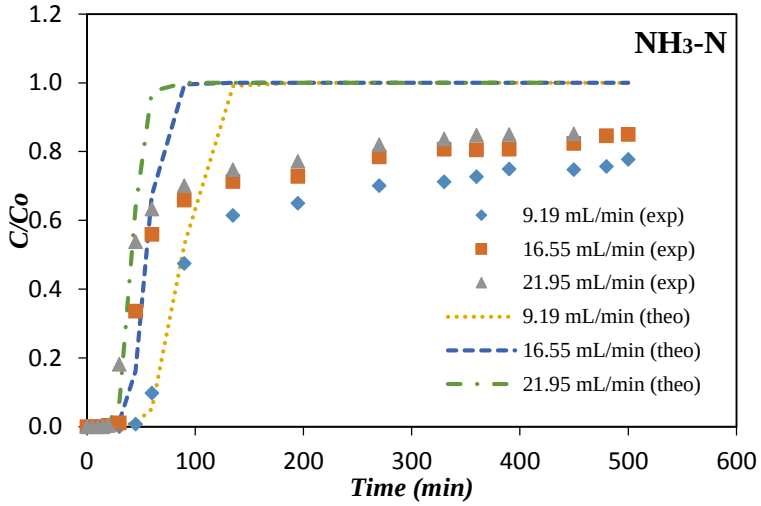


Figure 5.13 Experimental data of $NH_3$-N adsorption fitted with Yoon and Nelson model varying flow rates (Co = 0.5 mg/L; Depth = 19 cm; pH = 6-7)

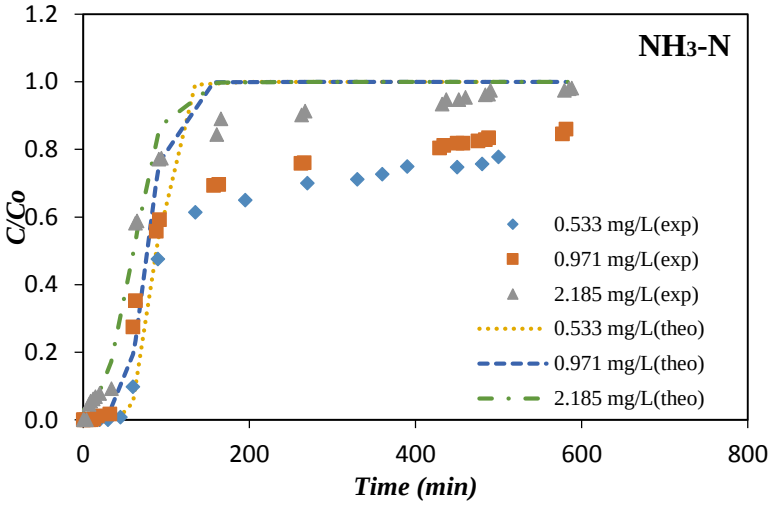


Figure 5.14 Experimental data of $NH_3$-N adsorption fitted with Yoon and Nelson model varying concentrations (Q = 9.8 mL/min; Depth = 19 cm; pH = 6-7)

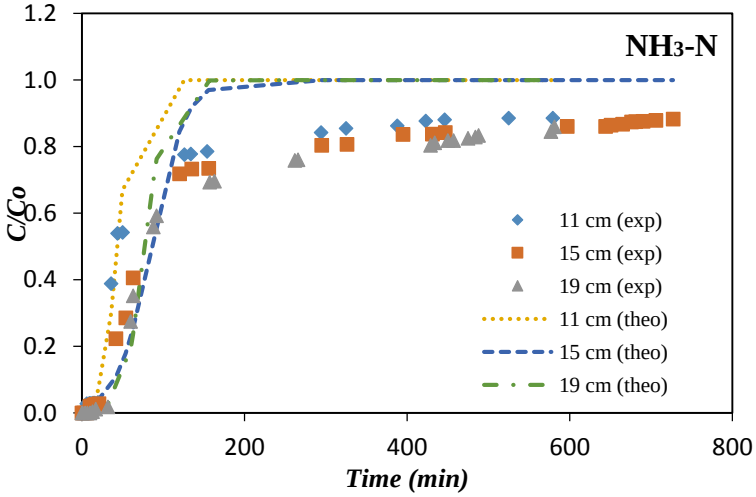


Figure 5.15 Experimental data of $NH_3$-N adsorption fitted with Yoon and Nelson model varying bed-heights (Q = 9.8 mL/min; Co = 1 mg/L; pH = 6-7)

- **Modelling of $NO_3$-N Adsorption**

The plots of the Yoon and Nelson model were applied for $NO_3$-N adsorption onto sawdust. These plots were obtained at different flow rates (9.58-21.95 mL/min), different concentrations (0.565-2.565 mg/L), and different bed-depths (11-19 cm). The parameters of the Yoon and Nelson model are tabled in Table 5.9. The rate constant ($k_{YN}$) increased and the 50% breakthrough time ($\tau$) decreased with increases in flow rates and inlet concentrations. However, the rate constant ($k_{YN}$) decreased and the 50% breakthrough time ($\tau$) increased with the increasing of bed heights. The comparison of 50% experimental breakthrough time was not in good agreement with 50% theoretical breakthrough time, particularly at the lowest flow rate.

The theoretical curves were also compared with the corresponding experimental data in Figs. 5.16-5.18 and the obtained average percentage error values are tabled in Table 5.9. The experimental breakthrough curves were closest to those predicted by the Yoon and Nelson model in the *C*/*Co* region above 0.01. Similarly, for the biosorption of phenol by immobilised activated sludge in a continuous packed bed, it was indicated that the breakthrough curves were well in agreement with those predicted by the Yoon and Nelson model in the *C*/*Co* region from 0.08 to 0.99 (Aksu and Gonen, 2004). Moreover, for sorption of methylene blue by cedar sawdust and crushed brick in fixed bed columns, the experimental breakthrough curves are very close to those predicted by the Yoon and Nelson model in the *C*/*Co* region above 0.07 (Hamdaoui, 2006). Therefore, the application of the Yoon and Nelson model in the experimental results of $NO_3$-N adsorption onto sawdust provided a good correlation of the effects of flow rates, inlet concentrations, and bed heights.

Table 5.9 Yoon and Nelson model parameters for $NO_3$-N adsorption by sawdust at different flow rates, initial concentrations, and bed heights.

| $Q$ | $Co$ | $H$ | $k_{YN}$ | $\tau_{theo}$ | $\tau_{exp}$ | $R^2$ | $APE$ |
|---|---|---|---|---|---|---|---|
| mL/min | (mg/L) | cm | L/ min | min | min | | (%) |
| 9.58 | 0.565 | 19 | 0.009 | 135 | 90 | 0.900 | 8.07 |
| 16.61 | 0.544 | 19 | 0.008 | 57 | 47 | 0.933 | 3.61 |
| 21.95 | 0.548 | 19 | 0.009 | 42 | 34 | 0.911 | 5.58 |
| 9.84 | 1.06 | 19 | 0.005 | 131 | 93 | 0.876 | 22.65 |
| 9.84 | 2.565 | 19 | 0.366 | 24 | 21 | 0.957 | 15.20 |
| 9.84 | 1.020 | 11 | 0.242 | 25 | 46 | 0.904 | 20.97 |
| 9.84 | 1.045 | 15 | 0.006 | 121 | 96 | 0.722 | 27.73 |

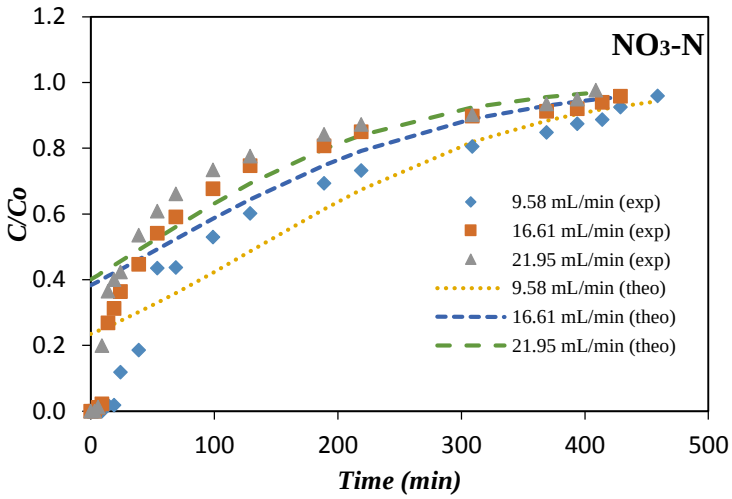


Figure 5.16 Experimental data of $NO_3$-N adsorption fitted with Yoon and Nelson model varying flow rates (Co = 0.5 mg/L; Depth = 19 cm; pH = 6-7)

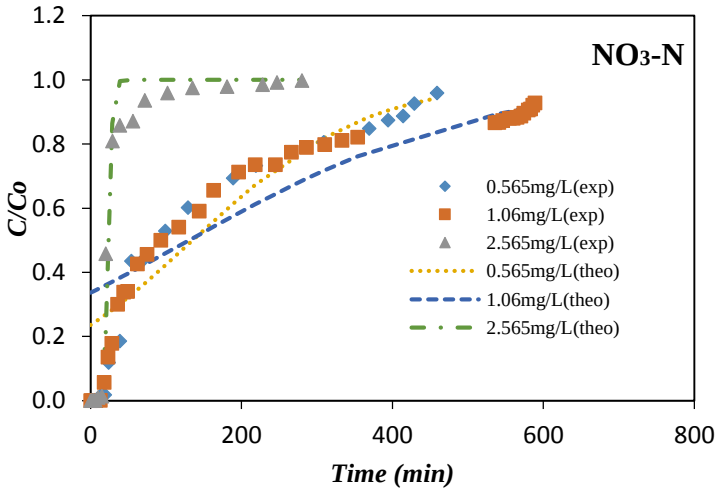


Figure 5.17 Experimental data of $NO_3$-N adsorption fitted with Yoon and Nelson model varying concentrations (Q = 9.8 mL/min; Depth = 19 cm; pH = 6-7)

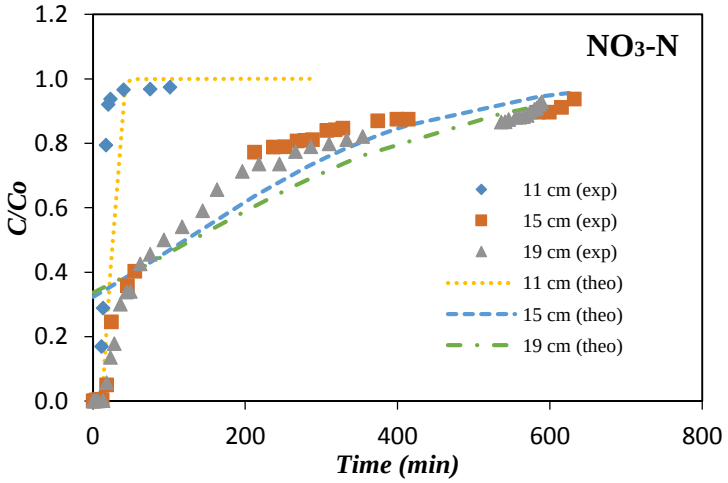


Figure 5.18 Experimental data of $NO_3$-N adsorption fitted with Yoon and Nelson model varying bed-heights (Q = 9.8 mL/min; Co = 1 mg/L; pH = 6-7)

- **Modelling of $NO_2$-N Adsorption**

The parameter values of the rate constant ($k_{YN}$) and the time required for 50% $NO_2$-N breakthrough ($\tau$) were determined from the variation of flow rates (9.44-22.43 mL/min), $NO_2$-N inlet concentration (0.537-5.260 mg/L), and the variation of bed heights (11-19 cm). These values were used to calculate the breakthrough curves and are listed in Table 5.10. According to Table 5.10, the rate constant ($k_{YN}$) increased and the 50% breakthrough time ($\tau$) decreased with increasing flow rate. However, the rate constant ($k_{YN}$) decreased and the 50% breakthrough time ($\tau$) increased with increases in the inlet concentrations, while the rate constant ($k_{YN}$) and the 50% breakthrough time ($\tau$) increased with increasing bed heights. The $\tau$ values were very similar to the experimental results.

The theoretical curves were compared with the corresponding experimental data, as seen in Figs. 5.19-5.21. The experimental breakthrough curves were very close to those predicted by the Yoon and Nelson model, with the average percentage error between 1.7-18.47.

Table 5.10 Yoon and Nelson model parameters for $NO_2$-N adsorption by sawdust at different flow rates, initial concentrations, and bed heights.

| $Q$ | $C_o$ | $H$ | $k_{YN}$ | $\tau_{theo}$ | $\tau_{exp}$ | $R^2$ | $APE$ |
|---|---|---|---|---|---|---|---|
| mL/min | (mg/L) | cm | L/ min | min | min | | (%) |
| 9.44 | 0.537 | 19 | 0.957 | 19 | 18 | 0.999 | 4.20 |
| 12.5 | 0.545 | 19 | 1.109 | 11 | 12 | 1.000 | 3.40 |
| 22.43 | 0.549 | 19 | 1.513 | 9 | 10 | 1.000 | 1.70 |
| 9.96 | 1.050 | 19 | 0.515 | 22 | 21 | 0.930 | 7.05 |
| 9.84 | 5.260 | 19 | 0.512 | 23 | 21 | 0.852 | 18.47 |
| 9.84 | 1.044 | 11 | 0.492 | 16 | 15 | 0.905 | 14.36 |
| 9.84 | 1.013 | 15 | 0.545 | 17 | 17 | 0.965 | 3.63 |

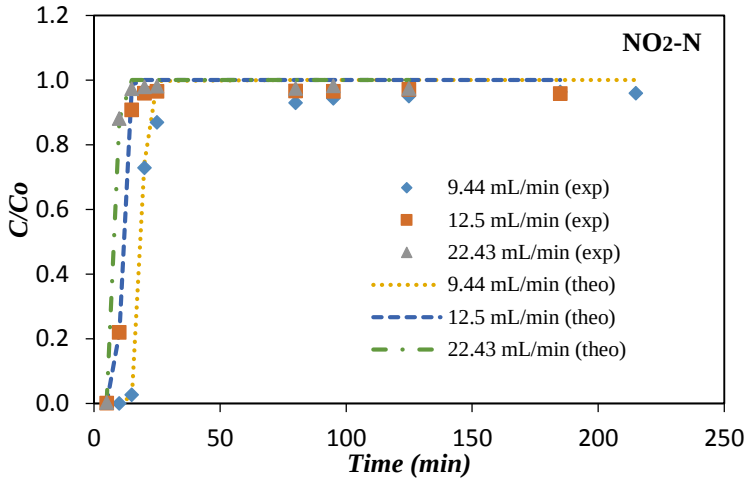


Figure 5.19 Experimental data of $NO_2$-N adsorption fitted with Yoon and Nelson model varying flow rates (Co = 0.5 mg/L; Depth = 19 cm; pH = 6-7)

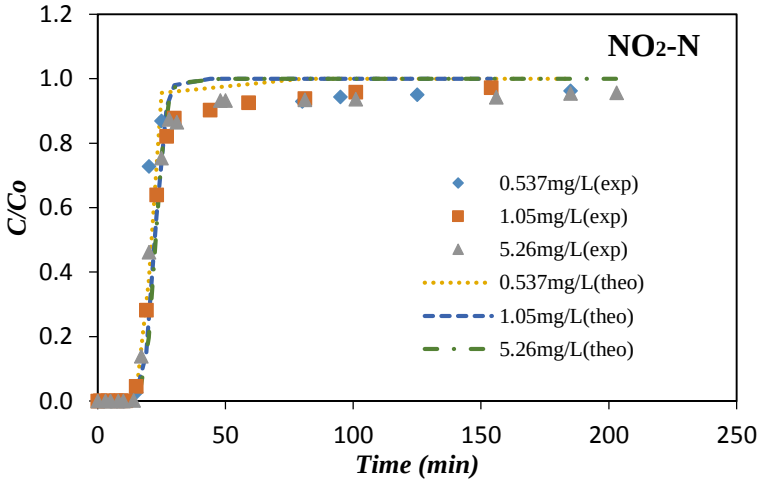


Figure 5.20 Experimental data of $NO_2$-N adsorption fitted with Yoon and Nelson model varying concentrations (Q = 9.8 mL/min; Depth = 19 cm; pH = 6-7)

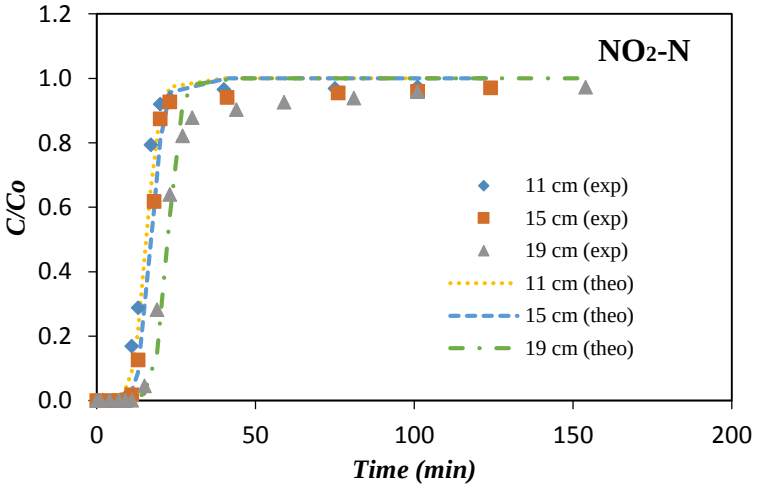


Figure 5.21 Experimental data of $NO_2$-N adsorption fitted with Yoon and Nelson model varying bed-heights (Q = 9.8 mL/min; Co = 1 mg/L; pH = 6-7)

## 5.3. Concluding Remarks

As sawdust from Radiata pinewood is considered to be a good carbon source and an appropriate electron donor, its adsorption characteristics in stormwater under dynamic conditions were investigated. Synthetic stormwater was prepared from aqueous solutions with differing nutrient ($NH_3$-N, $NO_3$-N, and $NO_2$-N) concentrations. A series of up-flow-mode column experiments were performed for three different flow rates, three different inlet concentrations, and three different bed heights under saturated conditions.

The results revealed that the sorption of $NH_3$-N, $NO_3$-N, and $NO_2$-N is dependent on the flow rate, the inlet concentration, and the heights of the bed. $NH_3$-N, $NO_3$-N, and $NO_2$-N removal and the breakpoint time decreased with increases in the flow rate, inlet concentration, and bed-depth.

In addition, the length-of-unused-bed (*LUB*) approach was used for designing the fixed-bed reactor. The *LUB* was obtained by analysing the breakthrough curve. The lower value of *LUB* was achieved at lower inlet concentrations, lower bed heights, and at a lower flow rate for $NH_3$-N and $NO_3$-N, but it appeared at higher flow rate for $NO_2$-N. This value of *LUB* can be added to the stoichiometric length of bed needed. This makes the actual column longer, in order to account for unused adsorption capacity under actual conditions

The Langmuir and Freundlich adsorption models were used for the mathematical description of the adsorption of $NH_3$-N, $NO_3$-N, and $NO_2$-N onto sawdust. The characteristic sorption parameters for each isotherm were determined. It was observed that the sorption equilibrium data fitted both the models, with $NH_3$-N and $NO_2$-N very well described by the Freundlich model, and $NO_3$-N more likely to follow the Langmuir model. However, compared with the values obtained from batch experiments, the values of isotherm constants from column experiments were less than those in the batches. This is because, in batch systems, the flow rate is zero and there is a much longer contact time between nutrient solution and sawdust.

The Clark and Yoon-Nelson models were used with the experimental data to determine the column kinetic parameters. In dynamic conditions, $NH_3$-N is well predicted by the Clark model at higher flow rates, at higher inlet concentrations, and at higher bed heights, while $NO_3$-N is well predicted by the Yoon and Nelson model at higher flow rates, at higher inlet concentrations, and lower bed heights. However,

both the Clark and Yoon and Nelson models were very effective for predicting the whole of the breakthrough curves obtained with $NO_2$-N.

# CHAPTER 6

# MASS TRANSFER CHARACTERISTICS FOR NUTRIENT ADSORPTION ONTO SAWDUST

## 6.1. The Mechanisms in Fixed-bed Adsorber

In most adsorption processes the adsorbent is contacted by the fluid phase in a packed column (Ruthven, 1984). A predictive mathematical model that accurately describes the concentration history profile of the effluent is possibly very useful in design models. Accurate input data are essential for the successful use of predictive design models. This is including mass transport and isotherm parameters (Liu and Weber, 1981). Three mechanisms which are responsible for the broadening of concentrations profile in fixed-bed adsorbers are axial dispersion both molecular and eddy molecular diffusion, the external fluid-phase mass transfer resistance, and the internal solid-phase mass transfer resistance (Cooney, 1991).

### 6.1.1. Mass Balance Equations

The complexity of the dynamic behavior of an adsorption column is directly related to the number of components and the nature of the operation (isothermal or adiabatic) since these factors determine the number of transitions or mass transfer zone (Ruthven, 1984). For this reason, some assumptions are made. First, it is assumed that the system involved is isothermal. Second assumption is that there is no variation of the axial liquid velocity in the radial direction (uniform flow or plug flow). Further, consistent with the concept of plug flow, the last assumption is no variation of solute concentration in either phase in the radial direction. Cooney (1998) states that if the ratio of the column diameter to particle diameter is 20 or greater, then the effects of "channeling" at the wall and of random variations in the interstitial velocity in the bed interior have a negligible effect. In this research, the ratio of the column diameter to the particle sawdust diameter is 69.09, therefore the column have no "channeling" effects.

As illustrated in Fig. 6.1, it is considered that $Z$ (mm) is axial distance coordinate; $\Delta Z$ (mm) is a short length of sawdust of cross-sectional area, $S$ (mm$^2$). $\varepsilon$ is

void fraction in the bed (calculation is provided afterward), *t* is time (sec/min), and *C* is the concentration of solute in the fluid phase (mg/L), $\bar{q}$ is the average concentration of solute in the solid phase (mass of solute per unit volume of solid), $\upsilon$ is the average axial velocity of the flowing fluid in the interstitial spaces (mm/min). The differential mass balance equation for adsorption dissolved nitrogen in sawdust column can be derived as below.

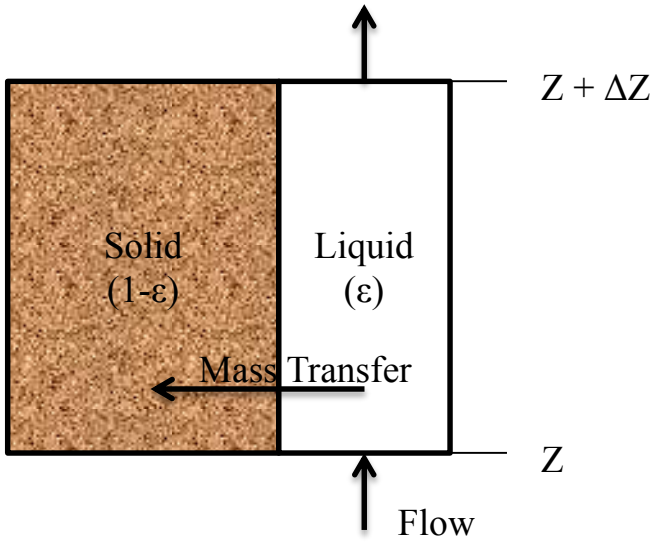


Figure 6.1 Schematic diagram of a segment of a fixed-bed adsorber (adapted from Cooney, 1998).

The space in which the fluid flows has volume $\varepsilon S\Delta Z$ and the solid phase occupies a volume $(1-\varepsilon)S\Delta Z$. *Q* is the rate at which fluid enters and leaves the section shown. The rate at which solute is carried into the column section by flow at plane *Z* is $Q(C)_z = \varepsilon v S(C)_Z$ and the rate at which solute is carried out of the column section by flow at plane $Z + \Delta Z$ is $Q(C)_{Z+\Delta Z}$ or $\varepsilon v S(C)_{Z+\Delta Z}$.

The rate at which solute accumulates in the fluid phase is equal to the volume of the fluid phase times the rate of change of the concentration *C* with time, or

$$\varepsilon S\ \Delta Z\ (\partial C/\partial t)_Z \tag{6.1}$$

where the subscript Z corresponds to an average value of Z over the section. The rate at which solute accumulates in the solid phase is:

$$(1-\varepsilon)S\Delta Z(\partial \bar{q}/\partial t)_Z \tag{6.2}$$

Another mechanism for solute to both enter and leave the column section is axial dispersion. This would make use Fick's law, which states that the dispersive flux

is equal to $-D_a(\partial C/\partial Z)_t$, where $D_a$ is an axial dispersion coefficient. As this flux is mass (or moles) per unit area per unit time, it needs to multiply by the cross-sectional area for dispersion, $\varepsilon S$, to get the rate of input or output in mass (or moles) per time. Hence, the mass balance on the solute over the section can be expressed in words as:

*Rate of solute in by flow + Rate of solute in by dispersion relative to the flow – Rate of solute out by flow – Rate of solute out by dispersion relative to the flow = Rate of accumulation of solute*

Substituting the terms as written above gives:

$$\varepsilon \upsilon S(C)_Z - \varepsilon S D_a \left[\left(\frac{\partial C}{\partial Z}\right)_t\right]_Z - \varepsilon \upsilon S(C)_{Z+\Delta Z} + \varepsilon S D_a \left[\left(\frac{\partial C}{\partial Z}\right)_t\right]_{Z+\Delta Z} = \varepsilon S \Delta Z \left(\frac{\partial C}{\partial t}\right)_Z + (1+\varepsilon) S \Delta Z \left(\frac{\partial \bar{q}}{\partial t}\right)_Z \quad (6.3)$$

Dividing by $\varepsilon S \Delta Z$ and rearranging the equation, and taking the limit $\Delta Z \rightarrow 0$ (Cooney, 1998):

$$\upsilon \left(\frac{\partial C}{\partial Z}\right)_t + \left(\frac{\partial C}{\partial t}\right)_Z + \frac{(1-\varepsilon)}{\varepsilon}\left(\frac{\partial \bar{q}}{\partial t}\right)_Z = D_a \left(\frac{\partial^2 C}{\partial Z^2}\right)_t \quad (6.4)$$

### 6.1.2. The Condition of Axial Dispersion

In all real systems, solute will be transported relative to the bulk fluid motion mainly by dispersion occurring from fluid mixing rather than by molecular diffusion. So, it can be established that $D_a$ is an overall dispersion coefficient which is equal to the molecular diffusivity of the solute *A* in fluid *B* and a mixing or "eddy" dispersion coefficient (Cooney, 1998). Therefore, Cooney (1998) have revealed that when the fluid phase is liquid, axial dispersion can be neglected as a significant factor in determining the behavior of an adsorber, except at extremely low flow rates (Ruthven, 1984; Cooney, 1998).

Considering that statement, this research is verified by some methods to clearly indentify whether the axial dispersion can be neglected or not. The methods are governed by Cooney (1991); it is limited to situations in which either particle diffusion or external film diffusion is the dominant mass transfer process (Cooney, 1991).

The method presents the value of $\gamma_f$ or $\gamma_p$ is a reliable indicator of whether axial dispersion is important. The parameters $\gamma_f$ and $\gamma_p$ reveals their physical significance. When these $\gamma$ values are >>1, axial dispersion can safely be ignored. $\gamma_f$ and $\gamma_p$ are parameters as below (Cooney, 1991):

$$\gamma_f = [\alpha^2(1-\varepsilon)/3\varepsilon]\,(RK_{db}^2/k_f D_a) \tag{6.5}$$

$$\gamma_p = [\alpha^2(1-\varepsilon)/15\varepsilon](R^2K_{db}/D_s D_a) \tag{6.6}$$

where α is velocity of constant pattern front, equal to $\varepsilon v/[\varepsilon+(1-\varepsilon)K]$; $R$ is particle radius; $K_{db}$ is distribution ratio, equal to $q_o/c_o$; $D_s$ is solute diffusivity in the solid phase ($cm^2$/min); $D_a$ is axial dispersion coefficient ($cm^2$/s); $k_f$ is convective fluid phase external film mass transfer coefficient (cm/min).

### 6.1.3. The Internal Solid-phase Mass Transfer Resistance

The simplest model for the solid phase is called Homogeneous Solid Diffusion Model (HSDM) (Cooney, 1998). The system is considered as an idealized bed of uniform spherical microparticles as illustrated in Fig. 6.2. The bed-depth is assumed to be much greater than the diameter of individual particle thus the concentration does not change significantly over the particle surface. Equilibrium is assumed between the adsorbed phase and fluid phase at the particle surface. The equilibrium correlation is taken to be linear (Ruthven, 1984).

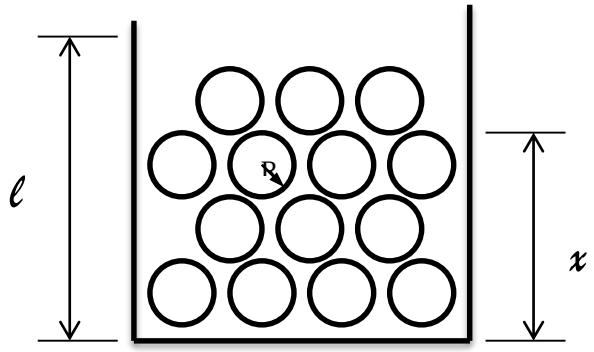


Figure 6.2 Idealized bed of uniform spherical microporous

The equation describing homogenous diffusion in a sphere, assuming a constant diffusivity, $D_s$, at all point in the particle (Cooney, 1998) is:

$$\frac{\partial q}{\partial t} = \frac{D_s}{r^2}\frac{\partial}{\partial r}\left(r^2\frac{\partial q}{\partial r}\right) \tag{6.7}$$

$$\frac{\partial q}{\partial r}(0,t) = 0 \tag{6.8}$$

$$\frac{\partial q}{\partial r}(R,t) = -\frac{k_f}{D_s}(q_s - q^*) \tag{6.9}$$

where $q_s$ is the surface concentration (just inside solid) and $q^*$ is the $q$ value in equilibrium with the bulk concentration in the liquid.

The average value of $q$ in a spherical particle, indicated by $\bar{q}$, is given by:

$$\bar{q} = \frac{3}{R^3}\int_0^R q(r) {r_d}^2 dr \tag{6.10}$$

where $q(r)$ is local values of $q$ in the solid, $r_d$ is a radial position coordinate originating in the centre of the solid spherical particle, and $R$ is the outer radius of the solid particle.

From Cooney (1998), the average concentration in the solid at infinite time ($q_e$):

$$\frac{\bar{q}}{q_e} = 1 - \frac{6}{\pi^2}\sum_{n=1}^{\sim}\frac{1}{n^2} exp\left[\frac{-D_s n^2 \pi^2 t}{R^2}\right] \tag{6.11}$$

For small times operation, or, more precisely, for $\bar{q}/q_e < 0.3$, this equation is written as (Cooney, 1998):

$$\frac{\bar{q}}{q_e} = 6\left[\frac{D_s t}{R^2}\right]^{1/2}\left[\pi^{-1/2} + L\right] \tag{6.12}$$

Thus, a plot of $\bar{q}/q_e$vs the square root of time should give a straight line of slope $6(D_s/\pi R^2)^{1/2}$ from which $D_s$ can be determined.

For long time process, the equation becomes (Cooney, 1998):

$$\frac{\bar{q}}{q_e} \approx 1 - \frac{6}{\pi^2}\exp\left[\frac{-D_s \pi^2 t}{R^2}\right] \tag{6.13}$$

A plot of ln $(1 - \bar{q}/q_e)$vs t should be linear with a slope of $-\pi^2 D_s/R^2$.

### 6.1.4. The External Fluid-phase Mass Transfer Resistance

External film mass transfer dominates mass transfer behavior during the early portion of breakthrough curve obtained from fixed-bed adsorbers. Thus, it is important to define the condition under which their assumptions and their method are valid (Cooney, 1991), as will be discussed below.

Considering the mass transfer through the stagnant liquid film which is usually modeled with the rate law:

$$\frac{\partial \bar{q}}{\partial t} = k_f a(C - C_i) \tag{6.14}$$

where $\bar{q}$ is the average solute concentration in the solid. $C$ is the uniform concentration of the solute in the bulk of the liquid at a distance from the surface; $C_i$ is the concentration of the solute in the liquid at the particle/liquid interface. $a$ is the surface area of the adsorbent particle, and $k_f$ is the film mass transfer coefficient.

Using the form with provision for axial dispersion, the liquid phase balance is same as Eq. 6.4. Stated that initially the fluid-phase concentration at the particle surface is zero, setting $C_i = 0$, substituting Eq. 6.14 into Eq. 6.4, and letting $(\partial c/\partial t)_z$ be zero based on the physical argument that is small, (this assumption is valid if the solid distribution ratio, $q_0/C_0$ is large), hence (Cooney, 1991):

$$v\frac{dC}{dZ} + \frac{(1-\varepsilon)}{\varepsilon} k_f a C = D_a \frac{d^2C}{dz^2} \tag{6.15}$$

Solving for $C$ as a function of $z$, with the boundary condition that $C = C_0$ at $z = 0$, yields:

$$\frac{C}{C_0} = exp\left\{\frac{v}{2D_a} - \left(\frac{v^2}{4D_a^2} + \frac{(1-\varepsilon)k_f a}{\varepsilon D_a}\right)^{1/2}\right\} z \tag{6.16}$$

Evaluating this at the end of the bed ($z = H$) gives:

$$\frac{C}{C_0} = exp\left\{\frac{vH}{2D_a} - \left((\frac{vH}{2D_a})^2 + \frac{(1-\varepsilon)k_f a H^2}{\varepsilon D_a}\right)^{1/2}\right\} \tag{6.17}$$

Plotting fractional concentration $C/C_0$ against the dimensionless residence time, $\theta$, then extrapolating back to $\theta = t/t` = 1$, where $t` = H/v$, is the time required for the first parcel of the solute-rich feed stream to transverse the length of the bed. In order for this method to work, it is necessary to consider that the flowrate in the bed must be large enough and/or the bed short enough to generate a nonzero value of $C/C_0$.

The solution for $D_a = 0$ is:

$$\frac{C}{C_0} = exp\left\{-\frac{(1-\varepsilon)k_f a H}{\varepsilon v}\right\} \tag{6.18}$$

### 6.1.5. Equilibrium Consideration

The equilibrium isotherm illustrates the completely general nature of a concentration front or mass transfer zone. Three general cases can be distinguished depending on whether the equilibrium relationship is linear, favorable, or unfavorable over the concentration range corresponding to the transition consideration (Ruthven, 1984).

Fig. 6.3 shows possible general forms for the equilibrium isotherm and the *X-Y* diagram. The *X-Y* diagram is a nondimensional representation of the equilibrium relationship. It is expressed in term of the reduced variable $(q^*-q`_o)/(q_o-q`_o)$ and $(c-c`_o)/(c_o-c`_o)$, where $q_o-q`_o$ and $c_o-c`_o$ represent the respective changes in adsorbed phase and fluid phase concentration over the mass transfer zone for the component considered.

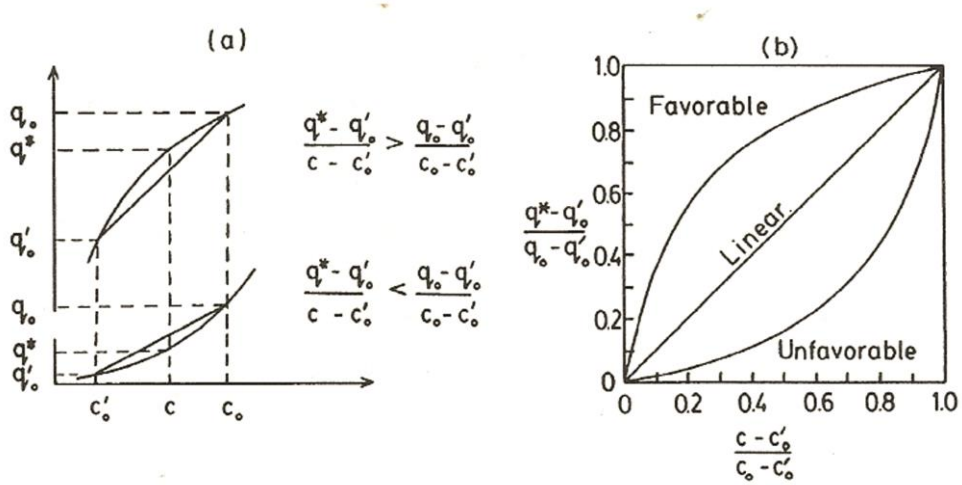


Figure 6.3 (a) Equilibrium isotherm and (b) equilibrium diagram showing distinction between "favorable", "unfavorable", and "linear" systems (adopted from Ruthven, 1984)

The three general cases illustrated in Fig. 6.3 correspond to (Ruthven, 1984):

Favorable $$\frac{q^*-q'_o}{q_o-q'_o} > \frac{c-c'_o}{c_o-c'_o} \quad (6.19)$$

Linear $$\frac{q^*-q'_o}{q_o-q'_o} = \frac{c-c'_o}{c_o-c'_o} \quad (6.20)$$

Unfavorable $$\frac{q^*-q'_o}{q_o-q'_o} < \frac{c-c'_o}{c_o-c'_o} \quad (6.21)$$

## 6.2. Available Correlations of Mass Transfer in Literature

### 6.2.1. Dimensionless Transforms

The mass transfer coefficients in fixed bed column can be correlated with dimensionless groups characterized by the flow and geometry of the column. The dimensionless groups are used for solving variety of problems in mass transfer and summarized as below.

$$Re = \frac{Inertial\ forces}{Viscous\ forces} = \frac{d_p \varepsilon v \rho}{\mu} \tag{6.22}$$

$$Sc = \frac{Viscous\ diffusion\ rate}{Molecular\ (mass) diffusion\ rate} = \frac{\mu}{\rho D_m} \tag{6.23}$$

$$Sh = \frac{Convective\ mass\ transfer\ coefficient}{Diffusive\ mass\ transfer\ coefficient} = \frac{k_f d_p}{D_m} \tag{6.24}$$

$$j_D = \frac{Mass\ transfer\ coefficient}{friction\ factor} = \left(\frac{k_f}{\varepsilon v}\right) Sc^{2/3} \tag{6.25}$$

$$Bi = \frac{Mass\ transfer\ coefficient}{Mass\ diffusivity} = \frac{k_f d_p}{2K_{db} D_s} \tag{6.26}$$

where *Re* is Reynold number, *Sc* is Schmidt number, *Sh* is Sherwood number, $j_D$ is Colburn factor, and *Bi* is Biot number. $d_p$ is particle diameter (cm), $\varepsilon$ is void fraction in packed bed, $v$ is interstitial fluid phase velocity(cm/min), $\rho$ is fluid phase density (g/cm$^3$), and μ is fluid phase viscosity (g/cm min). $D_m$ is solute molecular diffusivity in the fluid phase (cm$^2$/min), $k_f$ is convective fluid phase external film mass transfer coefficient (cm/min), $D_s$ is solute diffusivity in the solid phase (cm$^2$/min), and $K_{db} = q_0/c_0$.

### 6.2.2. Correlations for Axial Dispersion

Axial dispersion contributes to the broadening of the adsorption front due to flow in the void spaces between particles. The axial dispersion can be estimated by using the following correlation (Ruthven, 1984):

$$\frac{D_a}{v d_p} = \frac{20}{\varepsilon}\left(\frac{D_m}{v d_p}\right) + \frac{1}{2} \tag{6.27}$$

### 6.2.3. Correlations for Fluid Phase Mass Transfer Coefficients

The transport of the adsorable species from the bulk of the fluid phase to the external surface of the adsorbent consist of an important step in the overall uptake process. For modeling a fixed bed adsorber, a volumetric mass transfer coefficient in the liquid phase can be estimated from available mass transfer correlation.

Numerous researchers have investigated experiments for measuring mass transfer in fixed bed and have established correlations for their results (Wilson and Geankoplis, 1966; Suzuki, 1990). Thus, the $k_f$ value is also estimated using the following correlation.

Correlation of experimental data in the region of 0.0016 < Re < 55, Wilson and Geankoplis recommended as below (Wilson and Geankoplis, 1966):

$$j_D = \frac{1.09}{\varepsilon} Re^{-2/3} \qquad (6.28)$$

Based on this correlation, $k_f$ can be calculated also from relationship below (Suzuki, 1990):

$$Sh = \left(\frac{1.09}{\varepsilon}\right) Sc^{1/3} Re^{1/3} \qquad \text{for} \quad 0.0015 < \text{Re} < 55 \qquad (6.29)$$

## 6.3. Results and Discussion

### 6.3.1. Determination of the Bed Void Fraction

The total bed void fraction ($\varepsilon$) is the fraction of the space in the packed bed in which the fluid flows. The calculation is based on difference of the weight of saturated and dried sawdust. Several columns were measured at the end of experiments. The average of bed void fraction is 0.7 with standard deviation 0.7 ± 0.01.

### 6.3.2. Classification of Single-Transition Systems

#### 6.3.2.1. Equilibrium Relationship

Checking the relationship of isotherm according to Eq. 6.19-6.21 is significant to explain entirely the nature of mass transfer zone. Thus, based on concentration test in batch experiments, the summary of the equilibrium isotherm and its equation can be

seen at Table 6.1. $NO_3$-N is linear following Freundlich isotherm, while $NH_3$-N and $NO_2$-N are favorable isotherms with Langmuir and Freundlich forms respectively.

Table 6.1. The equation of equilibrium isotherm

| Species | Condition | Isotherm | Equation |
|---|---|---|---|
| $NH_3$-N | Favorable | Langmuir | $q = (0.059C)/(1+C)$ |
| $NO_3$-N | Linear | Freundlich | $q = 0.05C^{0.435}$ |
| $NO_2$-N | Favorable | Freundlich | $q = 0.163C^{0.388}$ |

#### 6.3.2.2. Isothermal and Adsorbable Components

In this research, it is assumed that heat transfer resistance can be neglected. The simplest type of system is an isothermal system with one adsorbable component in an inert carrier. Changes in fluid velocity across the mass transfer zone are therefore negligible.

#### 6.3.2.3. The Significant of Axial Dispersion

Based on Cooney method (Cooney, 1991), the significant of axial dispersion was proved by calculating equation 6.5. and 6.6. From Table 6.2, it can be seen that for $NH_3$-N and $NO_3$-N, all of the $\gamma_f$ or $\gamma_p$ values are below of 1. This indicates the axial dispersion is significant during the adsorption process which is its flow model is called dispersed flow model. Whereas, $\gamma_f$ or $\gamma_p$ values of $NO_2$-N are >> 1, which means axial dispersion can be ignored and its flow model can be assumed as plug flow model. In order to obtain the values of $\gamma_f$ and $\gamma_p$ for all species, axial dispersion coefficients were determined by Eq. 6.27.

#### 6.3.2.4. Complexity of Kinetic Model

Consider of the Biot number (*Bi*) which is the ratio of the liquid-phase mass transfer rate to the intraparticle mass transfer rate. As Bi increases, the liquid-phase mass transfer rate becomes faster as compared to the intraparticle mass transfer rate, so for the Biot numbers greater than 30, the intraparticle-phase mass transfer rate controls the adsorption rate (Hand et al., 1984). Also, Cooney has stated that if *Bi* value > 30 (approximately) the particle resistance essentially dominates and the external film

resistance may be ignored and when $Bi < 1$ (approximately) the reverse is true (Cooney, 1991).

Furthermore, Traegner and Suidan (1989) have stated in their research that first, liquid film mass transfer is the dominant transport mechanism if the Biot number is 1 or less. For such a Biot Number the model loses sensitivity to perturbations in *Ds*, and becomes very sensitive to variations in $k_f$. Second, surface diffusion is the dominant mass transfer mechanism if the Biot number is 100 or bigger and the equilibrium adsorption isotherm is favorable. In this case, the model is very sensitive to variations in *Ds* and is insensitive to the selected values of $k_f$. Finally, both transport mechanisms are important if Biot numbers between 1 and 100. Sensitivity to either of the kinetic parameters depends on whether the actual solution is closer to 1 or 100. The model is sensitive to $k_f$ and *Ds* in this Biot number range. Clearly if $Bi >> 100$, the experimental data are not suitable to determine liquid film mass transfer coefficients and if $Bi << 1$, computed solid diffusion coefficients will not be reliable (Traegner and Suidan, 1989). Thus, the experimental data is separated into two basic form of the complexion of kinetic model.

Since the Bi number of $NH_3$-N and $NO_3$-N obtained from experimental data (Table 6.2) varies between 33 and 163, in general (only 3 points more than 100), it can be said that both external film resistance and surface diffusion are considered in mathematical modeling. However, it should be noticed that only $NH_3$-N in this criteria has favorable isotherm.

Even though $NO_2$-N has Biot number greatly more than 100 which means all of the mass transfer resistance resides in the solid, but in any real system, the external film resistance is not negligible (Cooney, 1998). One can assume an experimental value for $k_f$ by noting that, near $t = 0$, there is no significant solute in the solid phase and thus the solid phase resistance is negligible, hence one can model the initial uptake using only the rate law which contains $k_f$ (Cooney, 1998). Also, the values of $\gamma_f$ or $\gamma_p$ are a large amount more than 1, therefore the second form is $NO_2$-N with no axial dispersion and the external film resistance is calculated by Eq. 6.18.

Table 6.2. Operating conditions and evaluated parameters of complexity of kinetic model.

| *Column Name* | *Q* (mL/s) | *Co* (mg/L) | *Z* (cm) | $\epsilon v$ (mL/s cm$^2$) | $K_{db}$ | *Bi* | α | $\gamma_p$ | $\gamma_f$ |
|---|---|---|---|---|---|---|---|---|---|
| $NH_3$-N-1 | 0.153 | 0.533 | 19 | 0.014 | 0.038 | 65 | 0.019 | 0.073 | 0.006 |
| $NH_3$-N-2 | 0.276 | 0.542 | 19 | 0.024 | 0.038 | 133 | 0.034 | 0.168 | 0.006 |
| $NH_3$-N-3 | 0.366 | 0.539 | 19 | 0.032 | 0.038 | 163 | 0.045 | 0.245 | 0.007 |
| $NH_3$-N-4 | 0.164 | 0.971 | 19 | 0.014 | 0.030 | 80 | 0.020 | 0.056 | 0.003 |
| $NH_3$-N-5 | 0.164 | 2.185 | 19 | 0.014 | 0.019 | 77 | 0.021 | 0.035 | 0.002 |
| $NH_3$-N-6 | 0.164 | 1.030 | 11 | 0.014 | 0.029 | 102 | 0.020 | 0.054 | 0.003 |
| $NH_3$-N-7 | 0.164 | 0.999 | 15 | 0.014 | 0.030 | 80 | 0.020 | 0.055 | 0.003 |
| $NO_3$-N-8 | 0.160 | 0.565 | 19 | 0.014 | 0.069 | 33 | 0.020 | 0.148 | 0.022 |
| $NO_3$-N-9 | 0.277 | 0.544 | 19 | 0.024 | 0.071 | 51 | 0.034 | 0.327 | 0.032 |
| $NO_3$-N-10 | 0.366 | 0.548 | 19 | 0.032 | 0.070 | 50 | 0.045 | 0.469 | 0.047 |
| $NO_3$-N-11 | 0.164 | 1.06 | 19 | 0.014 | 0.048 | 41 | 0.020 | 0.105 | 0.013 |
| $NO_3$-N-12 | 0.164 | 2.565 | 19 | 0.014 | 0.029 | 57 | 0.020 | 0.061 | 0.005 |
| $NO_3$-N-13 | 0.164 | 1.020 | 11 | 0.014 | 0.049 | 81 | 0.020 | 0.107 | 0.007 |
| $NO_3$-N-14 | 0.164 | 1.045 | 15 | 0.014 | 0.049 | 78 | 0.020 | 0.105 | 0.007 |
| $NO_2$-N-15 | 0.157 | 0.537 | 19 | 0.014 | 0.238 | 2198 | 0.018 | 227.564 | 0.520 |
| $NO_2$-N-16 | 0.208 | 0.545 | 19 | 0.018 | 0.236 | 1110 | 0.024 | 338.108 | 1.526 |
| $NO_2$-N-17 | 0.374 | 0.549 | 19 | 0.033 | 0.235 | 3454 | 0.043 | 735.425 | 1.067 |
| $NO_2$-N-18 | 0.166 | 1.050 | 19 | 0.015 | 0.158 | 5076 | 0.020 | 156.198 | 0.155 |
| $NO_2$-N-19 | 0.164 | 5.260 | 19 | 0.014 | 0.059 | 23213 | 0.020 | 113.097 | 0.025 |
| $NO_2$-N-20 | 0.164 | 1.044 | 11 | 0.014 | 0.159 | 13785 | 0.019 | 153.930 | 0.057 |
| $NO_2$-N-21 | 0.164 | 1.013 | 15 | 0.014 | 0.162 | 5457 | 0.019 | 156.424 | 0.145 |

### 6.3.3. Determination of Mass Transfer

#### 6.3.3.1. The Solid phase Mass Transfer Coefficients

The surface diffusion ($D_s$) was calculated by Eq. (6.12) for $NH_3$-N and $NO_3$-N, and Eq. (6.13) for $NO_2$-N. The surface diffusivity is usually obtained from rate studies of adsorption in batch reactor (Liu and Weber, 1981; Cooney, 1998). The reason of this is because of the difficulty in determining the surface diffusion in long column fixed-bed operation as that both film transfer and surface diffusion occur simultaneously along the entire range of the breakthrough curve and also the fact that $D_s$ theoretically is independent of flow rate (Liu and Weber, 1981). Therefore, all calculations for determining surface diffusions in this research were using batch experiments data.

The Results are shown in Fig. 6.4 and Fig. 6.5 for a range of 0.5 – 5 mg/L of concentration of solutions. It can be observed that $NH_3$-N and $NO_3$-N (Fig. 6.4), which have less sensitivity in solid phase mass transfer, the range of $D_s$ values is very little. It is in the range of 3.87–4.4×$10^{-6}$ $cm^2/s$ and 3.7–4.58×$10^{-6}$ $cm^2/s$ for $NH_3$-N and $NO_3$-N respectively. However, *Ds* values of $NO_2$-N (Fig. 6.5), the solid diffusivity are dissimilar in every single concentration of solutions. $D_s$ values of $NO_2$-N are in the range of 4.35–7.92×$10^{-9}$ $cm^2/s$. This sensitivity is approved by Traegner and Suidan statements (Traegner and Suidan, 1989). Accordingly, the surface diffusivity must also be recognized as concentration-dependent (Fettig and Sontheimer, 1987).

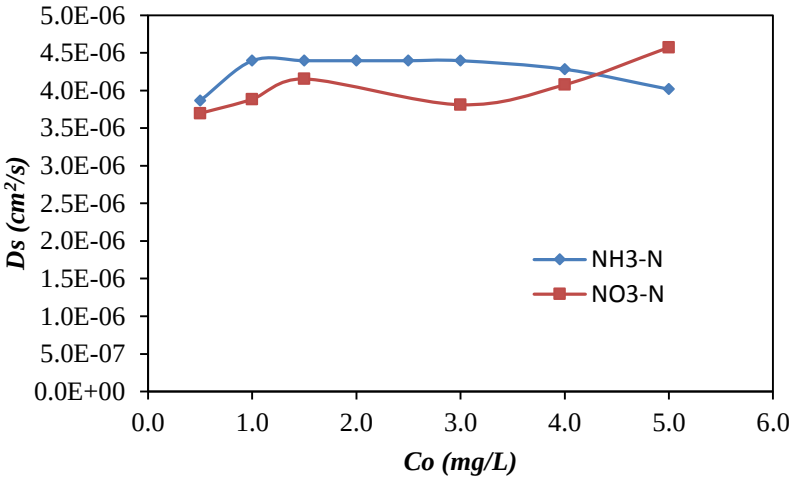


Figure 6.4 Surface diffusion coefficients for $NH_3$-N and $NO_3$-N

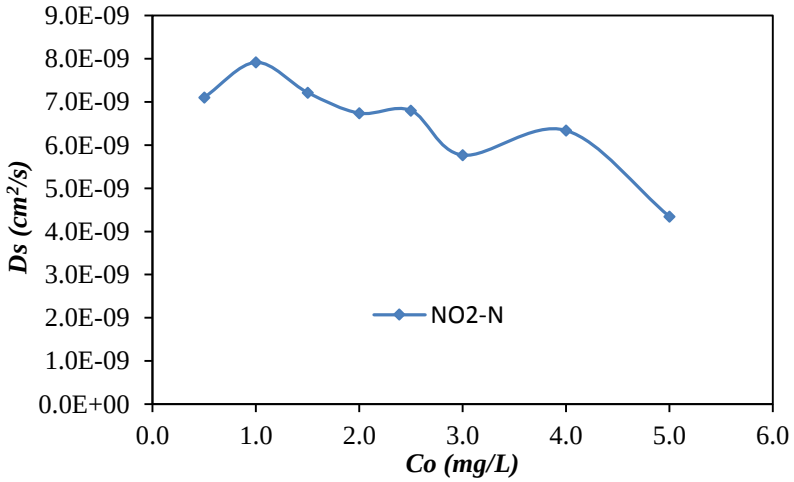


Figure 6.5 Surface diffusion coefficients for $NO_2$-N

### 6.3.3.2. Axial Dispersion

Axial dispersion coefficients were computed by Eq. 6.27. The molecular diffusivities ($D_M$) which used for analyzing these coefficients for all adsorbates are listed in Table 6.4. The results are shown in Table 6.5 for $NH_3$-N and $NO_3$-N. As axial dispersion affected by molecular diffusion and by the dispersion related fluid flow (Vazquez et al, 2006), in Fig. 6.6 shows the axial dispersion coefficient increases with increasing the flow rate. This result is also good agreement with Borba et al. (2006) which was removing nickel (II) ions from aqueous solutions by biosorption in a fixed bed column. The statement of dispersion effects are generally negligible for fixed-bed adsorbers with relative long length (Liu and Weber, 1981) can be approved by Fig. 6.7 which is illustrating there is no effect of bed-depth of axial dispersion. The values of axial dispersion are in the range of 1.05-1.8×$10^{-3}$ $cm^2/s$ for all experiment criterions.

Table 6.4. Diffusion coefficients adsorbates in water ($D_M$), (Picioreanu et al, 1997)

| Adsorbate | $D_M$ ($cm^2/s$) |
|---|---|
| $NH_3$-N | 1.86E-05 |
| $NO_3$-N | 1.70E-05 |
| $NO_2$-N | 1.70E-05 |

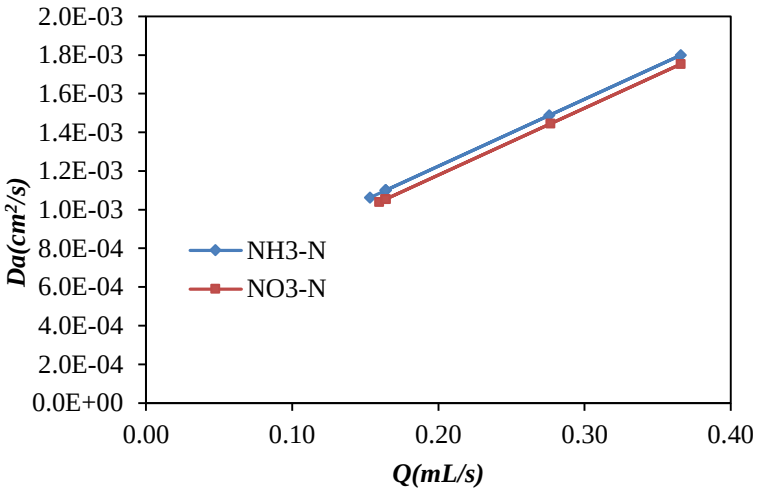


Figure 6.6 Axial Dispersion ($D_a$) vs Flow Rate ($Q$)

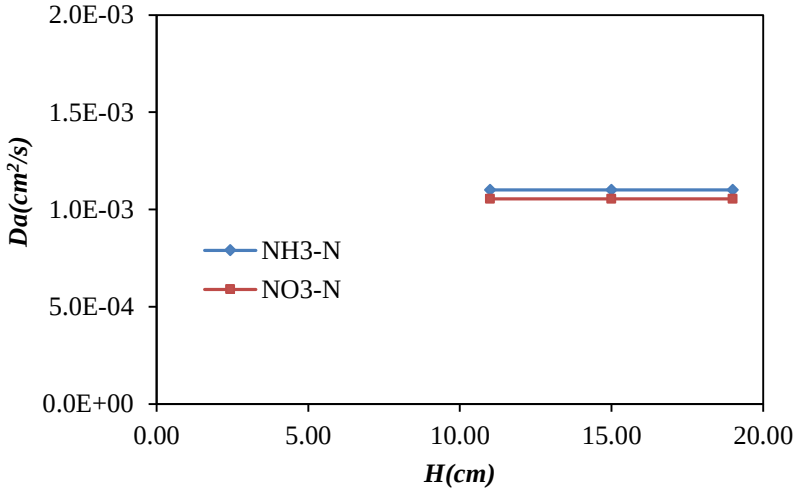


Figure 6.7 Axial Dispersion ($D_a$) vs bed-depth ($H$)

### 6.3.3.3. The External Fluid-phase Mass Transfer Resistance

After determining axial dispersion, film transfer coefficients ($k_f$) were calculated by Eq. (6.17) for $NH_3$-N and $NO_3$-N and Eq. (6.18) for $NO_2$-N, which is the mass-transfer area per unit volume of bed sawdust was calculated as: $a = 6(1-\varepsilon)/d_p$. The results are described in Table 6.5. Generally, it can be said that $k_f$ increases with increased flow rate and decreased bed-depth (Fig. 6.8 and Fig. 6.9). This result is same as other studies (Chatzopoulos and Varma, 1995; Vazquez et al, 2006).

The values of $k_f$ from experiment result ($k_{f\,(exp)}$) then was compared with $k_f$ correlation ($k_{f\,(correl)}$) (Eq. 6.29) (Table 6.5). Although this correlation was calculated based on the hydrodynamic conditions in the bed, the accuracy of this correlation is generally low (Chatzopoulos and Varma, 1995). This mainly due to approximation of the rough activated carbon granular as smooth spherical particle, the external GAC surface area $a$ is typically underestimated significantly in the model. Thus, since the rate of solute mass transfer to the particle-liquid interface is proportional to $k_f a$, the model requires using the artificially higher $k_f$ values to compensate for the underestimation of $a$ (Fettig and Sontheimer, 1987; Chatzopoulos and Varma, 1995). Moreover, even when applied to fixed bed adsorbers containing the same type of packing materials for which the mass transport correlations have been derived, this correlation procedure usually introduces a potentially error of approximately 20% (Liu and Weber, 1981). It is, consequently, finding out the film transfer coefficients

directly from fixed-bed adsorbers would provide much more accurate estimates for the film transfer coefficients, $k_f$.

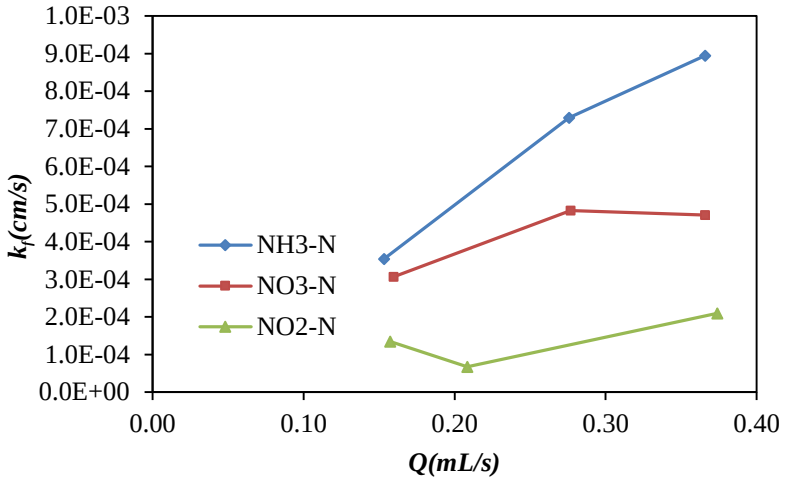


Figure 6.8. Correlation between $k_f$ and the flow rate ($Q$).

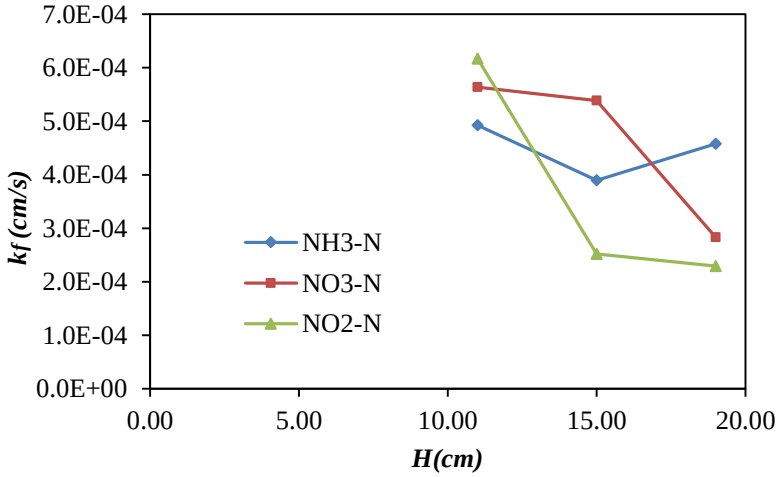


Figure 6.9 Correlation between $k_f$ and the bed-depth ($H$).

Table 6.5. Values of $D_a$, $k_f$ *experiments* and $k_f$ *correlation* with Eq. 6.29.

| *Column Name* | $D_a$ ($cm^2/s$) | $k_f a$ *1/s* | $k_f$ cm/s | $k_f$*(correl)* cm/s |
|---|---|---|---|---|
| $NH_3$-N-1 | 1.06E-03 | 0.012 | 3.55E-04 | 1.80E-03 |
| $NH_3$-N-2 | 1.49E-03 | 0.024 | 7.29E-04 | 2.19E-03 |
| $NH_3$-N-3 | 1.80E-03 | 0.029 | 8.94E-04 | 2.41E-03 |
| $NH_3$-N-4 | 1.10E-03 | 0.013 | 4.58E-04 | 1.84E-03 |
| $NH_3$-N-5 | 1.10E-03 | 0.007 | 2.41E-04 | 1.84E-03 |
| $NH_3$-N-6 | 1.10E-03 | 0.016 | 4.92E-04 | 1.84E-03 |
| $NH_3$-N-7 | 1.10E-03 | 0.013 | 3.90E-04 | 1.84E-03 |
| $NO_3$-N-8 | 1.04E-03 | 0.010 | 3.07E-04 | 1.72E-03 |
| $NO_3$-N-9 | 1.45E-03 | 0.016 | 4.83E-04 | 2.07E-03 |
| $NO_3$-N-10 | 1.75E-03 | 0.015 | 4.71E-04 | 2.27E-03 |
| $NO_3$-N-11 | 1.05E-03 | 0.009 | 2.83E-04 | 1.73E-03 |
| $NO_3$-N-12 | 1.05E-03 | 0.008 | 2.48E-04 | 1.73E-03 |
| $NO_3$-N-13 | 1.05E-03 | 0.018 | 5.64E-04 | 1.73E-03 |
| $NO_3$-N-14 | 1.05E-03 | 0.018 | 5.38E-04 | 1.73E-03 |
| $NO_2$-N-15 | - | 0.004 | 1.35E-04 | 1.71E-03 |
| $NO_2$-N-16 | - | 0.002 | 6.77E-05 | 1.88E-03 |
| $NO_2$-N-17 | - | 0.007 | 2.10E-04 | 2.28E-03 |
| $NO_2$-N-18 | - | 0.008 | 2.29E-04 | 1.74E-03 |
| $NO_2$-N-19 | - | 0.007 | 2.15E-04 | 1.73E-03 |
| $NO_2$-N-20 | - | 0.020 | 6.17E-04 | 1.73E-03 |
| $NO_2$-N-21 | - | 0.008 | 2.52E-04 | 1.73E-03 |

### 6.3.4. Development of Mass Transfer Correlation for Nutrient Adsorption

Usually correlations of dimensionless groups are formulated for predicting the rate constants for external transport in fixed-bed. Commonly, the external fluid-phase mass transfer coefficients, $k_f$, is fitted in the dimensionless Sherwood number, *Sh*, which is predicted as a function of the Reynolds number, *Re*, and the Schmidt number, *Sc*, characterizing hydrodynamic conditions and molecular diffusion, respectively (Robert et al, 1985).

Most of the previous authors who are working in solid-liquid mass transfer in porous media have neglected axial dispersion and used a plug flow model. However, one can note that it is necessary to use the axial dispersion model in the range of low velocities (Comiti and Renaud, 1991). In this research, based on the complexity of

model determined earlier, experimental data of $NH_3$-N has been selected to simulate of all data set for mass transfer coefficient as a function of Sherwood number.

The stepwise regression analyses were carried out to obtain the best fit of this model. It is begin with calculating Reynold number (*Re*), Schmidt number (*Sc*), and Sherwood number (*Sh*) by using Eq. 6.22 - 6.24. The strong correlation of mass transfer rate coefficients and velocity in terms of dimensionless of *Sh* and *Re* numbers is shown in Fig. 6.10. It can be confirmed that *Sh* number increases with increasing *Re* number.

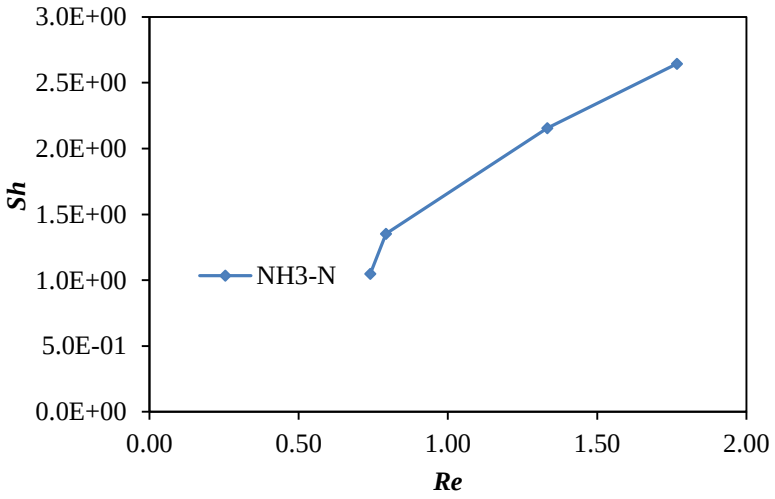


Figure 6.10 Sherwood number (*Sh*) vs Reynolds number (*Re*)

For all types of packed bed, most authors have been assumed that *Sh* is proportional to *Sc* to the power of 1/3 for liquid-solid mass transfer. Then it can be expressed in dimensionless form as:

$$Sh = a\, Re^m Sc^{1/3} \tag{6.30}$$

Where *a* and *m* are empirical constants obtained by fitting experimental data. The data was transformed to the logarithmic form and a linearization model was used for the correlation. Thus in *ln* linearized form, Eq. 6.30 become:

$$\ln\left(\frac{Sh}{Sc^{1/3}}\right) = \ln a + m \ln Re \tag{6.31}$$

The transformed data (Eq. 6.31) were fitted by a simple least-square analysis (Ayyub and McCuen, 2011). The standard error estimate of the model which is equal to the standard deviation of the errors is given by:

$$S_e = \sqrt{\frac{1}{n-2}\sum_{i=1}^{n}\left(ln(\frac{\widehat{Sh}}{Sc^{1/3}}) - \ln(\frac{Sh}{Sc^{1/3}})\right)^2} \tag{6.32}$$

where $n$ is the number of data points and $ln(\frac{\widehat{Sh}}{Sc^{1/3}})$ is the value of the particular data point of experiment. The optimum external fluid phase mass transfer model is found as:

$$Sh = 0.4059\, Re^{1.02} Sc^{1/3} \tag{6.33}$$

This model is valid for the condition of 0.74 < Re < 1.77 and *Sc* at 54. The standard error of estimate of this model was found *Se* = 0.12. The exponential value of 1.02 for the Reynolds number indicates that the mass transfer coefficient is proportional to the liquid velocity to the power of 1.02. Fig. 6.11 shows the plot of the model and experimental data.

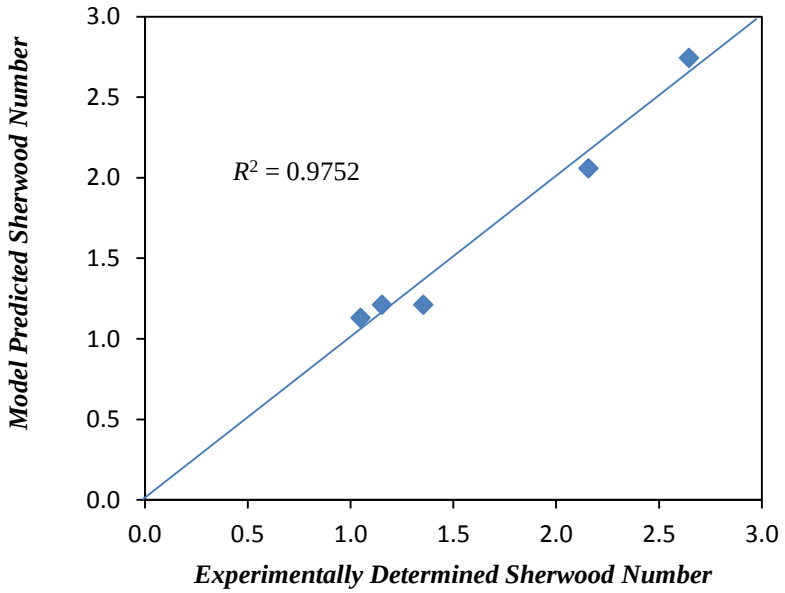


Figure 6.11 Plot of experimentally determined $Sh_{(exp)}$ with model predicted $Sh_{(model)}$.

## 6.4. Comparison to Other Studies

The numbers of liquid-solid mass transfer experimental studies have been performed previously. They have proposed general correlating of fluid-phase mass transfer. Most of the experimental studies deal with packed bed of spheres (Table 6.6). In almost all methods they have used as a plug flow model, until Wakao and Funazkri (1978) proposed the mass transfer correlation with considering axial dispersion in the liquid flow. One must be noted that the mean mass transfer coefficient $k_f$ is calculated from the rate of dissolution of solid particles in the liquid stream. As a result, the solid mass transfer surface area is modified slightly as a function of time with possible formation of small roughness which may affect the value of $k_f$ (Comiti and Renaud, 1991).

From table 6.6, it can be seen that the last three line of the Sherwood number contains the constant number of 2 which represents the minimum possible rate of mass transfer from an isolated active spherical particle in a stagnant fluid condition. Active particle mean a particle that is exchanging mass with the fluid phase because either a chemical reaction or a physical process is taking place (Scala 2013). However, the single active particle if surrounded by a bed of inert particles, this limiting value should be corrected for the effect of diffusion of the bed and of the decrease of the available fluid volume (Scala 2013). Many experimental works reported at low Reynolds number the predicted values of *Sh* were much lower than two and approached zero at $Re \rightarrow 0$ (Scala 2013). Thus, since this study was focusing at the low Reynolds number, the Sherwood limiting value was taken as zero.

The dependence of the experimental *Sh* that obtained from this investigation on the hydrodynamic condition in the bed as performed by the exponent of *Re* (1.02) is higher than those other researchers. However, this fluid flow around the particle which is affected to the constant of Reynolds number (0.4059) in this study was obtained less than other references. As noted earlier, this dissimilarity is influenced by the higher surface area obtained from previous references which is using solid particles. Additionally, this might be the fact that sawdust particle in this research is intraparticle adsorbate medium. Furthermore, the Reynolds number in the bed of sawdust is very low (0.74 - 1.77) which is mainly in the laminar flow regime (Suzuki, 1990), while other researchers investigated at higher Reynolds number up to 10.000.

These factors, lead to make the distinction of the exponent of Reynolds number in this research.

Table 6.6. Liquid-solid mass transfer in packed beds

| *Correlation Equation* | *Packed bed examined* | *Valid condition* | *Reference* |
|---|---|---|---|
| $Sh = 0.4059\ Re^{1.02} Sc^{1/3}$ | Sawdust – water<br>ε = 0.7 | 0.74 < *Re* < 1.77 | This study |
| $Sh = 2.4\ Re^{0.34} Sc^{1/3}$ | Benzoic acid spheres - water<br>ε = 0.436 | 0.08 < *Re* < 120<br>150 < *Sc* < 1300 | Williamson et al. (1963) |
| $Sh = 2.5\ Re^{1/3} Sc^{1/3}$ | Benzoic acid spheres - water<br>ε = 0.436 | 0.0016 < *Re* < 55<br>950 < *Sc* < 70000 | Wilson and Geankoplis (1966) |
| $Sh = 2 + 1.1\ Re^{0.6} Sc^{1/3}$ | Review 12 selected experimental data studies<br>ε = 0.4 | 3 < *Re* < 10000 | Wakao and Funazkri (1978) |
| $Sh = 2 + 3.44\ Re^{0.471} Sc^{1/3}$ | Filtrasorb-300 (F-300) -water ε = 0.41 | 1 < *Re* < 100 | Chatzopoulos and Varma (1995) |
| $Sh = 2 + 0.61\ Re^{0.34} Sc^{1/3}$ | Wheat straw - water | 18 < *Re* < 445 | Doan et al. (2008) |

## 6.5. Concluding Remarks

Mass transfer characteristics of nutrients adsorption onto sawdust were examined and a mass transfer correlation was develop. Three mechanisms are verified for the broadening of concentrations profile in fixed-bed adsorbers. There are axial dispersion, the external fluid-phase mass transfer resistance, and the internal solid-phase mass transfer resistance. The adsorption isotherm parameters and surface diffusion coefficients were determined independently in batch experiments.

In the variety of 0.5 – 5 mg/L of concentration of solutions, surface diffusion, $D_s$, was obtained in the range of 3.87–4.4×$10^{-6}$ $cm^2/s$, 3.7–4.58×$10^{-6}$ $cm^2/s$, for $NH_3$-N, $NO_3$-N respectively which was less sensitivity in solid phase mass transfer due to their Biot number range were less than 100. However, NO2-N which has range of Biot number more than 100 which means all of the mass transfer resistance resides in the solid, its surface diffusion $D_s$ was obtained in the range of 4.35–7.92×$10^{-9}$ $cm^2/s$. It can be concluded that the surface diffusion is concentration-dependent.

The values of axial dispersion are in the range of 1.05-1.8×$10^{-3}$ $cm^2/s$ for $NH_3$-N and $NO_3$-N. The axial dispersion coefficient increases with increasing flow rate. However, it was found that the length of bed has no effect of axial dispersion. External mass transfer coefficients, $k_f$, were obtained in the range of 2.41–8.94×$10^{-4}$ cm/s, 2.48–5.6×$10^{-4}$ cm/s, and 0.677–6.17×$10^{-4}$ cm/s for $NH_3$-N, $NO_3$-N, and $NO_2$-N, respectively. These results are higher than those predicted by literature correlations. This is probably due to the different estimation of specific external surface area.

In this research, based on $NH_3$-N results, the optimum mass transfer correlation was found as $Sh = 0.4059Re^{1.02}Sc^{1/3}$. This correlation is valid in the range of $0.74<Re<1.77$. The standard error of estimate of this model was found 0.12. The mass transfer coefficient is proportional to the liquid velocity to the power of 1.02. This relationship can be useful for the designing a stormwater treatment particularly in nitrogen removal.

# CHAPTER 7

# CONCLUSIONS AND RECOMMENDATIONS

## 7.1. Conclusions

An increased impervious area causes an increase total volume of rainfall runoff and its pollutants. As a result, stormwater runoff contains varieties of contaminants such as hydrocarbons, trace metals and nutrients. Nutrients include phosphorous and nitrogenous compounds such as ammonia-nitrogen ($NH_3$-N), nitrate-nitrogen ($NO_3$-N), and nitrite-nitrogen ($NO_2$-N). This contaminated water is harmful to human health and the surrounding ecosystem. It is therefore essential to remove these contaminants before it goes to water bodies.

A combined natural-engineered system known as biological retention (bioretention/biofiltration) has recently been suggested as a simple but effective strategy to manage stormwater runoff. If nitrogen removal is of concern, one strategy to overcome this environmental threat is to design the bioretention/biofiltration system with a SAZ (Saturated Zone) to enhance anaerobic denitrification. Usually an additional carbon source is included in the SAZ as an electron donor to facilitate denitrification. In the research carried out for this paper, wood sawdust from Radiata pine was chosen as the additional carbon source, in order to determine its effectiveness as a superior and cheaper resource. Investigations were carried out on the removal of nutrients from stormwater using the sawdust. First, a series of batch experiments was carried out for different initial nutrient concentrations, dosages, particle sizes, contact times and pH. Next, a series of column experiments were performed at different flow rates, with differing nutrient concentrations, and varying heights of sawdust columns.

The results of the batch experiments show that sawdust is an effective adsorbent in removing $NH_3$-N, $NO_3$-N, and $NO_2$-N from aqueous solutions, particularly at lower concentrations. The maximum of 55% removal was obtained for $NH_3$-N adsorption and 100% removal was obtained for $NO_3$-N and $NO_2$-N adsorption. Maximum removal was obtained after 10 minutes for $NH_3$-N and $NO_3$-N, while it took 45 hours to reach maximum removal of $NO_2$-N. In the dosage test, the percentage removal increased due to the greater availability of a surface area for adsorption.

However, pH and particle sizes did not show any significant effect in the removal process. The $NH_3$-N adsorption followed the Langmuir model ($R^2$ = 0.96±0.01) but the adsorption of $NO_3$-N and $NO_2$-N followed the Freundlich model ($R^2$ =0.99±0.01). The sawdust surface is made up of small heterogeneous adsorption patches and thus most of the nutrients followed Freundlich model.

The kinetics of the adsorption process were checked for different nutrient adsorption onto sawdust. The results revealed that the kinetics of $NO_2$-N adsorption follows the pseudo-first and second order respectively but that $NH_3$-N and $NO_3$-N adsorption follows the pseudo-second order only. This is due to equilibrium being reached more rapidly in $NH_3$-N and $NO_3$-N adsorption than the $NO_2$-N adsorption. This explains why intraparticle diffusion and film liquid diffusion were the predominant processes in $NO_2$-N adsorption.

The dynamic behaviour of adsorption characteristics of nutrient onto sawdust was studied with breakthrough curves. The results revealed that nutrient adsorption in dynamic conditions depend upon several experimental conditions. The nutrient removal and breakthrough time decreases with the increasing flow rate, inlet concentration and bed depth. Further, the length of unused bed (LUB) was calculated to check how much sawdust took part in the solute adsorption process prior to breakthrough. The value of the LUB could then be added to the stoichiometric length of bed needed. This made the actual column longer, to account for any unused adsorption capacity under actual conditions.

Clark (1987) and Yoon and Nelson (1984) models were then used for the column data, to simulate the breakthrough curves and to determine the column kinetic parameters. The adsorption of different nutrients was explained by these models differently. Both models showed effective predictions for $NO_2$-N adsorption; the Clark model (1987) provided good predictions for $NH_3$-N adsorption, and the Yoon and Nelson (1984) model proved effective at predicting $NO_3$-N adsorption.

Fluid-solid interphase mass transfer is an important process in nutrient adsorption and this was tested in this study. Surface diffusion was calculated from the batches, and axial dispersion was calculated from the columns. Results revealed that surface diffusion is concentration-dependent, but that axial dispersion depends on the flow rate. The liquid-solid phase mass transfer coefficient ($k_f$) was calculated and found to be directly proportional to the flow rate but inversely proportional to the bed

depth. The Biot number calculated for different nutrient adsorptions shows that surface diffusion and interphase mass transfer are the two dominant processes for $NH_3$-N and $NO_3$-N adsorption, but that $NO_2$-N adsorption is dominated by surface diffusion only.

Finally, a liquid-solid phase mass transfer correlation for nutrient adsorption onto sawdust was developed. Based on the Biot number and sorption isotherm, only $NH_3$-N data was used to develop this relationship. $NH_3$-N has Biot number range of 1 to 100 which means have both external film resistance and surface diffusion and also it has favorable isotherm. A stepwise regression analysis was performed to obtain the optimum mass transfer correlation. The optimum liquid-solid phase mass transfer correlation was found as $Sh=0.4059Re^{1.02}Sc^{1/3}$. This correlation was valid in the range of $0.74<Re<1.77$ and the standard error of estimate for this model was found to be ±0.12. The mass transfer was found to be proportional to the liquid flow rate to the power of 1.02. This value was higher compared to that which was reported by other researchers. This may have been due to differences in experimental conditions. This study was conducted under laminar flow conditions whereas some other studies were undertaken in turbulent flow conditions. Laminar flow was chosen in this study as stormwater in wetlands is in this flow condition and adsorption will occur in anaerobic conditions in stormwater treatment wetlands when sawdust in used. Moreover, sawdust particles used in this research were intraparticle adsorbate medium while other studies used porous media which did not show intraparticle diffusion.

Therefore, it can be concluded that sawdust of Radiata pine wood can be considered as a promising adsorbent medium for the treatment of stormwater. Sawdust can act as electron donor and is an excellent source of carbon, which contributes to the denitrification process. As a waste material, the sawdust can be used as a renewable resource for the treatment of stormwater in a sustainable way. The results found in this study may be useful for designing saturated zone biofiltration/bioretention systems for stormwater treatment.

## 7.2. Recommendations

Based on the results of batch and column experiments, it was concluded that Radiata pine wood sawdust is an effective adsorbent medium for the removal of nutrient from stormwater. There is always a need for finding cost effective medium

for wastewater/stormwaster treatment. This study provides important information regarding this issue. The following recommendations are made for future study:

- Since this research uses a single pollutant of interest in aqueous solution, the complexity of compounds should be extended by using multiple pollutants or actual stormwater samples. Stormwater should be collected from flashflood surface runoff as it contains more possible pollutants.

- Radiata pine sawdust can be mixed with other medium including soil, sand, and other organic media, using natural or engineered filtration methods to improve its ability to remove pollutants in stormwater .

- Theoretically, literature shows that the wood material has such chemical composition which is able to adsorb nutrient, heavy metals, and hydrocarbon. These need to be verified by further study. All of the results obtained in this research are based on a laboratory scale. A pilot study may be undertaken to determine the long-term performance of sawdust and its life expectancy. This should be followed by a practical application in the field to confirm the effectiveness of sawdust as an adsorbent. Furthermore, the possibility of growing native plant species on a sorption media should then be investigated in a subsurface wetland treatment process, as it enables dual processes for nutrient removal.

- The capability of Radiata pine wood sawdust requires further investigation as it may be a potential candidate for removing contaminants from wastewater, groundwater or greywater.

- It is recommended that appropriate practices for the disposal of the spent medium be adequately examined to avoid further secondary pollution. This might be explored by the use of fungus or other organisms for biological treatment in anaerobic conditions.

# REFERENCES


Acar, F. N. and Eren, Z., 2006. Removal of Cu (II) ions by activated poplar sawdust (Samsun Clone) from aqueous solutions. *Journal of Hazardous Materials* B 137: 909-914.

Achak, M., Hafidi, A., Ouazzani, N., Sayadi, S., Mandi, L., 2009. Low cost biosorbent "banana peel" for the removal of phenolic compounds from olive mill wastewater: Kinetic and equilibrium studies. *Journal of Hazardous Materials* 166: 117–125.

Ahmad, A., Rafatullah, M., Sulaiman, O., Ibrahim, M. H., and Hashim, R. 2009. Scavenging behavior of meranti sawdust in the removal of methylene blue from aqueous solution. *Journal of Hazardous Materials* 170: 357-365.

Ahmad, F., Daud, W. M. A. W., Ahmad, M. A., Radzi, R., 2012. Cocoa (Theobroma cacao) shell-based activated carbon by $CO_2$ activation in removing of Cationic dye from aqueous solution: Kinetics and equilibrium studies. *Chemical engineering research and design* 90: 1480–1490.

Ajmal, M., Khan, A. H., Ahmad, S., Ahmad, A., 1998. Role of sawdust in the removal of copper (II) from industrial wastes, *Water Resources* 32: 3085-3091.

Aksu, Z., 2005. Application of biosorption for the removal of organic pollutants: a review. *Process Biochemistry*, 40: 997-1026.

Aksu, Z., Gonen, F., 2004. Biosorption of phenol by immobilized activated sludge in a continuous packed bed: prediction of breakthrough curves. *Process Biochemistry*, 39: 599-613.

Albarelli, J. Q., Rabelo, R. B., Santos, D. T., Beppu, M. M., Meireles, M. A. A., 2011. Effects of supercritical carbon dioxide on waste banana peels for heavy metal removal. *J. of Supercritical Fluids* 58: 343– 351.

Amel, K., Hassena, M. A., Kerroum, D., 2012. Isotherm and Kinetics Study of Biosorption of Cationic Dye onto Banana Peel. *Energy Procedia* 19: 286 – 295.

Argun, M. E., Dursun, S., Ozdemir, C., and Karatas, M., 2007. Heavy metal adsorption by modified oak sawdust: Thermodynamic and kinetics. *Journal of Hazardous Materials* 141: 77-85.

Ashish, S., Aniruddha, M., Prathmesh, S., Dattatraya, P., Prakash, R., Mansing, A., Sanjay, K., 2012. Removal of Bi (III) with Adsorption Technique Using Coconut Shell Activated Carbon. *Chinese Journal of Chemical Engineering*, 20 (4) 768-775.

Ates, F., Un, U. T., 2013. Production of Char from Hornbeam Sawdust and its Performance Evaluation in the Dye Removal. *Journal of Analytical and Applied Pyrolysis*, 103: 159-166.

Ayyub, B. M., McCuen, R. H., 2011. Probability, Statistics, and Reliability for Engineers and Scientists, Third Edition. *Taylor and Francis Group*, United State of America.

Azizian, S., 2004. Kinetic models of sorption: a theoretical analysis, *Journal of Colloid and Interface Science* 276: 47–52.

Babu, B. V. and Gupta, S., 2008. Adsorption of Cr(VI) using activated neem leaves: kinetic studies. *Adsorption* 14: 85–92.

Baker, L. A., 1992. Introduction to nonpoint source pollution in the United States and prospects for wetland use. *Ecological Engineering*, 1: 1-26.

Batzias, F. A., Sidiras, D. K., 2007. Simulation of methylene blue adsorption by salts-treated beech sawdust in batch and fixed-bed systems. *Journal Hazardous Materials* 149: 8-17.

Bhatnagar, A., Sillanpaa, M., 2010. Utilization of agro-industrial and municipal waste materials as potential adsorbents for water treatment—A review. *Chemical Engineering Journal* 157: 277–296

Bhatnagar, A., Vilar, V. J. P., Botelho, C. M. S., Boaventura, R. A. R., 2010. Coconut-based biosorbents for water treatment — A review of the recent literature. *Advances in Colloid and Interface Science* 160: 1–15.

Bhattacharyya, K. G., Gupta, S. S., 2006. Adsorption of Fe (III) from water by natural and acid activated clays: Studies on equilibrium isotherm, kinetics and thermodynamics of interactions, *Adsorption* 12: 185-204.

Bohart, G. S., Adam, E. Q, 1920. Some aspects of the behavior of charcoal with respect to chlorine. *Journal of the American Chemical Society*, 42: 523-544.

Borba, C. E., Guirardello, R., Silva, E. A., Veit, M. T., Tavares, C. R. G., 2006. Removal of nickel (II) ions from aqueous solution by biosorption in a fixed bed column: Experimental and theoretical breakthrough curves. *Biochemical Engineering Journal*, 30: 184-191.

Boving T. B., Neary K., 2007. Attenuation of polycyclic aromatic hydrocarbons from urban stormwater runoff by wood filters. *Journal of Contaminant Hydrology* 91 (1-2):43-57.

Boyd, G. E., Adamson, A. W., Myers, Jr. L. S., 1947. The exchange adsorption of ions from aqueous solution by organic zeolites. II. Kinetics. *Journal of the American Chemical Society* 69: 2836.

Bozic, D., Gorgievski, M., Stankovic, V., Strbac, N., Serbula, S., Petrovic, N., 2013. Adsorption of heavy metal ions by beech sawdust – Kinetics, mechanism and equilibrium of the process. *Ecological Engineering* 58: 202-206.

Bratieres, K., Fletcher, T. D., Deletic, A., Zinger, Y., 2008. Nutrient and sediment removal by stormwater biofilters: A large-scale design optimization study. *Water Research* 42: 3930-3940.

Bulut, Y., Aydin, H., 2006. A kinetics and thermodynamics study of methylene blue adsorption on wheat shells, *Desalination* 194: 259-267.

Chang, N., Hossain, F., Wanielista, M., 2010**.** Filter Media for Nutrient Removal in Natural Systems and Built Environments: I—Previous Trends and Perspectives. *Environmental Engineering Science*, 27(9): 689-706.

Chang-jun, L. Yan-zhong, L., Zhao-kun, L., Zhao-yang, C., Zhong-guo, Z., Zhi-ping, J., 2007. Adsorption removal of phosphate from aqueous solution by active red mud. *Journal of Environmental Sciences* 19: 1166–1170.

Chatzapoulos, D., Varma, A., 1995. Aqueous-phase adsorption and desorption of toluene in activated carbon fixed beds: experiments and model. *Chemical Engineering Science*, 50 (1): 127-141.

Chen, B., Chen, Z., 2009. Sorption of naphthalene and 1-naphthol by biochars of orange peels with different pyrolytic temperatures. *Chemosphere* 76: 127–133.

Chen, S., Yue, Q., Gao, B., Li, Q., Xu, X., 2011. Removal of Cr (VI) from aqueous solution using modified corn stalks: Characteristic, equilibrium, kinetic and thermodynamic study. *Chemical Engineering Journal* 168: 909–917.

Cho,K.W., Song, K.G., Cho,J. W., Kim,T.G., Ahn, K. H. 2009. Removal of nitrogen by a layered soil infiltration system during intermittent storm events. *Chemosphere* 76: 690–696.

Chong, H. L. H., Chia, P. S., Ahmad, M. N.., 2013. The Adsorption of Heavy metal by Bornean Oil Palm Shell and its Potential Application as Constructed Wetland Media. *Bioresource Technology* 130: 181-186.

Clark, R. M., 1987. Evaluating the cost and performance of field-scale granular activated carbon systems. *Environmental Science Technology*, 21 (6): 573-580.

Collins, K. A., Lawrenceb, T. J., Standerc, E. K., Jontosd, R. J., Kaushale, S. S., Newcomerf, T. A., Grimmg, N. B., Ekbergh, M. L. C., 2010. Opportunities and challenges for managing nitrogen in urban stormwater: A review and synthesis. *Ecological Engineering* 36:1507–1519.

Comiti, J., Renaud, M., 1991. Liquid-solid mass transfer in packed beds of parallelepipedal particles: energetic correlation. *Chemical Engineering Science*, 46 (1): 143-154.

Cooney, D. O., 1998. Adsorption Design for Wastewater Treatment. *Lewis Publisher*, Florida.

Cooney, D. O., 1991. Determining external film mass transfer coefficients for adsorption columns. *AIChE journal*, 37 (8): 1270-1274.

Cooney, D. O., 1991. The importance of axial dispersion in liquid-phase fixed-bed adsorption operations. *Chemical Engineering Community*, 110: 217-231.

Crittenden, J. C., Trussell, R. R., Hand, D. W., Howe, K. J., Tchobanoglous, G., 2005. Water Treatment: Principles and Design, Second Edition. *John Willey & Sons, Inc,* New Jersey.

Cussler, E. L., 2009. Diffusion Mass Transfer in Fluid Systems, Third Edition. *Cambridge University Press*, United Kingdom.

Daifullah, A.A.M., Girgis, B.S., Gad, H.M.H., 2004. A study of the factors affecting the removal of humic acid by activated carbon prepared from biomass material. *Colloids and Surfaces A: Physicochem. Eng. Aspects* 235: 1–10.

Davis, A. P., Shokouhian, M., Sharma, H., and Minami, C., 2001. Laboratory Study of Biological Retention for Urban Stormwater Management. *Water Environment Research*, 73 (1): 5-14.

Deliyani, E.A., Peleka, E.N., Matis, K.A., 2009. Review Modeling the sorption of metal ions from aqueous solution by iron-based adsorbents. *Journal of Hazardous Materials*, 172: 550-558.

Department of Environment, Government of Western Australia, 2004. Stromwater Manajemen Manual for Western Australia.

Doan, H. D., Lohi, A., Dang, V. B. H., Dang-Vu, T., 2008. Removal of $Zn^{+2}$ and $Ni^{+2}$ by adsorption in a fixed bed of wheat straw. *Process Safety and Environment Protection*, 86: 259-267.

Dobrowolski. R, Otto. M, 2010. Study of chromium (VI) adsorption onto modified activated carbons with respect to analytical application, *Adsorption* 16: 279-286.

Dursun, G., Cicek, H., Dursun, A. Y. 2005. Adsorption of phenol from aqueous solution by using carbonised beet pulp. *Journal of Hazardous Materials* B125: 175–182.

Dutta, B. K., 2007. Principles of Mass Transfer and Separation Processes. PHI Learning Private Limited, New Delhi.

Ekpete, O. A., Horsfall, J. M., Spiff, A. I., 2011. Fixed Bed Adsorption Of Chlorophenol On To Fluted Pumpkin And Commercial Activated Carbon. *Australian Journal of Basic and Applied Sciences*, 5(11): 1149-1155.

El-Hendawy, A.-N. A., Alexander, A. J., Andrews, R. J., Forrest, G., 2008. Effects of activation schemes on porous, surface and thermal properties of activated carbons prepared from cotton stalks. *J. Anal. Appl. Pyrolysis* 82: 272–278.

Escudero, C., Gabald´on, C., Marzal, P., Villaescusa, I., 2008. Effect of EDTA on divalent metal adsorption onto grape stalk and exhausted coffee wastes. *Journal of Hazardous Materials* 152: 476–485.

Facility for Advancing Water Biofiltration (FAWB), 2008. Advancing the Design of Stormwater Biofitration, Australia.

Faucette, L.B. and Tyler, R. Organic BMPs used for stormwater management. http://www.ieca.org/membersonly/cms/content/Proceedings/Object168PDFEnglish.pdf

Febrianto, J., Kosasih, A. N., Sunarso, J., Ju, Y-H, Indraswati, N., Ismadji, S., 2009. Review Equilibrium and kinetic studies in adsorption of heavy metals using biosorbent: A summary of recent studies. Journal of Hazardous Materials 162: 616-645.

Fetter C W, 1999. Contaminant Hydrogeology, Second Edition, Prentice Hall, Inc. New Jersey.

Fettig, J., Sontheimer, H., 1987. Kinetics of adsorption on activated carbon: I. single-solute systems. *Journal of Environmental Engineering*, 113 (4): 764-778.

Foo, K. Y. and Hameed, B. H., 2010a. Insights into the modeling of adsorption isotherm systems. *Chemical Engineering Journal* 156: 2-10.

Foo, K.Y., Hameed, B.H., 2010b. Review - Detoxification of pesticide waste via activated carbon adsorption process. *Journal of Hazardous Materials* 175: 1–11.

Gobel, P., Dierkes, C., and Coldewey, W.G., 2007. Storm water runoff concentration matrix for urban areas. *Journal of Contaminant Hydrology* 91: 26–42

Greenway, M., Lucas, B., 2010. Improved media and plant species for long term sustainability of nutrient retention in bioretention systems. *Proc. National Conf. of the Stormwater Industry Association*, pp.1-13.

Gupta, N., Kushawa, A. K. Chattopadhyaya, M. C., 2012. Adsorption studies of cationic dyes onto Ashoka (*Saraca asoca*) leaf powder, *Journal of the Taiwan Institute of Chemical Engineers* 43: 604-613.

Gupta, S. Babu, B. V., 2009. Modeling, simulitaion, and experimental validation for continuous Cr (VI) removal from aqueous solutions using sawdust as an adsorbent. *Bioresource Technology* 100: 5633-5640.

Gupta, S. S., Bhattacharyya, K. G., 2006. Adsorption of Ni (II) on clays. *Journal of Colloid and Interface Science* 295: 21–32

Gupta, V. K., Rastogi, A., Nayak, A., 2010. Adsorption studies on the removal of hexavalent chromium from aqueous solution using a low cost fertilizer industry waste material. *Journal of Colloid and Interface Science* 342: 135–141.

Hamdaoui, O., 2006. Batch study of liquid-phase adsorption of methylene blue using cedar sawdust and crushed brick. *Journal of Hazardous Materials* B135: 264–273

Hamdaoui, O., 2006. Dynamic sorption of methylene blue by cedar sawdust and crushed brick in fixed bed columns. *Journal of Hazardous Materials*, B138: 293-303.

Hameed, B. H., Mahmoud, D. K., and Ahmad, A. L., 2008. Sorption equilibrium and kinetics of basic dye from aqueous solution using banana stalk waste. *Journal of Hazardous Materials*, 158: 499-506.

Hameed, B.H., Daud, F.B.M., 2008. Adsorption studies of basic dye on activated carbon derived from agricultural waste: *Hevea brasiliensis* seed coat. *Chemical Engineering Journal* 139: 48–55.

Han, R., Zhang, L., Song, C., Zhang, M., Zhu, H., Zhang, L., 2010. Characterization of modified wheat straw, kinetic and equilibrium study about copper ion and methylene blue adsorption in batch mode. *Carbohydrate Polymers* 79: 1140–1149.

Hand, D. W., Crittenden, J. C., ASCE, M., Thacker, W. E., 1984. Simplified models for design of fixed-bed adsorption systems. *Journal of Environmental Engineering*, 110: 440-456.

Hatt, B. E., Fletcher,T. D., and Deletic, A. Treatment performance of gravel filter media: Implications for design and application of stormwater infiltration systems. *Water Research* 41 (2007) 2513 – 2524.

Ho, Y-S., Mckay. G., 1998. A comparison of chemisorption kinetic models applied to pollutant removal on various sorbents, *Trans IChemE* B (76) 332-340.

Ho, Y-S, 2006. Review of second-order models for adsorption systems, *Journal of Hazardous Materials* B (136) 681–689.

Ho, Y. S., Ng, J. C. Y., McKay, G., 2000. Kinetics of pollutant sorption by biosorbents: Review, *Separation and Purification Reviews*, 29(2): 189-232.

Ho, Y. S., Porter, J. F. McKay, G., 2002. Equilibrium Isotherm Studies for The Sorption of Divalent Metal Ions onto Peat Copper, Nickel and Lead Single Component Systems. *Water, Air, and Soil Pollution* 141: 1–33.

Hossain, F., Chang, N. Wanielista, M., 2009. Modeling Kinetics and Isotherms of Functionalized Filter Media for Nutrient Removal from Stormwater Dry Ponds, *Environmental Progress & Sustainable Energy* 29 (3): 319-333.

Hsieh, C., Davis, A. P., 2005. Evaluation and Optimization of Bioretention Media for Treatment of Urban Storm Water Runoff. *Journal of Environmental © ASCE*: 1521-1531.

Ignatowicz, K., 2009. Selection of sorbent for removing pesticides during water treatment. *Journal of Hazardous Materials* 169: 953–957.

Ignatowicz, K., 2011. A mass transfer model for the adsorption of pesticide on coconut shell based activated carbon. *International Journal of Heat and Mass Transfer* 54: 4931–4938.

Jansson-Charrier, W., Guibal, E., Roussy, J., Delanghe, B., Le Cloirec. P., 1996. Vanadium (IV) sorption by chitosan: kinetics and equilibrium, *Water Reasearch* 30 (2): 465-475.

Johengen, T.H., LaRock, P.A., 1993. Quantifying nutrient removal processes within a constructed wetland designed to treat urban stormwater runoff. *Ecological Engineering* 2: 347-366.

Jusoh, A., Hartini, W.J.H., Ali, N., Endut, A., 2011. Study on the removal of pesticide in agricultural runoff by granular activated carbon. *Bioresource Technology* 102: 5312–5318.

Kalavathy, M. H., Karthikeyan, T., Rajgopal, S., Miranda, L. R., 2005. Kinetic and isotherm studies of Cu (II) adsorption onto $H_3PO_4$-activated rubber wood sawdust, *Journal of Colloid and Interface Science* 292: 354-362.

Kantarli, I. C., Yanik, J., 2010. Activated carbon from leather shaving wastes and its application in removal of toxic materials. *Journal of Hazardous Materials* 179: 348–356.

Kapur, M. Mondal, M. K., 2013. Mass transfer and related phenomena for Cr(VI) adsorption from aqueous solutions onto Mangifera indica sawdust. *Chemical Engineering Journal*, 218: 138-146.

Karadag, D., Koc, Y., Turan, M,, Armagan, B., 2006. Removal of ammonium ion from aqueous solution using natural Turkish clinoptilolite, *Journal of Hazardous Materials* B (136): 604-609.

Kayranli, B., 2011. Adsorption of textile dyes onto iron based waterworks sludge from aqueous solution; isotherm, kinetic and thermodynamic study. *Chemical Engineering Journal* 173: 782– 791.

Khaled, A., Nemr, A. E., El-Sikaily, A., Abdelwahab, O., 2009. Treatment of artificial textile dye effluent containing Direct Yellow 12 by orange peel carbon. *Desalination* 238: 210–232.

Khavidavi, H. D., Aghaie, H, 2013. Adsorption of Thallium (I) Ions Using Eucalyptus Leaves Powder. *CLEAN-Soil Air Water*, 41(7): 673-679.

Khraisheha, M., Al-Ghouti, M. A., Stanford, C. A., 2010. The application of iron coated activated alumina, ferric oxihydroxide and granular activated carbon in removing humic substances from water and wastewater: Column studies. *Chemical Engineering Journal* 161: 114–121.

Kim, H., Seagren E. A., Davis, A. P., 2003. Engineered Bioretention for Removal of Nitrate from Stormwater Runoff. *Water Environment Research* 75 (4): 355-367.

Klasson, K. T., Wartelle, L. H., Lima, I. M., Marshall, W. E., Akin, D. E., 2009. Activated carbons from flax shive and cotton gin waste as environmental adsorbents for the chlorinated hydrocarbon trichloroethylene. *Bioresource Technology* 100: 5045–5050.

Korkusuz, E. A., Bekliog˘lu, M., Demirer, G. N., 2007. Use of blast furnace granulated slag as a substrate in vertical flow reed beds: Field application. *Bioresource Technology* 98: 2089–2101.

Lach, J., Okoniewska, E., Neczaj, E., Kacprzak, M., 2007. Removal of Cr(III) cations and Cr(VI) anions on activated carbons oxidized by $CO_2$. *Desalination* 206: 259–269.

Lagergren, S., 1898. Zur theorie der sogenannten adsorption geloster stoffe. Kungliga Svenska Vetenkapsakademiens, handlingar, Handlingar 24: 1–39.

Langmuir, I., 1918. The adsorption of gases on plane surface of glass, mica and platinum. *Journal of the American Chemical Society,* 40, 1361–1403.

Larous, S., Meniai, A-H., 2012. The use of sawdust as by product adsorbent of organic pollutant from wastewater: adsorption of phenol. *Energy Procedia* 18: 905-914.

Lee S I, Weon S Y, Lee C W, and Koopman B, 2002. Removal of nitrogen and phosphate from wastewater by addition of bittern, *Chemosphere* 51: 265–271.

Lemus, J., Palomar, J., Heras, F., Gilarranz, M. A., Rodriguez, J. J., 2012. Developing criteria for the recovery of ionic liquids from aqueous phase by adsorption with activated carbon. *Separation and Purification Technology* 97: 11–19.

Liang, S., Guo, X., Feng, N., Tian, Q., 2010. Isotherms, kinetics and thermodynamic studies of adsorption of Cu2+ from aqueous solutions by $Mg^{2+/}K^{+}$ type orange peel adsorbents. *Journal of Hazardous Materials* 174: 756–762.

Limousin, G., Gaudet, J.-P., Charlet, L., Szenknect, S., Barthes, V., Krimissa, M., 2007. Sorption isotherms: A review on physical bases, modeling and measurement. *Applied Geochemistry*, 22: 249-275.

Liu, K-T., Weber, Jr., W. J., 1981. Characterization of Mass Transfer Parameters for Adsorber Modeling and Design. *Journal Water Pollution Control Federation*, 53 (10): 1541-1550.

Lloyd, S.D. Fletcher, T.D., Wong, T.H.F., Wootton, R.M. 2001. Assessment of Pollutant Removal in a Newly Constructed Bio-retention System," in *Proc*. 2nd *Conf*. *South Pacific Stormwater* , Auckland, New Zealand, pp.20-30.

Lorenc-Grabowska, E., Gryglewicz, G., Diez, M.A., 2012. Kinetics and equilibrium study of phenol adsorption on nitrogen-enriched activated carbons. Fuel ( Aticle in press).

Lu, S.G., Bai, S.Q., Zhu, L., Shan, H.D., 2009. Removal mechanism of phosphate from aqueous solution by fly ash. *Journal of Hazardous Materials* 161: 95–101.

Lugo-Lugo, V., Herna´ndez-Lo´ pez, S., Barrera-Dı´az, C., Uren˜a-Nu´ n˜ez, F., Bilyeu, B., 2009. A comparative study of natural, formaldehyde-treated and copolymer-grafted orange peel for Pb(II) adsorption under batch and continuous mode. *Journal of Hazardous Materials* 161: 1255–1264.

Madrakian, T., Afkhami, A., Ahmadi, M., 2012. Adsorption and kinetic studies of seven different organic dyes onto magnetite nanoparticles loaded tea waste and removal of them from wastewater samples. *Spectrochimica Acta Part A: Molecular and Biomolecular Spectroscopy* 99: 102–109.

Malkoc, E., Nuhoglu, Y., Dundar, M., 2006. Adsorption of chromium (VI) on pomace – An olive oil industry waste: Batch and column studies, *Journal of Hazardous Materials* B138: 142-151.

Marin, A. B. P., Aguilar, M. I., Meseguer, V. F., Ortuno, J. F., Saez, J., and Llorens, M., 2009. Biosorption of chromium (III) by orange (citrus cinensis) waste: Batch and continuous studies, *Chemical Engineering Journal* 155: 199-206.

Martin, C., Ruperd, Y., Legret, M, 2007. Urban stormwater drainage management: The development of a multicriteria decision aid approach for best management practices. *European Journal of Operational Research*, 181: 338–349.

Me´ndez-Dı´az, J.D., Sa´nchez-Polo, M., Rivera-Utrilla, J., Bautista-Toledo, M.I., 2009. Effectiveness of different oxidizing agents for removing sodium dodecylbenzenesulphonate in aqueous systems. *Water Research* 43: 1621 – 1629.

Memon, S. Q., Memon N., Shah, S.W., Khuhawar, M.Y., Bhanger M.I., 2007. Sawdust - A green and economical sorbent for the removal of cadmium (II) ions. *Journal of Hazardous Materials* B139: 116–121.

Mondal, M.K., 2009. Removal of Pb(II) ions from aqueous solution using activated tea waste: Adsorption on a fixed-bed column. *Journal of Environmental Management* 90: 3266–3271.

Nehrenheim, E., Gustafsson, J.P., 2008. Kinetic sorption modelling of Cu, Ni, Zn, Pb and Cr ions to pine bark and blast furnace slag by using batch experiments. *Bioresource Technology* 99: 1571–1577.

Noonpui, S., Thiravetyan, P., Nakbanpote, W., Netpradit, S., 2010. Color removal from water-based ink wastewater by bagasse fly ash, sawdust fly ash and activated carbon. *Chemical Engineering Journal* 162: 503–508.

NSW Environment Protection Authority. 1997 Managing Urban Stormwater: Treatment Techniques; Draft http://www.epa.nsw.gov.au.

O¨ zer, D., Dursun, G., O¨ zer, A., 2007. Methylene blue adsorption from aqueous solution by dehydrated peanut hull. *Journal of Hazardous Materials* 144: 171–179.

Oliveira, L. C. A., Coura, C. V. Z., Guimarães, I. R., Goncalves, M., 2011. Removal of organic dyes using Cr-containing activated carbon prepared from leather waste. *Journal of Hazardous Materials* 192: 1094–1099.

Öztürk, N., Bekta, T. E., 2004. Nitrate removal from aqueous solution by adsorption onto various materials, *Journal of Hazardous Materials* B (112): 155–162.

Pełech, R., Milchert, E., Wr´obel, R., 2006. Adsorption dynamics of chlorinated hydrocarbons from multi-component aqueous solution onto activated carbon. *Journal of Hazardous Materials* B137: 1479–1487.

Petrova, B., Budinova, T., Tsyntsarski, B., Kochkodan, V., Shkavro, Z., Petrov, N., 2010. Removal of aromatic hydrocarbons from water by activated carbon from apricot stones. *Chemical Engineering Journal* 165: 258–264.

Plazinski, W., Rudzinski, W., Plazinska, A., 2009. Theoretical models of sorption kinetics including a surface reaction mechanism: A review. *Advances in Colloid and Interface Science* 152: 2-13.

Politi, D., Sidiras, D., 2012. Wastewater treatment for dyes and heavy metals using modified pine sawdust as adsorbent. *Procedia Engineering* 42: 1969 – 1982.

Prado, A. G.S., Moura, A. O., Holanda, M. S., Carvalho, T. O., Andrade, R. D. A., Pescara, I. C., de Oliveira, A. H. A., Okino, E. Y.A., Pastore, T. C.M., Silva, D. J., Zara, L. F., 2010. Thermodynamic aspects of the Pb adsorption using Brazilian sawdust samples: Removal of metal ions from battery industry wastewater. *Chemical Engineering Journal* 160: 549–555.

Radiata Pine, Department of Agriculture, Fisheries and Forestry, Queensland Government, Australia http://www.daff.qld.gov.au/29_5424.htm (accessed on 15/01/2013).

Radiata Pine, http://www.weeds.org.au/cgi (accessed on 9/04/2013).

Ragland, K. W., Aerts, D. J., 1991. Properties of wood for combustion analysis, *Bioresource Technology* 37: 161-168.

Ramakrishna, K. R., Viraraghavan, T., 1997. Dye removal using low cost adsorbents, *Water Science Technology* 36 (2-3): 189.

Ray, A., Selvakumar, A., Tafuri, A. N., 2006. Removal of selected pollutants from aqueous media by hardwood mulch, *Journal of Hazardous Materials* B (136): 213–218.

Read, J., Wevill, T., Fletcher, T., Deletic, A., 2008. Variation among plant species in pollutant removal from stormwater in biofiltration systems. *Water Research* 42: 893-902.

Reffas, A., Bernardet, V., David, B., Reinert, L., M., Lehocine, B., Dubois, M., Batisse, N., Duclaux, L., 2010. Carbons prepared from coffee grounds by H3PO4 activation: Characterization and adsorption of methylene blue and Nylosan Red N-2RBL. *Journal of Hazardous Materials* 175: 779–788.

Rudzinski, W., Plazinski, W., 2007. Theoretical description of the kinetics of solute adsorption at heterogeneous solid/solution interfaces on the possibility of distinguishing between the diffusional and the surface reaction kinetics models. *Applied Surface Science,* 253: 5827-5840.

Runping, H., Pan., Zhaohui, C., Zhenhui, Z., Mingsheng, T., 2008. Kinetics and isotherms of Neutral Red adsorption on peanut husk. *Journal of Environmental Sciences* 20: 1035–1041.

Ruthven, D. M., 1984. Principles of adsorption and adsorption Processes. *John Wiley & Sons, Inc*, Canada.

Saliling, W. J. B., Westerman, P. W., Losordo, T. M., 2007. Wood chips and wheat straw as alternative biofilter media for denitrification reactors treating aquaculture and other wastewaters with high nitrate concentrations. *Aquacultural Engineering* 37: 222-233.

Sari A, Tuzen M, Citak D, and Soylak M, 2007. Equilibrium, kinetic and thermodynamic studies of adsorption of Pb(II) from aqueous solution onto Turkish kaolinite clay. *Journal of Hazardous Materials* 149: 283-291.

Sawyer, C. N, McCarty, P. L, Parkin, G. F, 2003. Chemistry for Environmental Engineering and Science, fifth edition. *Tata McGraw-Hill*, New York.

Scala, F., 2013. Particle-fluid mass transfer in multiparticle systems at low Reynolds numbers. *Chemical Engineering Science*, 91: 90-101.

Schipper, L. A., Barkle, G. F.,Vojvodic-Vukovic, M., 2005. Maximum Rates of Nitrate Removal in a denitrification Wall. *Journal of Environmental Quality*, 34: 1270-1276.

Shukla, A., Zhang, Y., Dubey, P., Margrave, J. L., Shukla, S. S., 2002. The role of sawdust in the removal of unwanted materials from water, *Journal of Hazardous Materials* B (95): 137–152.

Shukla, S.R., Pai, R. S., 2005. Adsorption of Cu(II), Ni(II) and Zn(II) on dye loaded groundnut shells and sawdust. *Separation and Purification Technology* 43: 1–8.

Suzuki, M., 1990. Adsorption Engineering. *Kodansha LTD*, Japan

Taylor, G. D., Fletcher, T. D., Wong, T. H. F., Breen, P. F., Duncan, H. P., 2005. Nitrogen composition in urban runoff – implications for stormwater management, *Water Research* 39: 1982-1989.

Thomas, H. C., 1944. Heterogeneous ion exchange in a flowing system. *Journal of American Chemistry Society*, 66: 1664-1666.

Tien, C., 1994. Adsorption Calculations and Modeling. Butterworth-Heinemann, United State of America.

Traegner, U. K., Suidan, M. T., 1989. Parameter evaluation for carbon adsorption. *Journal of Environmental Engineering*, 115 (1): 109-128.

Trowsdale, S. A., Simcock, R., 2010. Urban stormwater treatment using bioretention. *Journal of Hydrology* 397: 167–174.

Tsai, W-T., Chang, C-Y., Ho, C-Y., and Chen, L-Y., 1999. Adsorption properties and breakthrough model of 1,1-dichloro-1-fluoroethane on activated carbons, *Journal of Hazardous Materials*, B69: 53-66.

United States Environmental Protection Agency, 1997. Innovative Uses of Compost Bioremediation and Pollution Prevention. *Solid Waste and Emergency Response*. EPA530-F-97-042. www.epa.gov

United States Environmental Protection Agency, 1999. Preliminary Data Summary of Urban Storm Water Best Management Practices. EPA-821-R-99-012. Office of Water, Washington, DC

United States Environmental Protection Agency, 2003. National Primary Drinking Water Standards. EPA-816-F-03-016. Office of Water, Washington, DC.

Uprichard, J. M., 2002. Pulp and Paper from Radiata Pine, Apita & Forest Research Victoria, Australia.

V´azquez, G., Alonso, R., Freire, S., Gonza´lez-A´ lvarez, J., Antorrena, G., 2006. Uptake of phenol from aqueous solutions by adsorption in a *Pinus pinaster* bark packed bed. *Journal of Hazardous Materials* B133: 61–67.

Wahab, M. A., Jellali, S., Jedidi, N., 2010. Ammonium biosorption onto sawdust: FTIR analysis, kinetics and adsorption isotherms modeling. Bio*resource Technology* 101: 5070-5075.

Waldrop, R.J., Beck, M., Daniels, W.L., Erick, M., Maguire, R., Hunt, J., Joiner, B., 2009. Removal of nutrients from stormwater using CCPs. *World of Coal Ash (WOCA) conference*.

Wang, Y., Liu, S., Xu, Z., Han, T., Chuan, S., Zhu, T., 2006. Ammonia removal from leachate solution using natural Chinese clinoptilolite. *Journal of Hazardous Materials* B (136): 735–740.

Wang, X. S., Lu, Z. P., Miao, H. H., He, W., Shen, H. L., 2011. Kinetics of Pb (II) adsorption on black carbon derived from wheat residue. *Chemical Engineering Journal* 166: 986–993.

Wanielista, M., Chang, N. B., 2008. Alternative Stormwater Sorption Media for the Control of Nutrients, Stormwater Management Academy, University of Central Florida, Orlando, Florida.

Williamson, J. E., Bazaire, K. E., Geankoplis, C. J., 1963. Liquid phase mass transfer at low Reynolds numbers. *Industrial Engineering Chemistry Fundamentals*, 2 (2): 126-129.

Wolborska, A., 1989. Adsorption on activated carbon of *ρ*-nitrophenol from aqueous solution. *Water Research*, 23: 85-91.

Wong, T., Breen, P., Lloyd, S., 2000. Water Sensitive Road Design-Design Options for Improving Stormwater Quality of Road Runoff, Technical Report, Report 00/1. *Cooperative Research Centre for Catchment Hydrology*, Australia.

Xuan, Z., Chang, N., Wanielista, M., Hossain, F., 2010. Laboratory-scale Characterization of a green sorption medium for on-site sewage treatment and disposal to improve nutrient removal, *Environmental Engineering Sciene* 27 (4): 301-312.

Yasemin, B. Zeki, T., 2007. Removal of heavy metals from aqueous solution by sawdust adsorption. *Journal of Environmental Sciences* 19: 160-166.

Yoon, Y. H., Nelson, J. H., 1984. Application of gas adsorption kinetics. I. A theoretical model for respirator cartridge service time. *American Indian Hygiene Association Journal*, 45: 509-516.

Zaini, M. A. A., Okayama, R., Machida, M., 2009. Adsorption of aqueous metal ions on cattle manure-compost based activated carbons. *Journal of Hazardous Materials* 170: 1119–1124.

ZZaiZhong, M., Wang, Y., Yu, J., Tian, Y., Xu, G., 2012. Porous carbon from vinegar lees for phenol adsorption. Particuology 10: 35-41.

Zinger, Y. Blecken, G-T., Fletcher, T. D., Viklander, M., Deletic, A., 2013. Optimising Nitrogen Removal in Existing Stormwater Biofilters: Benefits and Tradeoffs of a Retrofitted Saturated Zone. *Ecological Engineering*, 51: 75-82.

Zinger, Y., Fletcher,T.D., Deletic, A., Blecken G.T., Viklander M., 2007. Optimisation of the nitrogen retention capacity of stormwater biofiltration systems. *Novatech*.

# Appendix

## Graphs of Langmuir and Freundlich Isotherm of Batch Experiments

## 1. Langmuir Isotherm Model Based on Concentration Test

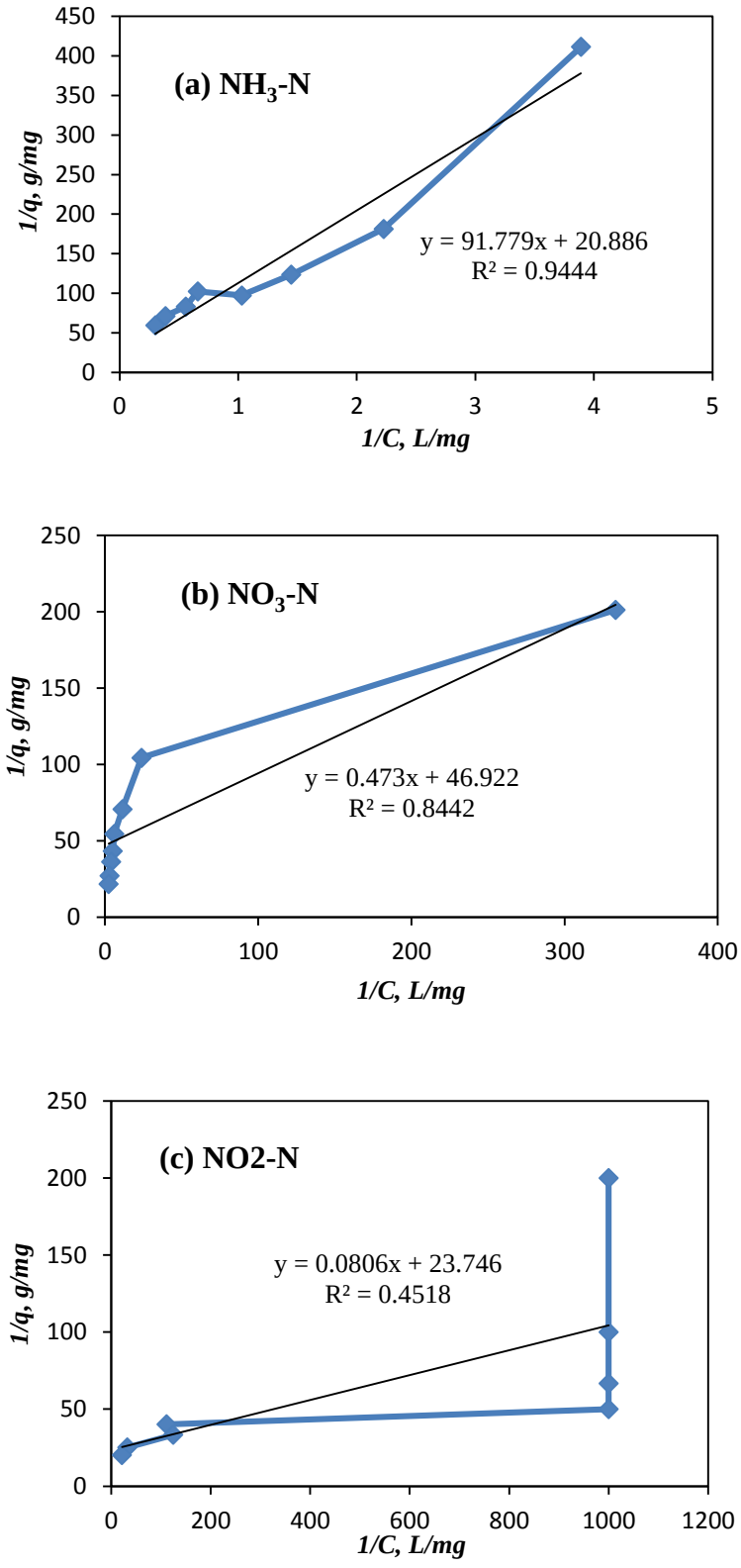


Figure A1 Langmuir isotherm plot of (a) $NH_3$-N, (b) $NO_3$-N, and (c) $NO_2$-N based on concentration test

## 2. Langmuir Isotherm Model Based on Dosage Test

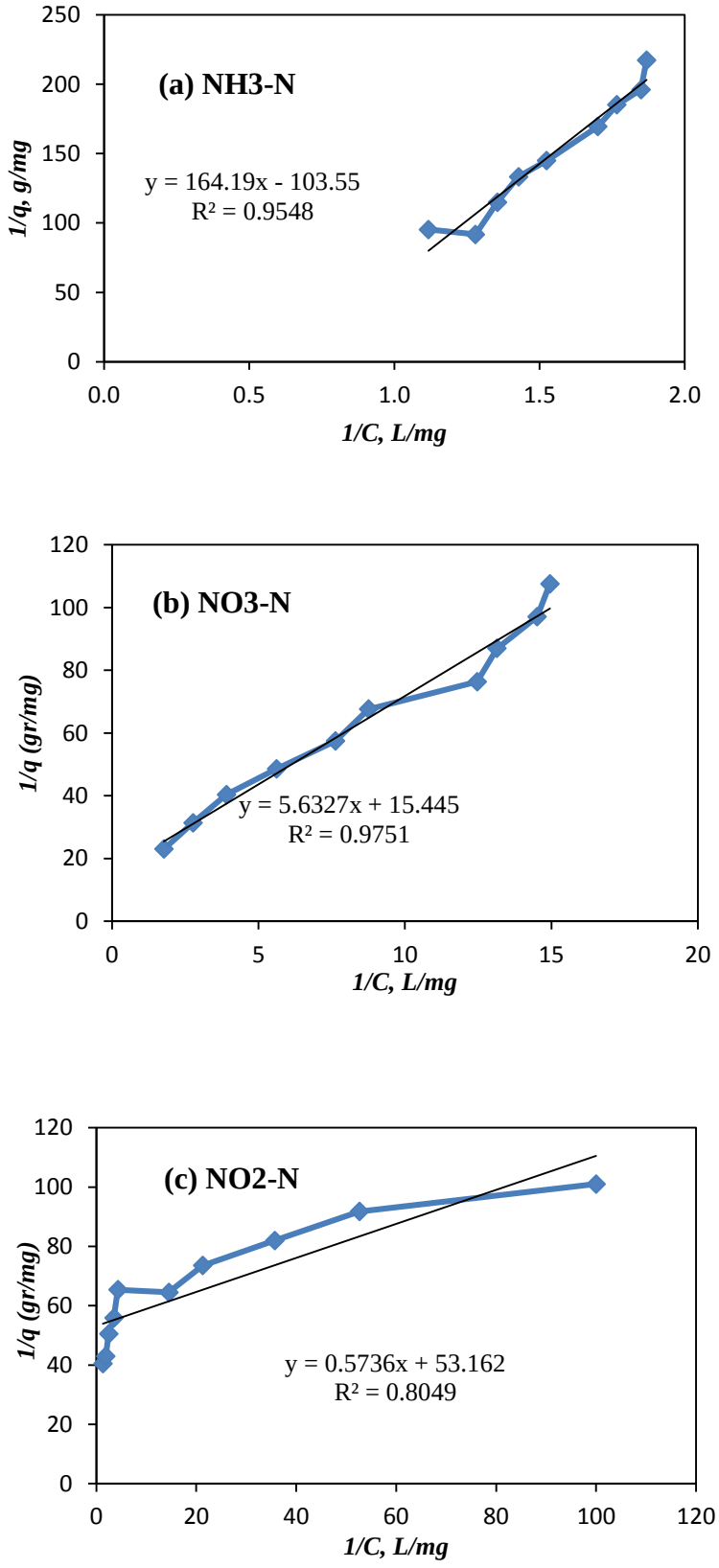


Figure A2 Langmuir isotherm plot of (a) $NH_3$-N, (b) $NO_3$-N, and (c) $NO_2$-N based on dosage test

### 3. Freundlich Isotherm Model Based on Concentration Test

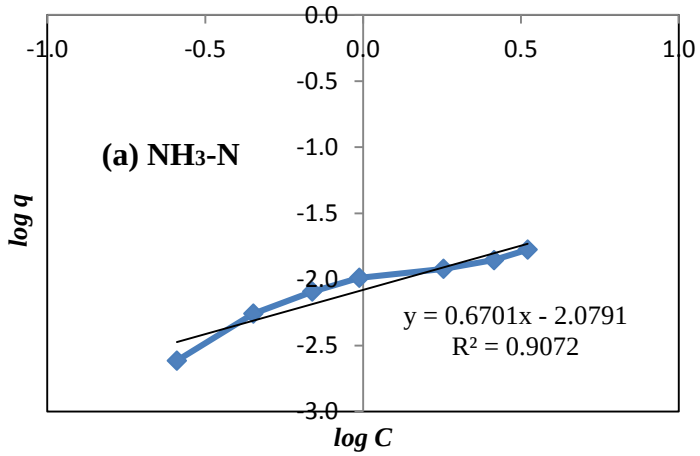


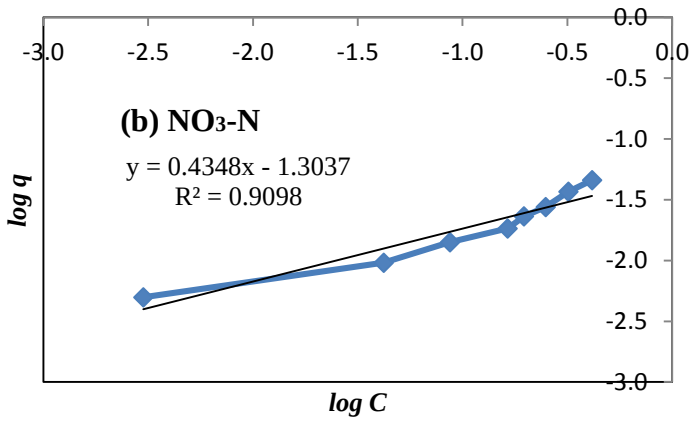


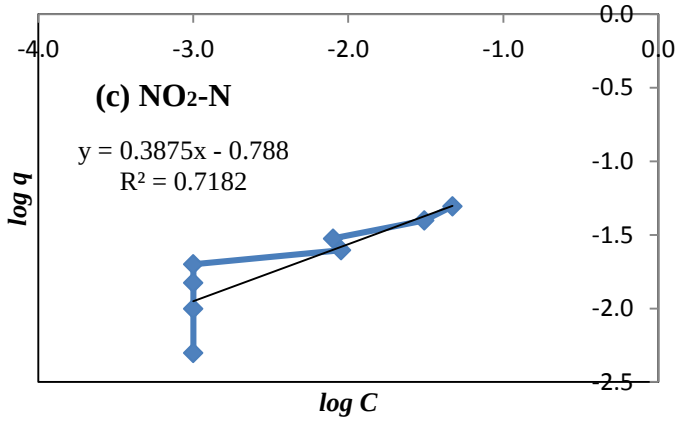


Figure A3 Freundlich isotherm plot of (a) $NH_3$-N, (b) $NO_3$-N, and (c) $NO_2$-N based on concentrations test

## 4. Freundlich Isotherm Model Based on Dosage Test

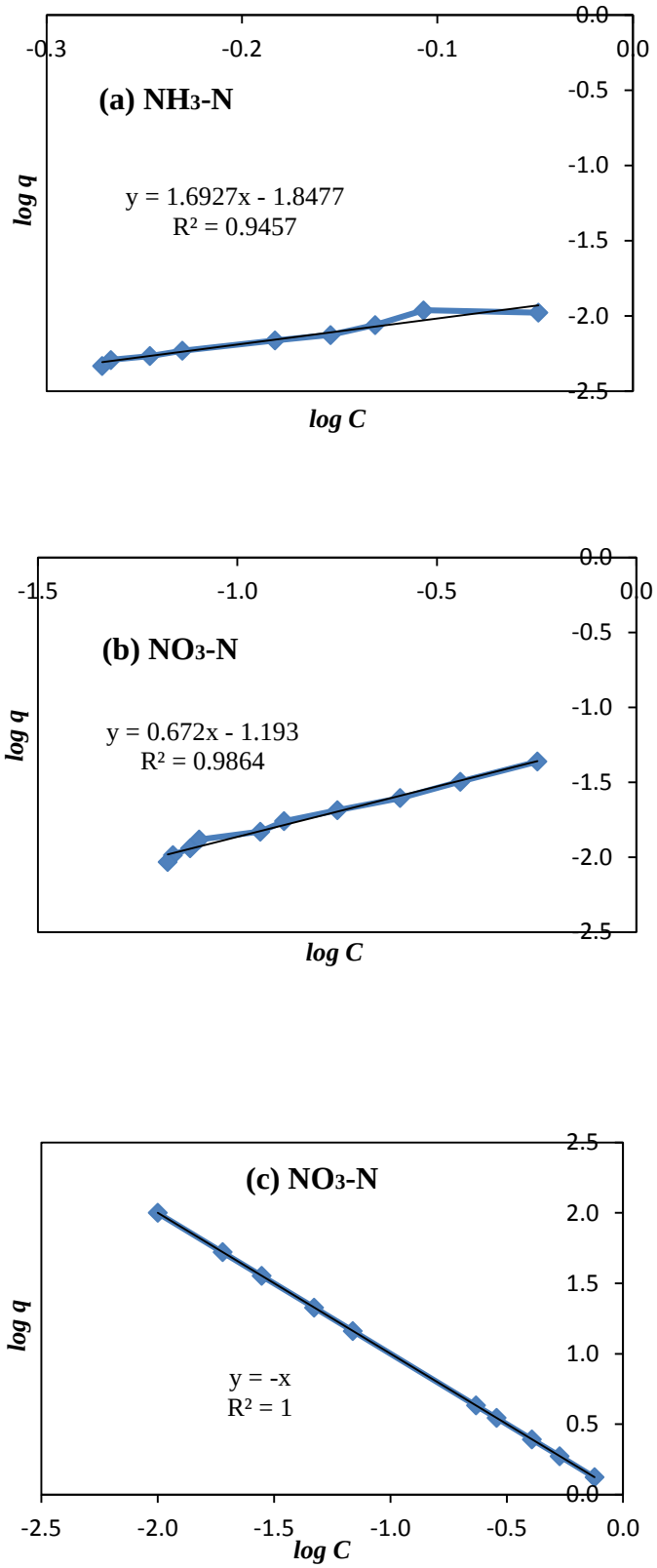


Figure A4 Freundlich isotherm plot of (a) $NH_3$-N, (b) $NO_3$-N, and (c) $NO_2$-N based on dosage test